Characterization of De Novo Protien Aggregate Formation in S. Cerevisiae

Douglas Lyke
Marquette University

CHARACTERIZATION OF *DE NOVO* PROTEIN AGGREGATE FORMATION IN *S. CEREVISIAE*

by

Douglas R. Lyke, B.S.

A Dissertation submitted to the Faculty of the Graduate School,
Marquette University,
in Partial Fulfillment of the Requirements for
the Degree of Doctor of Philosophy

Milwaukee, Wisconsin

May 2020

ABSTRACT

CHARACTERIZATION OF *DE NOVO* PROTEIN AGGREGATE FORMATION IN *S. CEREVISIAE*

Douglas R. Lyke, B.S.

Marquette University, 2020

Misfolded proteins are commonly refolded to a functional conformation or degraded by quality control mechanisms. When misfolded proteins evade quality control, they often form aggregates that are sequestered to specific sites in the cell. The proper sequestration of aggregates is thought to prevent potential dysfunction, toxicity and disease that is often associated with the presence of aggregates. However, the cellular mechanisms that underlie the management of newly formed protein aggregates are unclear. To understand the cellular response to protein aggregate formation, I used the aggregation prone prion domain of the Sup35 protein (Sup35NM) in yeast. Previous work observing GFP-tagged Sup35NM (Sup35NM-GFP) through 3D time-lapse microscopy observed consistent two-step behavior of newly formed aggregates. The first step involves the formation of small foci that are highly mobile. These foci can coalesce to form larger mature aggregates. The second step is the sequestration of matured aggregates near the periphery of the cell. In this study I developed novel quantitative techniques to measure aggregate behavior during both steps of formation. Using these techniques, I determined that the mobility and coalescence of protein aggregates, step 1, is dependent on both the actin cytoskeleton and the Myo2p motor protein. However, step 2 is dependent upon actin networks, but not Myo2p. It was unclear whether this behavior was specific to Sup35NM-GFP or part of a general response to protein aggregation; therefore I also quantified the formation of other types of aggregates. Chemically induced stress granules and a human aggregating protein associated with amyotrophic lateral sclerosis, TDP-43, both undergo a two-step formation process that is dependent upon actin. These data suggest that there is a general cellular process in responding to different types of newly formed aggregates. Together, this study provides new insights into the mechanisms used to respond to the formation of protein aggregates, changing the current dogma of the field, and suggests for future consideration.

ACKNOLEDGMENTS

Douglas R. Lyke, B.S.

I would like to first thank my dissertation advisor, Dr. Anita Manogaran. It was a privilege to be the first of what will be many successful, graduate students to earn their doctorate through your mentoring. The patience, diligence, and encouragement from your mentoring style helped shape me not only into the scientist that I am today, but also into a more confident individual including outside of the lab. My ability to think critically, synthesize ideas, and analyze I owe to you. I hope that I was able to set the expectations high for future graduate students in your lab and will always be looked back on fondly as your first student.

I would also like to thank the many individuals who were a part of the Manogaran Lab, and my dissertation committee. There were many talented undergrads that I had the opportunity to work along side, too many to list, that inspired me to continue striving for excellence in my work. Dr. Jaya Sharma, a former post-doc in our lab, was always incredibly friendly and helpful when I first joined the lab. Dr. Jane Dorweiler, a researcher in our lab, deserves her own personal thank you. She was always willing to help me with any problem that I came across, wanted to push me as a scientist, and helped develop my writing skills through her critiques. Jane was more like a second mentor to me than a colleague in the lab, and I feel extremely fortunate to have had the opportunity to work with and learn from her. Lastly, my dissertation committee, Dr. Hristova, Dr. Petrella, Dr. Schlappi, and Dr. Yang, the diversity of background that each of you brought to my committee meetings over the past years really helped me think broader as a scientist and become someone who is great at multiple facets rather than being specialized in only one.

Finally, I would like to thank my family and friends, who have endured the rigor of graduate school in some ways as much as I have. I would like to especially thank my parents for always giving me support and offering to help in my life in whatever way they can. I would also like to thank my brother and sister-in-law for always their continuous support. Most importantly though, I need to thank my amazing wife Abbie, whom without I would not be the person that I am today. Abbie, you are an incredible person who makes me want to be the best person that I can be. Your love and support sincerely fueled me through graduate school, and I cannot thank you enough for everything you have done and sacrificed to allow me to accomplish my goals.

Table of Contents

LIST OF TABLES

LIST OF FIGURES

Chapter 1: Introduction

1.1: Overview

Cell biology is the study of the structure, function, and components of the simplest unit of life, the cell. In the cell, proteins serve multi-functional tasks in all organisms from single celled up to humans. The tasks that proteins provide can be very diverse including structure, transport, enzymatic activity, chaperones, messengers, antibodies, etc. To provide these various functions, polypeptides fold into 3D conformations based on amino acids and cellular interactions. Some conformations are more thermodynamically favorable than others, and are typically associated with function. However, not all folds are favorable or functional, and the cell must manage these misfolded proteins by either refolding, sequestering, or degrading the protein. If misfolded proteins are not managed quickly by the cell, they are capable of forming large protein aggregates that are often associated with cellular dysfunction, toxicity, and disease (Labaddia and Morimoto, 2015). Protein aggregation is not always detrimental to the cell, however the cellular mechanisms that recognize and manage protein aggregates to prevent cellular dysfunction are not well understood. This dissertation aims to identify factors involved in the cellular mechanisms that manage the initial formation of protein aggregates in hopes of understanding associated diseases better.

1.2: Protein Misfolding and Aggregation

Misfolding of proteins is a much more common phenomenon than one might expect. Misfolding occurs in a number of ways such as during translation

through misincorporation of amino acids or mutation, by mislocalization or molecular crowding on the nascent polypeptide, post-translational modifications, or later through spontaneous misfolding. The initial synthesis of proteins happens through translation at the ribosome, which is not perfect and has been described as the most error prone step in protein synthesis (Ogle and Ramakrishnan, 2005). Scientists conservatively estimate that at least 15% of average length proteins contain one or more misincorporated amino acids (Drummond and Wilke, 2009). Errors to the amino acid sequence or mutations can occur spontaneously as a result of transcriptional or translational misincorporation, splicing errors, ribosome stalling, and premature termination (Drummond and Wilke, 2009). Mutations can also be inherited, referred to as familial mutations. For example, mutations in the human protein Transthyretin (TTR) can be inherited, and lead to the development of familial amyloidotic polyneuropathies (Hund, 2012).

Misfolding can occur even after the polypeptide is properly translated. Post-translational modification errors can result in misfolding (Drummond and Wilke, 2009). If the polypeptide is not localized properly in the cell it may not fold properly. For example it is thought that proteins destined for secretory pathways that remain in the cytosol will not fold properly (Levine et al., 2005). Molecular crowding can also be a cause of protein misfolding (Ellis, 2001).

Even after proteins have been folded subsequent misfolding can occur spontaneously. Protein folds are not static, but rather dynamic influenced by their surroundings and chemical properties. “Folding Funnels” predict that

polypeptides are directed towards, stable, low energy state folds. There could be multiple possible conformations of different stabilities (Leopold et al., 1992). The dynamic properties of proteins allows them to take on less stable conformations periodically, which can be considered misfolded forms (Shakhnovich et al., 2006). Changes to the cellular environment through things such as aging or stress have the potential to cause alternate or misfolded conformations to be favored in the cell (Hipkiss, 2006; Gidalevitz et al., 2011).

The cell has protein quality control (PQC) machinery to refold or degrade proteins using chaperones, autophagy, or the proteasome. Often the first response is an attempt of molecular chaperones to refold the protein to a correct conformation using an ATP dependent process (Saibil, 2013). Chaperones, acting in complex with co-chaperones, often associate directly with the ribosome to facilitate folding as polypeptides are being synthesized, either in the ER to aid in folding of secreted or membrane bound proteins, or in the cytosol to assist in the refolding of proteins (Gautschi et al., 2002; Nishikawa et al., 2001; Young et al., 2004). If misfolded proteins cannot be refolded, they can be degraded through either autophagy or the proteasome-mediate proteolysis (Labaddia and Morimoto, 2015). There are two types of autophagy in the cell: macroautophagy and microautophagy which break down bulk cytoplasmic material or distinct organelles or molecules through selective respectively (Reggiori and Klionsky, 2013). Degradation by the proteasome is much more targeted, with proteins destined to be degraded being tagged with ubiquitins that are recognized by the proteasome complex (Nandi et al., 2006; Wang et al., 2013). However, when

misfolded proteins escape either refolding or degradation, they will commonly form aggregates with other misfolded proteins (Moreno-Gonzalez and Soto, 2011).

Misfolded proteins are prone to associate together based on their biochemical properties and form aggregates (Hipp et al., 2014). There are two types of protein aggregates in yeast: amorphous and amyloid. Amorphous aggregates are normally unorganized, typically made of multiple types of protein, and not commonly associated with disease (Weids et al., 2016). This type of aggregate usually forms as the cell responds to a transient stress in which proteins associated with processes such as translation that need to be down regulated are sequestered into aggregates or inclusions until the stress is removed leading to reversal of the aggregate (Buchnan and Parker, 2009). Conversely, amyloid aggregates are highly structured and insoluble formations, comprised of many copies of the same protein (Greenwald and Riek, 2010). Amyloids are also resistant to heat, detergent, and proteases, making these aggregates difficult to resolve (Rambaran and Serpall, 2008, Greenwald and Riek, 2010). Amyloids may have biological benefits (Bleem and Daggett, 2017), however they are commonly associated with disease such as Alzheimer's and Type-II Diabetes (Rambaran and Serpall, 2008). While not all amyloids are infectious such as TDP-43 aggregates that are associated with ALS, a subset of amyloids called prions are infectious. Prions are self-propagating amyloids that cause monomeric versions of the protein to misfold to the prion conformation and

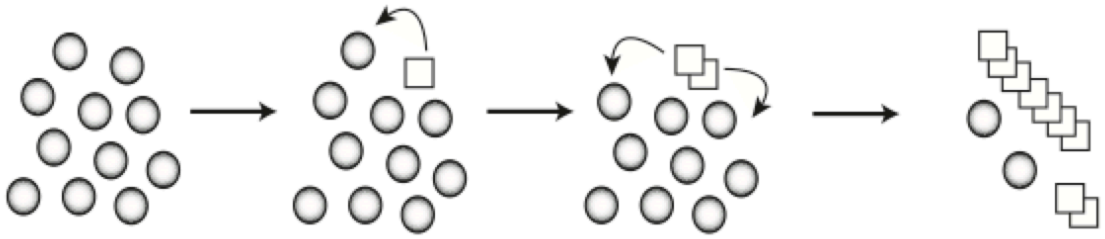

Figure 1.1: Prion Protein Aggregate Formation. In this model the circles represent functionally folded proteins, while the squares are misfolded, prion version of the protein. In the first panel proteins are normally folded, however over time it is possible for a protein to take on a misfolded conformation (square, panel 2). Prion protein aggregates are capable of influencing other normally folded versions of the same protein to become misfolded to the prion conformation, as shown by the arrows in panel 2 and 3. As more protein becomes misfolded, the aggregate is able to grow larger (panel 4).

associate with the aggregate (Figure 1.1; Prusiner, 2006), and are associated with diseases such as Creutzfeldt-Jakob's (Imran and Mahmood, 2011).

Proteins that form either amorphous or amyloid aggregates often contain intrinsically disordered regions (IDR) are susceptible to aggregation as this region is prone to associating with many binding partners, including other proteins. Exposure of the IDR in a misfolded protein increases the ability of the protein to bind and interact with others, leading to aggregation (Uemura et al., 2018). Another biochemical property that leads to protein aggregation is the exposure of hydrophobic residues. Typically, at least for cytosolic proteins, hydrophobic residues are buried within the protein and not exposed to avoid interaction with cytosol. However, when a protein is misfolded, it is possible for these residues to become exposed. This exposure leads to protein aggregation as proteins clump together in an effort to hide their hydrophobic residues (Chiti

and Dobson, 2006; Song, 2013). Once protein aggregates form, they can be dealt with by similar mechanisms to misfolded proteins, degradation or refolding, or incorporated into protein inclusions that sequester aggregates from the cellular environment for later management (Hipp et al., 2014).

1.3: Mammalian Protein Aggregation

Protein aggregation is associated with a variety of diseases, many of which are age related (Gregersen et al., 2006). While it is unclear, the infrequency of protein aggregate diseases in younger individuals suggests that management of misfolded proteins is more efficient but becomes less robust over time. Similar to mutations that cause protein misfolding, diseases can be characterized as spontaneous or familial. Spontaneous disease is typically associated with later onset with disease progression commonly associated with declining protein quality control with age, whereas familial diseases have earlier onset due to inherited mutations affecting the associated protein causing thermodynamics to favor the formation of misfiled, aggregated proteins. For example aggregation of Wildtype TTR causing senile systemic amyloidosis is associated with an onset after 60 years of age, however TTR-V30M is an inherited mutation that leads to onset of familial amyloid cardiomyopathy around 45-50 years of age (Ruberg and Burk, 2012).

While much focus has been placed on curing or treating protein aggregation diseases, the initial formation of aggregates is not well understood and why older individuals are more susceptible to disease. It is possible that in

younger cells PQC mechanisms are more robust to handle protein aggregation, and as cells age misfolded proteins are allowed to accumulate with the addition of other aging factors such as reactive oxygen species and DNA damage, overloading the remaining PQC to efficiently recognize and manage aggregates. Regardless of age, it is still unknown how the cell recognizes and manages newly formed protein aggregates. The study of *de novo* protein aggregate formation in particular is rather difficult in mammalian models. The spontaneous formation of protein aggregates is very rare, with mouse models taking 1-2 years to observe aggregate formation (Scholtzova et al., 2014). With such rare appearance of aggregates, in a multicellular system it is difficult to capture the formation of protein aggregates. Understanding the cellular biology in these systems is also quite difficult as making genetic manipulations to alter a single process is hard.

1.4: Yeast Protein Aggregation and Inclusions

To study the de novo formation of protein aggregates more efficiently, the single celled model system of budding yeast, *Saccharomyces cerevisiae*, can be used. The generation time of yeast is only 2 hours allowing high throughput screens to be performed easily, and has 23% genome identity to humans (Liu et al., 2017). The genome of yeast is also relatively small compared to mammalian systems and can easily be genetically manipulated, allowing for more directed investigation of cellular processes. This system allows for the formation of protein

aggregates to be observed on a reliable scale to pursue directed approaches in higher order organisms.

Yeast protein aggregation is commonly studied and induced using three different methods: protein overexpression, stress, or heterologous expression. To induce protein aggregation through overexpression, an endogenous protein that is prone to aggregation is transiently overexpressed. This additional expression increases the likelihood that a misfolded conformation of the protein will ensue and spontaneous aggregation can take place. A protein called Sup35p in yeast is commonly used for aggregation by overexpression as it contains an IDR (Ter-Avanesyan et al., 1994). The advantage to using transient overexpression to induce protein aggregation is that a reduced cellular stress response is elicited, however as this method requires spontaneous formation aggregation can still be a relatively rare event.

Stress induced aggregation is one of the more studied methods of induction due to rapid aggregation and the biological relevance of understanding stress response. Stress granules, or stress foci, form in response to a variety of cellular stresses such as heat, pH, and nutrient deprivation (Leeuwen and Rabouille, 2019). Stress granules are composed of protein and RNA, which upon the addition of stress are quickly sequestered into aggregates (Buchan and Parker, 2009). Upon the removal of stress, stress granules are also quickly dissolved returning proteins and RNA to their normal function (Wallace et al., 2015). This rapid reversibility is likely fostered through phase separation. During phase separation, proteins are locally organized into membraneless

compartments so that are quickly accessible back under normal conditions (Franzmann and Alberti, 2018; Franzmann et al., 2018; Kato et al., 2012; Kroschwald et al., 2018; Molliex et al., 2015; Riback et al., 2017). Proteins that are rich in IDR's are thought to undergo phase separation more rapidly than other proteins due to an inherent stress sensing ability (Alberti, 2017). To observe stress granules in yeast, the heat shock protein Hsp104p has commonly been used. Hsp104p is a heat shock protein functioning in disaggregation and is needed for the characteristic reversibility (Cherkasov et al., 2013). However, there are a large number of proteins and RNA that localize to stress granules, including at least over 100 proteins identified to go through phase separation alone (Wallace et al., 2015). The incorporation of this magnitude of proteins is reflective of the global response that occurs in yeast from stress. This global, reversible response can make it difficult to draw conclusions of specific protein aggregate behavior in yeast that can be related to disease related aggregation that would occur in the absence of a significant stress.

Finally, heterologous expression can be used to induce aggregation in yeast. As described above, protein aggregation in mammalian models can be difficult as a result of timing and tracking aggregation in a multicellular system, however researchers still wanted to study the proteins directly associated with human disease. These particular proteins can be expressed in "humanized yeast", where the proteins quickly aggregate (Laurent et al., 2016). The use of heterologous proteins in yeast has greatly facilitated our understanding of how aggregates impact cellular behavior and has provided some indications to how

aggregates are associated with disease. While this method allows for rapid aggregation of a single protein in yeast, constant overexpression is needed and cellular response may not be as efficient. Given that the protein is not endogenous to yeast, it may be difficult for protein quality control to recognize the formation of the aggregate and respond accordingly. Therefore, humanized yeast models are often associated with a high level of toxicity. Expression the Huntingtin Protein with expanded glutamine repeats (Htt-Q103) is very toxic as the glutamine repeats can interact with endogenous proteins that contain similar repeats resulting in a loss of function (Meriin et al., 2002). Similarly, TDP-43, which is aggregated in ALS patients, also forms toxic aggregates when expressed in yeast (Johnson et al., 2009).

With each of the three models to induce protein aggregation, aggregates are associated with different protein inclusions. These inclusions are distinct sites in the cell where damaged, misfolded, and aggregating proteins are sequestered for proper PQC. Amyloid aggregates formed through overexpression or heterologous expression are usually found at one of two inclusions, IPOD or JUNQ/INQ. The Insoluble Protein Deposit (IPOD) is a perivacuolar site that houses insoluble, amyloid protein aggregates. The yeast prions [*PSI*$^{+}$], [*PIN*$^{+}$], and [*URE3*] localize here along with expression of the Huntintin Protein (HttQ103) or TDP-43 in humanized yeast (Kaganovich et al, 2008; Tyedmers et al., 2010; Saibil et al., 2012; Farrawell et al., 2015). The Juxtanuclear quality control compartment (JUNQ) or Intranuclear quality control compartment (INQ) are nucleus based inclusions that house aggregates that are marked for

degradation by the proteasome (Kaganovich et al., 2008; Gallina et al., 2015; Miller et al., 2015). Aggregates, such as VHLp and Ubc9p, are ubiquitinated and are sequestered to this inclusion for degradation (Kaganovich et al., 2008). An Age Associated Protein Deposit, APOD, has recently been proposed to house amyloid aggregates as well that appears only in old cells, however only Sup35p aggregates have been found at this cytosolic inclusion so far (Saarikangas et al., 2015).

Stress induced aggregates however, which are amorphous, are thought to localize to inclusions known as Q-Bodies (Escusa-Toret et al., 2013). While Q-Bodies are described to be cytoplasmic, localization of the stress induced aggregates through the associated chaperone Hsp104p suggests they may also be localized to the surface of organelles such as the mitochondria and ER (Zhou et al., 2014). As expected, there are over 100 proteins reported to localize to Q-Bodies in yeast (Buchan et al., 2013). Degradation of aggregates localized to Q-Bodies can be through both the proteasome and autophagy (Escusa-Toret et al., 2013; Buchan et al., 2013)

1.5: Sup35 Protein Aggregation and [*PSI*$^{+}$] Propagation

Yeast has multiple proteins capable of forming prions or amyloid aggregates. The protein Sup35p has become a standard in the field to observe protein aggregate formation as part of the protein induced method. Sup35p is a translation termination protein in yeast, and is essential in yeast. The protein is modular in nature, with the C-terminal domain having translational termination

function (Salas-Marco and Bedwell, 2004; Stansfield et al., 1993), and the N-terminal and Middle domain of the protein, while indispensible for translation termination function, contains an IDR that makes the protein prone to aggregation and is thought to provide stress sensing ability to enter phase separation condensates in times of stress (Franzmann et al., 2018). The N and M domains also allow Sup35p to form a prion called [*PSI*$^{+}$], while the C domain is not required (Ter-Avanesyan et al., 1994).

The [*PSI*$^{+}$] prion is found in two different variants depending upon the size and conformation of the aggregate. Strong [*PSI*$^{+}$] aggregates are smaller in size and are thought to be more infectious as a result as they can be transferred more easily to daughter cells. Meanwhile, weak [*PSI*$^{+}$] aggregates are large, with less efficient propagation to daughters and are more easily cured by chaperone manipulation (Derkatch et al., 1996; Bradley and Liebman, 2004). The size of the aggregate allows for differentiation between the two variants, as on SDD-AGE gels protein complexes are separated based on size (Kryndushkin et al., 2013). Variants of prions are not unique to [*PSI*$^{+}$] as another yeast prion, [*PIN*$^{+}$] can be found in multiple variations dependent on its ability to induce the formation of [*PSI*$^{+}$] rather than size (Bradley et al., 2002).

The propagation of [*PSI*$^{+}$] for generations requires the chaperone Hsp104p (Chernoff et al., 1995). Hsp104p is a AAA+ ATPase with dissaggregase activity originally identified in stress tolerance (Sanchez and Lindquist, 1990). The chaperone requires co-chaperones Sis1p and Ssa1p for dissaggregase function (Glover and Lindquist, 1998). To perform this function, the chaperone

complex binds to the protein aggregate, and pulls part of the aggregate through a central pore via ATP hydrolysis, breaking the aggregate into two pieces (Halsberger et al., 2008). The generation of two smaller aggregates can propagate prions in two different ways. First it can provide two ends that monomeric misfolded proteins can be added to (Kryndushkin et al., 2003). Second, it can generate small aggregate fragments that can be transmitted to daughter cells (Paushkin et al., 1996). This constant fragmenting and growing of aggregates allows for the population to maintain the prion as cell division occurs. Without Hsp104p, this shearing action does not take place, and the propagation of [PSI+] does not happen, while too much Hsp104p activity also fragments aggregates to a point where seeding cannot occur, also preventing propagation (Ness et al., 2002; Shorter and Lindquist, 2004).

1.6: *de novo* [*PSI*$^+$] Formation

The spontaneous *de novo* formation of [*PSI*$^+$] happens at an extremely low rate of 5.8×10^{-7} (Lancaster et al., 2010). Formation is enhanced through overexpression of Sup35p to increase the chances of protein misfolding (Wickner et al., 1994). The formation rate with overexpression can be dramatically increased further up to 10^{-2} by the presence of a second prion such as [*PIN*$^+$], the prion version of Rnq1p (Derkatch et al., 1998). The presence of a second prion is thought to seed [*PSI*$^+$] formation through two possible mechanisms. The first cross-seeding, where [*PIN*$^+$] is used as a template by which overexpressed Sup35p is misfolded and allowed to aggregate (Derkatch et al., 2001; Osherovich

and Weissman, 2001). The second mechanism is by a titration model where [*PIN*$^+$] interacts with another protein or chaperone that is preventing the formation of [*PSI*$^+$]. The interaction with [*PIN*$^+$] prevents the unknown factor from stopping [*PSI*$^+$] formation (Derkatch et al., 2001; Osherovich and Weissman, 2001).

In the *de novo* formation of Sup35p aggregates a seed is still required for aggregate formation. The most common cross-seed for Sup35p is a second prion called [PIN+], the prion version of Rnq1p. While this protein does not have a known function, [PIN+] was identified for its ability to induce [PSI+] formation (Sondheimer and Lindquist, 2000; Derkatch et al., 2001; Osherovich and Weissman, 2001). Cells lacking [PIN+] have trouble forming Sup35p aggregates unless another amyloid character protein aggregate is introduced into the cell to provide seeding quality (Derkatch et al., 2000).

Overexpression of the prion domain of Sup35p, Sup35NM, is enough to induce [*PSI*$^+$] formation in [*PIN*$^+$] cells (Figure 1.2). Using a conditional promoter, Sup35NM fused to a fluorescent reporter such as GFP (Sup35NM-GFP) allows for visualization of aggregate formation, leading to leading to fluorescent rings, lines, and dots in cells (Figure 1.2; Zhou et al., 2001). During division, ring aggregates are retained in the mother cell, however the daughter is thought to inherit the prion through non-visible aggregates formed by Hsp104p function (Ganusova et al., 2006; Mathur et al., 2009; Sharma and Liebman, 2012). These ring and line aggregates are hallmarks of [*PSI*$^+$] cells (Ganusova et al., 2006; Vishveshwara et al., 2009; Manogaran et al., 2011).

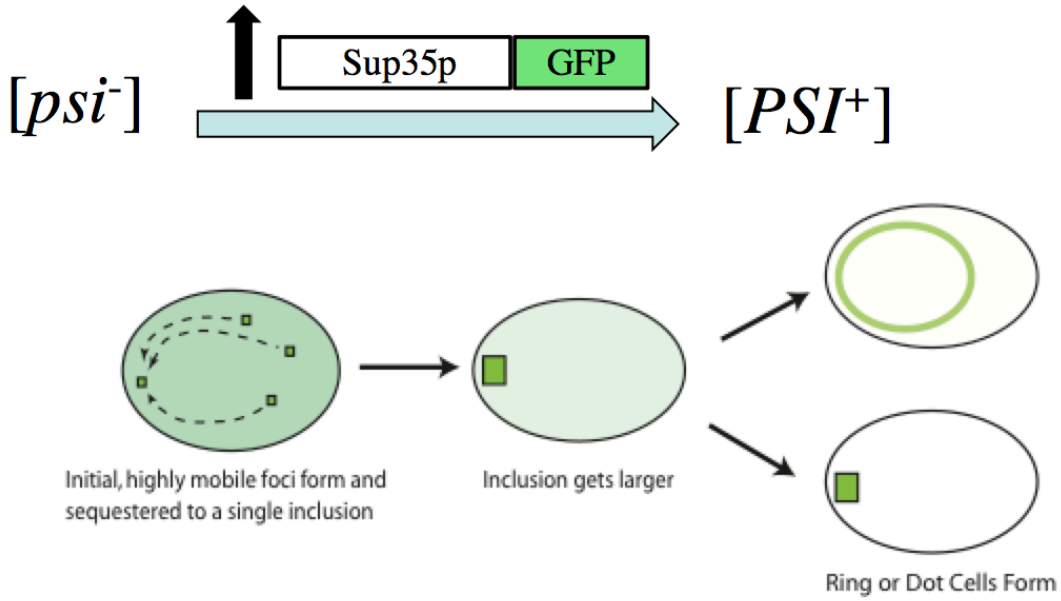

Figure 1.2: Transient overexpression of Sup35p fusion protein allows aggregate formation to be observed. Top: Transient overexpression of Sup35p fused to a fluorescent protein such as GFP increases the likelihood of protein aggregation and subsequent formation of [*PSI*$^{+}$] cells. Bottom: After transient expression of Sup35NM-GFP, small early foci become visible in cells that are highly mobile. Over time early foci become statically localized to a single site in the cell, where the foci continues to grow into a large aggregate that can take on either a dot-like or ring appearance.

The role of different cellular factors on the formation of Sup35NM-GFP aggregates has been previously investigated. Proteins associated with cortical endocytic patches, such as End3p, Sla2p, and Sla1p, all reduced the number of cells that contained aggregates (Ganusova et al., 2006). A large scale genetic screen using the yeast deletion library found several other factors that were classified into two categories that influenced aggregate formation. Early class genes, including some proteins associated with cortical actin patches such as Las17p and Sac6p, reduced the formation of Sup35NM-GFP aggregates and

propagation of [*PSI*$^{+}$]. Late class genes had normal aggregate formation, however still displayed a reduction in [*PSI*$^{+}$] propagation. Interestingly, authors found that each of the genetic deletions that altered [*PSI*$^{+}$] formation contained fragmented vacuoles, and as amyloid aggregates are thought to localize to the perivacuolar IPOD, together it was suggested that there is a link between the vacuole and protein aggregate formation (Manogaran et al., 2011; Tyedmers et al., 2010). A later study found that the disruption of genes in the autophagy pathway and vacuole function caused Sup35NM-GFP aggregate formation at a faster rate and increased [*PSI*$^{+}$] induction frequencies (Speldewinde et al., 2015). Together, this work suggests that both actin and autophagy may be important factors that influence the ability of Sup35NM-GFP to form aggregates and propagate to future generations.

1.7: Initial Cellular Response to Protein Aggregation in Yeast

To study the formation of Sup35NM-GFP aggregates, most studies take a snap shot approach. In this approach, aggregate formation is induced, and at varying time points microscopic images are acquired in an attempt to extrapolate dynamics and interaction. Our lab however, uses 3D-timelapse microscopy to observe Sup35NM-GFP aggregate formation. This approach removes the speculation aspect to the dynamics of formation as these details are visualized throughout the process. Using this approach, Sharma et al (2017) found that the induction of Sup35NM-GFP begins with diffuse cells, meaning GFP fluorescence is cytoplasmic with no distinct foci. Between 12-16 hours of induction small foci

appear in the cell that are highly mobile, which are termed early foci. These early foci move around in the cell for about 30 minutes before becoming static at a single location in the cell. This formation is characterized into a two step process: step 1 is high mobility of early foci and step 2 is the static sequestration of the larger protein aggregate. The dynamic details of this formation could not be extrapolated from snapshot microscopy providing support that 3D-timelapse microscopy is necessary to fully appreciate the behavior of newly formed protein aggregates.

Given the association of Sup35NM-GFP aggregate formation with components of the actin cytoskeleton (Ganusova et al., 2006; Manogaran et al., 2011), studies have been performed to investigate the influence of the yeast actin trafficking system on Sup35NM-GFP. Recent work depleting the Myo2p motor protein, which moves cargo along the actin cytoskeleton, found that the number of Sup35NM-GFP aggregates in [*PSI*$^{+}$] cells increased through snap shot microscopy (Kumar et al., 2016). While Myo2p had an effect on the number of aggregates, the use of snap shot microscopy and pre-existing Sup35NM-GFP aggregates is not informative towards understanding the dynamic relationship that may exist. Meanwhile, work done with stress induced aggregates rather than Sup35NM-GFP and time-lapse microscopy have found that disruption of the actin cytoskeleton through pharmacological agents can alter aggregate movement, abundance, and localization within the cell (Liu et al., 2010; Zhou et al., 2011; Song et al., 2014). It is possible that the effect of disruptions on an actin mediated trafficking mechanism has similar effects on Sup35NM-GFP relating to

both the mobile behavior of newly formed aggregates and localization in the cell, however this relationship unclear given the lack of time-lapse microscopy studies using newly formed Sup35NM-GFP.

1.8: Summary and Significance

While recent work has revealed the formation of Sup35NM-GFP aggregates is dynamic, it is not well understood what cellular mechanisms manage aggregates. Expanding our knowledge of cellular response mechanisms in yeast may enhance our ability to understand protein aggregate related diseases in mammalian systems and provide directed approaches for further studies in higher organisms that are difficult to study. In this dissertation I explore the dynamics of *de novo* Sup35NM-GFP formation, establishing innovative methods to quantify both step 1 and 2 of formation. The methods are then applied to understand how both the actin cytoskeleton and Myo2p motor protein may be involved in the formation of aggregates, as well as whether similar mechanisms are observed for the formation of different types of protein aggregates. Together, this work adds to our limited understanding of the formation of protein aggregates and will help influence further studies to eventually understand the role of the cellular response in managing protein aggregation and preventing disease.

Chapter 2: Materials and Methods

2.1 Yeast Strains and Growth Conditions

All strains were grown at 30^{o}C using standard media and cultivation procedures (Sherman, Fink, and Hicks, 1986). Yeast strains and plasmids used in this study can be found in Table 2.1 and 2.2. Unless otherwise specified, cultures were grown in rich media (YPD, 2% dextrose) or synthetic media containing 2% dextrose (SD) or galactose (SGal) as indicated and the appropriate amino acids. Yeast transformations were performed with the lithium acetate protocol (Geitz and Woods, 2002).

2.2 Genetic Disruptions

Strains with genetic disruptions created in this study were made by homologous recombination similar to Manogaran et al., 2011. Briefly, the HIS3 gene was amplified with primers (Table 2.3) adjacent to sequences (approximately 39 nucleotides) flaking the 5' or 3' ends of the candidate gene. PCR product was purified and transformed into the 74D-694 strain, and disruption strains were confirmed by PCR.

Lab Number	Strain Name	Genotype	Reference
D158	74-D694 *sac6*	MatA ade1-14, ura3-52, leu2-3,112, trp1-289, his3-200, *sac6*::HIS3 high [*PIN*+]	Manogaran et al. 2011
D228	BY4741 Hsp104-GFP	MatA, ura3, leu2, his3, met15, Hsp104-GFP High *[PIN*+]	Invitrogen (YLL026w), BY4741 GFP Tagged Library
D229	BY4741 Hsp42-GFP	MatA, ura3, leu2, his3, met15, Hsp42-GFP High [*PIN*+]	Invitrogen (YDR171w), BY4741 GFP Tagged Library
D233	74-D694 [psi-] High [*PIN*+]	MatA ade1-14, ura3-52, leu2-3,112, trp1-289, his3-200, high [*PIN*+]	Derkatch et al. 1997
D267	Wildtype Myo2 Strain	Mat A, ura3-52, leu2-3,112, his3-200, trp1-901, lys2-801, suc2-9	Catlett et al. 1998
D268	*myo2-2*	Mat A, ura3-52, leu2-3,112, his3-200, trp1-901, lys2-801, suc2-9, pep4-137, *myo2-2*(G1248D)	Catlett et al. 1998
D269	*myo2Δ*	Mat Alpha, ura3-52, leu2-3,112, his3-200, trp1-901, lys2-801, suc2-9, pep4-137, myo2::TRP1, pRS416-Myo2-Pep4	Catlett et al. 1998
JD067	BY4741 *act1-122* High [*PIN*+]	Mat A, his3-delta1, leu2, ura3, met15, lys2 act1-122::NATr High [*PIN*+]	Dorweiler et al., in revision
M102	BY4741 [psi-] High [*PIN*+]	Mat A, leu2, his3, ura3, met15, [psi-], High [*PIN*+]	Dorweiler et al., in revision
M208	74D-694 High [*PIN*+] bug1::HIS3	Mat A, ade1-14, leu2-3,115, ura3-52, trp1-289, his3-200 bug1::HIS3, high [PIN+]	Manogaran et al. 2011
M212	74D-694 High [*PIN*+] bem1::HIS3	Mat A, ade1-14, leu2-3,115, ura3-52, trp1-289, his3-200 bem1::HIS3, high [PIN+]	Manogaran et al. 2011
M216	74D-694 High [*PIN*+] vps5::HIS3	Mat A, ade1-14, leu2-3,115, ura3-52, trp1-289, his3-200 vps5::HIS3, high [PIN+]	Manogaran et al. 2011
M254	BY4741 microdot [*PIN*+]*act1-122*::NATr	MatA his3, leu2, ura3, *act1-122*::NATr, MET15, LYS2, microdot [*PIN*+]	Dorweiler et al., in revision
M256	BY4741 High [*PIN*+] *act1-101*::NATr	MatA his3, leu2, ura3, *act1-101*::NATr, met15, LYS2, High [*PIN*+]	Dorweiler et al., in revision
M261	BY4741 High *[PIN*+] with Sis1-GFP	Mat A ade1-14 his3-200 trp1-289 ura3-52 leu2-3112 SIS1GFP::KANMX6 [psi-] High [PIN+]	Invitrogen (YLL026w), BY4741 GFP Tagged Library
M262	BY4741 High [*PIN*+] with Ssa1-GFP	Mat A ade1-14 his3-200 trp1-289 ura3-52 leu2-3112 SSA1GFP::KANMX6 [psi-] High [PIN+]	Invitrogen (YLL026w), BY4741 GFP Tagged Library
M310	BY4741 High [*PIN*+] *act1-120*::NATr	MatA his3, leu2, ura3, *act1-120*::NATr, met15, LYS2, High [*PIN*+]	Dorweiler et al., in revision
M327	74-D694 High [*PIN*+] *atg40*::HIS3	Mat A, ade1-14, leu2-3,115, ura3-52, trp1-289, his3-200 *atg40*::HIS3, high [*PIN*+]	This Study
M353	74-D694 High [*PIN*+] *fis1*::HIS3	Mat A, ade1-14, leu2-3,115, ura3-52, trp1-289, his3-200 *fis1*::HIS3, high [*PIN*+]	This Study
M356	74-D694 High [*PIN*+] *num1*::HIS3	Mat A, ade1-14, leu2-3,115, ura3-52, trp1-289, his3-200 *num1*::HIS3, high [*PIN*+]	This Study
M359	74-D694 High [*PIN*+] *mdm36*::HIS3	Mat A, ade1-14, leu2-3,115, ura3-52, trp1-289, his3-200 *mdm36*::HIS3, high [*PIN*+]	This Study
M373	74-D694 High [*PIN*+] *mmm1*::HIS3	Mat A, ade1-14, leu2-3,115, ura3-52, trp1-289, his3-200 *mmm1*::HIS3, high [*PIN*+]	This Study
M375	74-D694 High [*PIN*+] *mdm12*::HIS3	Mat A, ade1-14, leu2-3,115, ura3-52, trp1-289, his3-200 *mdm12*::HIS3, high [*PIN*+]	This Study
M380	74-D694 High [*PIN*+] *cho2*::HIS3	Mat A, ade1-14, leu2-3,115, ura3-52, trp1-289, his3-200 *cho2*::HIS3, high [*PIN*+]	This Study
M383	74-D694 High [*PIN*+] *hsp42*::HIS3	Mat A, ade1-14, leu2-3,115, ura3-52, trp1-289, his3-200 *hsp42*::HIS3, high [*PIN*+]	This Study
M384	74-D694 High [*PIN*+] *ice2*::HIS3	Mat A, ade1-14, leu2-3,115, ura3-52, trp1-289, his3-200 *ice2*::HIS3, high [*PIN*+]	This Study
M386	74-D694 High [*PIN*+] atg32::HIS3	Mat A, ade1-14, leu2-3,115, ura3-52, trp1-289, his3-200 atg32::HIS3, high [*PIN*+]	This Study
M438	Wildtype High [PIN+] Myo2p Strain	Mat A Wild Type ura3-52, leu2-3,112, his3-200, trp1-901, lys2-801, suc2-9 High [PIN+]	This Study
M440	*myo2-2* High [*PIN*+]	Mat A myo2-2 mutant: ura3-52, leu2-3,112, his3-200, trp1-901, lys2-801, suc2-9, pep4-137, myo2-2(G1248D) High [PIN+]	This Study
M442	myo2-AflII High [PIN+]	mat alpha, myo2 deletion: ura3-52, leu2-3,112, his3-200, trp1-901, lys2-801, suc2-9, pep4-137, myo2::TRP1, pRS416-Myo2-Pep4 (lost by 5-FOA), pRS413-myo2-Af1II [PIN+]	This Study
M443	myo2-D1297G High [PIN+]	mat alpha, myo2 deletion: ura3-52, leu2-3,112, his3-200, trp1-901, lys2-801, suc2-9, pep4-137, myo2::TRP1, pRS416-Myo2-Pep4 (lost by 5-FOA), pRS413-myo2-D1297G [PIN+]	This Study
M444	myo2-D1297N High [PIN+]	mat alpha, myo2 deletion: ura3-52, leu2-3,112, his3-200, trp1-901, lys2-801, suc2-9, pep4-137, myo2::TRP1, pRS416-Myo2-Pep4 (lost by 5-FOA), pRS413-myo2-D1297N [PIN+]	This Study
M515	74D-694 *hsp104*::HIS3	Mat A, ade1-14, leu2-3,115, ura3-52, trp1-289, his3-200 hsp104::HIS3	Manogaran Lab

Table 2.1: Yeast Strains

Lab Number	Plasmid Name	Marker	Original Reference
p3032	pCU1P-SUP35NM-GFP	LEU2, CEN	Zhou et al. 2001
p3053	pRS413-pCUP1-SUP35NM-CFP	HIS3, CEN	Zu et al. 2014
p3068	pRS416 pCUP1-GFP-ATG8	URA3, CEN	Addgene # 49423
p3069	pBJ1808 pRS416-COF1RFP	URA3, CEN	Lin et al. 2010, Addgene #
p3071	pRS416 GAL1-TDP43WT-YFP	URA3, CEN	Addgene # 27447
p3085	pRS416-GAL1-SUP35NM-RFP	URA3, CEN	Arslan et al. 2015
p3089	pABP140-ABP140-3XYFP	URA3, Digest with Hpa1 for Int	Buttery et al. 2007
p3121	pRS316-pCUP1-SUP35NM-RFP	URA3, CEN	Arslan et al. 2015
p3162	pYX142 MITO-dsRED	LEU2, CEN	Naylor et al. 2005
p3165	pRS416-pSEC63-SEC63-mCherry-Tcyc1	URA3, CEN	Wang et al. 2014
p3167	pRS416-pGPD-mCherry-SKL-Tcyc1	URA3, CEN	Wang et al. 2014
p3172	pAG415GPD-Hsp104-mCherry	Leu, Cen	Malinovska et al., 2012
p3203	pRS413-MYO2-AFlII	HIS3, CEN	Catlett et al. 2000
p3204	pRS413-MYO2-D1297G	HIS3, CEN	Catlett et al. 2000
p3205	pRS413-MYO2-D1297N	HIS3, CEN	Catlett et al. 2000

Table 2.2: Plasmids Used

Lab Number	Name and Number	Sequence	Description
AM200	AM200 His Primer	CTTATGGCAACCGCAAGAGC	HIS3 complementary primer ("470")
		GTGAGTAGGAACGTGTATGTTTGTGTATATTGGAAAAAGGCCTACA	
AM250	AM250 Atg32 Antisense	TAAGAACACCTTTGGTGG	ATG32 AntiSense Primer for Disruption
AM251	AM251 Atg32 promoter	GCGGAACATAGCACCAAAGAGG	ATG32 Promoter Region for Disruption Confirmation
		TATTGAAGTCCTAATCACAAAAGCAAAAAAAATCTGCCAGGAACAG	
AM288	AM288 Atg32 Corrected Sense	TAAACATATGACAGAGCAGAAAGCCCTAGTAAAGC	ATG32 Sense Primer for Disruption
		CTACCATTATGGTAAAATGGAAAAACTATTCTAATCCAATCCTACAT	
AM256	AM256 Atg40 Antisense	AAGAACACCTTTGGTGG	ATG40 AntiSense Primer for Disruption
AM257	AM257 Atg40 Promoter	TCCCAGAGAACGCTTCCTTTG	ATG40 Promoter Region for Disruption Confirmation
		ACGTTCTTTCTGCTGTGCTTCACTCCACCATAGAAAACTA	
AM290	AM290 Atg40 Corrected Sense	ATGACAGAGCAGAAAGCCCTAGTAAAGC	ATG40 Sense Primer for Disruption
		ATAGAAGCACAGATCAGAGCACAGCCATACAACATAAGTATGACA	
AM311	AM311_Fis1::His3 Sense	GAGCAGAAAGCCCTAGTAAAGC	FIS1 Sense Primer for Disruption
		ATGTATGTACGTATGTGCTGATTTTTTATGTGCTTGCTACATAAGAA	
AM312	AM312_Fis1::His3 Antisense	CACCTTTGGTGG	FIS1 AntiSense Primer for Disruption
AM313	AM313_Fis1::His3 Diagnostic Sense	CTGCCGTGCCCTGCATCTG	FIS1 Promoter Region for Disruption Confirmation
		AAGACGCAACGGTCAAGGCTTTCCACGAGACGTTCGAATATGA	
AM316	AM316_Num1 Sense	CAGAGCAGAAAGCCCTAGTAAAGC	NUM1 Sense Primer for Disruption
		TATTGTTCTTAATTTACTTAGAGTTATTTAGTTTTTTTAACTA	
AM317	AM317_Num1 AntiSense	CATAAGAACACCTTTGGTGG	NUM1 AntiSense Primer for Disruption
AM318	AM318_Num1 Diagnostic	ATCGGTTCTAATAGGACCAC	NUM1 Promoter Region for Disruption Confirmation
		AGTTAAAAACCCTCCAGAGAGAACACTTACTACTATAGCATGA	
AM319	AM319_Mdm36 Sense	CAGAGCAGAAAGCCCTAGTAAAGC	MDM36 Sense Primer for Disruption
		CATTTAGTTTGTTTACATAGCAATGATATCCTTATTCTTACTA	
AM320	AM320_Mdm36 AntiSense	CATAAGAACACCTTTGGTGG	MDM36 AntiSense Primer for Disruption
AM321	AM321_Mdm36 Diagnostic	CATTACTGTCATGGGATCCG	MDM36 Promoter Region for Disruption Confirmation
		TTGAGAGAGTCAATATAATACCTGTAGCCTTTTTCTGAAAATG	
AM335	AM335_Mmm1 Sense	ACAGAGCAGAAAGCCCTAGTAAAGC	MMM1 Sense Primer for Disruption
		ATAGGAAAAAGATAGAACAAAAAATTTGTACATAAATATCTA	
AM336	AM336_Mmm1 AntiSense	CATAAGAACACCTTTGGTGG	MMM1 AntiSense Primer for Disruption
AM337	AM337_Mmm1 Diagnostic	CTCGTAAGTGACTTGACTGGC	MMM1 Promoter Region for Disruption Confirmation
		CGGTTGAAACAGATCATAAGCTGGCTTCAACTAATCCAAATGA	
AM339	AM339_Mdm12 Sense	CAGAGCAGAAAGCCCTAGTAAAGC	MDM12 Sense Primer for Disruption
		TTATGTAGACACTATTTTCAAACTATCTTTGTTAAACTACATA	
AM340	AM340_Mdm12 AntiSense	AGAACACCTTTGGTGG	MDM12 AntiSense Primer for Disruption
AM341	AM341_Mdm12 Diagnostic	AGAAGTTCTACCATGGCCG	MDM12 Promoter Region for Disruption Confirmation
		GGTGCTGTTTGTGGCCGATCACGCTAAAGATTAGGCAACGATG	
AM346	AM346_Ice2 Sense	ACAGAGCAGAAAGCCCTAGTAAAGC	ICE2 Sense Primer for Disruption
		CAATCCCTTCATGATCCTGCGACTCTTGCGCAACTGCTACATA	
AM355	AM355_Ice2 New AntiSense	AGAACACCTTTGGTGG	ICE2 AntiSense Primer for Disruption
AM348	AM348_Ice2 Diagnostic	AGCGGTTACTGGTTTCGGAG	ICE2 Promoter Region for Disruption Confirmation
		AGTGATTTTCTTAGTGACAAAGCTTTTTCTTCATCTGTAGATG	
AM349	AM349_Cho2 Sense	ACAGAGCAGAAAGCCCTAGTAAAGC	CHO2 Primer for Disruption
		CCTAGTACTTTTTAAATATATATACTCAAAAAAAAAAAACCTA	
AM350	AM350_Cho2 AntiSense	CATAAGAACACCTTTGGTGG	CHO2 AntiSense Primer for Disruption
AM351	AM351_Cho2 Diagnostic	GAACGGCGATGCCAGAAACGGC	CHO2 Promoter Region for Disruption Confirmation
		CATATCCCACACAAATTAAGATCATACCAAGCCGAAGCAATGA	
AM352	AM352_Hsp42 Sense	CAGAGCAAAAAGCCCTAGTAAAGC	HSP42 Sense Primer for Disruption
		AATATAAATGTATGTATGTGTGTATAAACAGATACGATATCT	
AM353	AM353_Hsp42 AntiSense	ACATAAGAACACCTTTGGTGG	HSP42 AntiSense Primer for Disruption
AM354	AM354_Hsp42 Diagnostic	GCAACGCCTGGAACACGCGC	HSP42 Promoter Region for Disruption Confirmation

Table 2.3: Primers Used in This Study

2.3: Induction of Sup35NM Fusion Protein Expression

Plasmids containing copper inducible promoters (Sup35NM-GFP, p3032; Sup35NM-RFP, p3121) were transformed into indicated strains and grown in 5mL of synthetic media with 50μM copper sulfate overnight (16-18 hours). Our previous work showed that most cell still retained diffuse fluorescence at these time points (Sharma et al., 2017). Plasmids containing galactose inducible promoters (Sup35NM-RFP, p3085) were transformed into indicated strains and grown for (18-22 hours) in 5mL of synthetic media containing 2% galactose. Note for time-lapse microscopy, induction was performed for the indicated times and then removed during image capture.

2.4: Snapshot Fluorescent Microscopy

Snapshot microscopy was used to take single 3D images of cells. Cell imaging was performed using Leica DMI 6000 deconvolution microscope (63X oil immersion with N.A. 1.4 magnifier) with DFC365FX camera. DIC, brightfield, GFP, texas red, CFP, DAPI, and YFP filters were used where appropriate with fluorescent protein expression or chemical stains. Cells expressing Sup35NM-GFP were selected based on the appearance of low levels of diffuse background fluorescence in the cell; ensuring aggregates were at their sequestration state. Leica LASX software was used to capture images with approximately 21 z-stack steps (step size around .5-.75μm) The Z-stack was set by setting the top and bottom points at which the cells lost focus and the DIC/brightfield channel would become small for that individual cell signaling either the top or bottom of the cell.

Images were subjected to 3D deconvolution using Autoquant deconvolution algorithms (Media Cybernetics) with intensity boost and background reduction unless otherwise indicated.

2.5: Time-lapse Fluorescent Microscopy

3D-Time-lapse Microscopy was performed in two different ways: short term and long term. Short-term microscopy was used to capture early formation events as they were occurring. Induced cells were placed on a glass slide with coverslip similar to snapshot microscopy. Diffuse cells or cells that contained an extremely early foci (barely visible aggregates with a brightly diffuse background) were subject to 3D-time-lapse microscopy. Upon finding a cell for timelapse, the z-stack was set to the same parameters as in snapshot microscopy, and image acquisition was set for every 30 seconds to 1 minute. Recordings were taken for 1-2 hours to capture the full visualization of aggregate formation.

Long-term microscopy was used to capture the initial formation of foci and was followed through sequestration. Long-term microscopy was often chosen for cells that were difficult to image (such as those containing Sup35NM-RFP), or those that we were particularly interested in observing how early foci were forming. 20μL of overnight induced cell cultures was added to 230μL of fresh media lacking copper or galactose in a single well of an Ibidi 8-Well Slide that was previously treated with ConcavalinA (ConA). Cells were allowed to settle for 10-15 minutes before imaging was performed. Images were recorded every 4 minutes in 3D for 6-8 hours with 10 or 21 step z-stacks.

2.6: Cell Staining

Budscar staining and quantification: 1mL of cell culture from 5mL of overnight growth was removed into a 1.5mL Eppendorf Microcentrifuge Tube. The sample was spun at 3000rpm for 2 minutes to pellet the cells. The supernatant was dumped off, and the pellet was resuspended in 1mL of 1X PBS. 1µL of 25µM Calcafluor White Stain (Sigma) was added to the sample. Cells were incubated for 20 minutes at 30°C. After incubation, cells were again pelleted and the supernatant was removed. The pellet was resuspended with 1mL of 1X PBS. Cells were pelleted once more, and resuspended in 250µL 1X PBS. An additional wash was performed at the discretion of the user. 2.2µL of stained cells were placed on a slide and a coverslip was put over the top of the sample. Cells were observed at 630X for discernable bud scars and protein aggregates identified in the DAPI and GFP filter sets respectively. Images were recorded in 3D as described in Snapshot Microscopy. Images were double blinded and analyzed by an independent investigator for aggregate profile and bud scar number.

Vacuole Staining: Cell cultures were grown overnight under standard conditions. 1mL of culture was removed from overnight growth, and pelleted at 3000 rpm for 2 minutes in a 1.5mL Eppendorf Microcentrifuge Tube. The supernatant was dumped off, and the pelleted cells were resuspended in 1mL of water. Resuspened cells were treated with 6.6µM FM4-64 stain (Molecular Probes). Cells were incubated for 20 minutes at 30°C. After incubation cells were

pelleted, supernatant was removed, and the pellet was resuspended in water. The wash was repeated. After the second wash, cells were resuspended in 250μL of water for imaging. 2.2μL of the sample were placed on a slide and covered with a coverslip. Cells were observed at 630X for vacuole appearance and protein aggregates using the Texas Red and GFP Filter Sets respectively. Images were acquired in 3D as described in Snapshot Microscopy and further analyzed as described in Adjacent and Co-localization Analysis.

Phalloidin Staining: Cells were grown under standard conditions overnight. 1mL of culture was removed in a 1.5mL Eppendorf Microcentrifuge Tube. 10μL of 3.7% formaldehyde was added to the cells and incubated at room temperature for 10 minutes. The sample was then pelleted at 3000 rpm for 2 minutes, with the supernatant dumped off. Pelleted cells were resuspended in 1mL of 1X PBS and 10μL of 3.7% formaldehyde. The sample was allowed to sit for 1 hour at room temperature before being pelleted again. The pellet was resuspended in 250μL of 1X PBS and 8.8μM rhodamine-phalloidin (Invitrogen) was added. The sample was kept in the dark using aluminum foil, and placed in the 30°C incubator for one hour. Following incubation, cells were pelleted and resuspended in 250μL of 1X PBS for washing. The wash was repeated a second time. Cells were then imaged using Snapshot Microscopy Methods and the Texas Red Filter to observe staining.

DAPI Staining: Cell cultures were grown overnight under standard conditions. 1mL of culture was removed from overnight growth, and pelleted at 3000 rpm for 2 minutes in a 1.5mL Eppendorf Microcentrifuge Tube. The

supernatant was dumped off, and the pelleted cells were resuspended in 1mL of 1X PBS. 2.5µL of DAPI from 1mg/mL stock was added to the resuspended sample, and incubated for 30 minutes at 30°C. After incubation cells were pelleted, supernatant was removed, and the pellet was resuspended in 1X PBS. The wash was repeated. After the second wash, cells were resuspended in 250µL of 1X PBS for imaging. 2.2µL of the sample were placed on a slide and covered with a coverslip. Cells were observed at 630X for vacuole appearance and protein aggregates using the DAPI and GFP Filter Sets respectively. Images were acquired in 3D as described in Snapshot Microscopy and further analyzed as described in Adjacent and Co-localization Analysis.

Quinacrine Staining: Cell cultures were grown to mid-log phase (OD = 0.7-1.0). Culture was cooled in ice for 5 minutes, and then 1mL of culture was pelleted at 3000 rpm for 2 minutes. The remaining pellet was resuspended in YPD with 100µM HEPES added for pH buffering. 200µM Quinacrine was added to the sample (1µL of 200mM stock). Sample was incubated for 10 minutes at 30°C, and then cooled briefly on ice. Sample was washed three times at 3000 rpm for 2 minutes each was using water containing 100µM HEPES and 0.2% glucose at pH 7.6. After washes the sample is resuspended in 200µL of the water solution for imaging. Protocol was adapated from Brett et al., 2011.

2.7: Imaging of Fluorescent Proteins

Hsp104-mCherry Stress Granules: Cell cultures expressing Hsp104-mCherry (p3172) were grown in 3mL of synthetic media for 3 hours at standard

conditions. Stress granule formation was induced following methods used by Buchan, Yoon, and Parker, 2011. 1mL of culture was removed from overnight growth in a 1.5mL Eppendorf Microcentrifuge Tube. The sample was then treated with 0.5% NaN_3 and left at room temperature for approximately 5 minutes before 2.2μL of sample were placed on a slide and covered with a coverslip for imaging. Stress foci were observed at 630X using the Texas Red Filter. Stress foci formation typically took place within the first 15 minutes of exposure to NaN_3, and cells on slides could be imaged in 3D for up to 90 minutes with acquisition every minute before either bleaching the sample or the slide dried.

TDP43 Imaging: For snapshot microscopy, cells expressing TDP43-YFP (p3071) were grown in synthetic media containing 2% galactose overnight. 2.2μL of sample were placed on a slide and covered with a coverslip for imaging. Cells were observed at 630X using the YFP filer and images were acquired in 3D following Snapshot Microscopy Methods. For Time-lapse microscopy, cells expressing TDP43-YFP were grown in synthetic media containing 2% galactose for 3 hours. After growth, Long-term Time-lapse microscopy methods were then used to observe aggregate formation.

Abp140 Imaging: Strains containing Abp140-YFP (p3089) were grown overnight under standard conditions. 1mL of the overnight culture was pelleted at 3000 rpm for two minutes and the supernatant was dumped off. The pellet was resuspended in 100μL of water. 10μL of the resuspended pellet was added to 5mL of fresh synthetic media and subsequently grown overnight for a maximum

of 18 hours under standard conditions. After overnight growth, the culture was imaged following Snapshot Microscopy Methods.

Cof1-RFP, Mito-dsRed, Sec63-mCherry, and SKL-mCherry Imaging: Cells expressing Cof1-RFP (p3069), Mito-dsRed (p3162), Sec63-mCherry (p3163), and SKL-mCherry (p3165) were grown in synthetic media containing 2% dextrose overnight for snap shot images. Cultures were imaged following Snapshot Microscopy Methods. The Texas Red filter was used for visualization.

2.8: Pharmacological Treatment

Cell cultures were grown under standard conditions overnight. Cultures were equally divided into two halves. 3μL of 200 proof ethanol was added to one half of the culture. The other half of the culture was treated with either 100μM LatrunculinA (Santa Cruz Biochemical), 100μM CytochlasinB (Cayman Chemical Company), or 25μM Jasplinkinolide (Cayman Chemical Company). Drug concentrations were determined to be effective in Lyke et al., 2018 (BioRx). Cultures were subsequently incubated for an additional 30-60 minutes at 30°C. After incubation, cultures were imaged following Snapshot Microscopy Methods.

Drug	Product Description	Company
Protease Inhibitor	Protease Inhibitor Cocktail (P8215)	Sigma
Rhodamine Phalloidin	Rhodamine Phalloidin (R415)	Invitrogen
FM4-64	FM4-64 Membrane Stain (T13320)	Molecular Probes
Cytochlasin B	Cytochlasin B (11328)	Cayman Chemical Company
Jasplakinolide	Jasplakinolide (11705)	Cayman Chemical Compnay
Latrunculin A	LatA (sc-202691)	Santa Cruz Biochemcial
Calcafluor	Fluorescent Brightener 28 (F3543-1G)	Sigma
PMSF	Phenylmethanesulfonyl fluoride (P7626)	Sigma
5-FOA	5-Fluoroorotic acid (R0811)	Thermo Scientific
Cycloheximide	Cycloheximide (C-6255)	Sigma
ConA	Concanavalin A (L7647)	Sigma
DAPI	DAPI (D9542)	Sigma
Sodium Azide	Sodium Azide (S-2002)	Sigma

Table 2.4: Pharmacological Agents Used

2.9 Heat Shock Treatment

Cultures subject to heat shock were grown overnight under standard conditions. 1mL of the culture was removed for imaging to confirm cellular phenotype prior to heat shock conditions. The remaining culture was incubated at 40°C, shaking for 30 minutes. The heat-shocked culture was removed from incubation and imaged promptly within 30 minutes of completing the heat shock.

2.10: Pathway Distribution

3 individual transformants of Sup35NM-GFP for each strain were grown overnight under standard conditions. After overnight growth, cells were imaged at 630X following Snapshot Microscopy Methods. Each transformant was blinded and images from each were quantified for the type of aggregate they contained (single dot, multiple dot, single line/ring, or multiple lines/rings). Categorization of

aggregates is based on Sharma et al., 2017 and performed with assistance by Abbey Kuborn.

2.11: Adjacent and Colocalization Analysis

For adjacent analysis, designated structures were scored as either adjacent or non-adjacent based on the distance between the structures. If structures were found in 2 or more z-steps away from each other, the structures were determined to be non-adjacent. If the distance in either the X or Y direction was more than 500nm apart, the structures were considered non-adjacent. Only cells that were in question were measured; those that were clearly non-adjacent were not measured. Images were rendered by deconvolution with intensity boost and background reduction.

For colocalization analysis, images were exported from LASX software as .avi files to maintain full z-stacks. Files were then imported to ImagePro software, where the co-localization was quantified for regions of interest encompassing the aggregate. This analysis provided Pearson's Correlation Coefficient Scores (PCC) that were used to determine levels of colocalization. PCC scores range from 1 to -1, indicating perfect co-localization to the absence of any co-localization respectively. Cells used for colocalization were not edited by deconvolution, and were the cropped version of the raw image.

2.12: Vacuole Quantification

FM4-64: Images of vacuoles stained by FM4-64 were quantified through visual categorization. The number of aggregates per cell was recorded and binned into separate class categories: Wildtype Class = 1-3 vacuoles, Class B = 4-6 vacuoles, and Class C = 7+ vacuoles. To quantify vacuole class, images were analyzed by scrolling through the z stack, and counting the number of individual stained vacuole membranes were observed. In the case that two vacuole membranes were not distinguishable from one another, that was classified as a single vacuole. This was performed for each strain in triplicate, with at least 100 cells in each trial.

Quinacrine: Images of quinacrine stained cells were assessed for fluorescent intensity. Using the region of interest tool in Leica LASX software, an ellipse is drawn around the stained vacuole region. The software gives an average fluorescent intensity value for the region of interest, which was then recorded. This was performed for each strain in triplicate, with at least 100 cells in each trial.

2.13: GFP-Atg8 Foci Quantification

Quantification of GFP-Atg8 foci was performed by analyzing images on the Leica LASX software. The number of distinguishable GFP-Atg8 foci per cell was counted for each strain in triplicate. To find the average area of each foci, the region of interest tool was used to draw an ellipse around individual foci. This tool provided the area of the ellipse drawn, giving a rough estimate of the area of

the foci. To quantify the average intensity of the foci, the cursor was placed over the brightest pixel within the foci and that value was recorded. All quantification was done in triplicate for each strain with at least 100 cells quantified in each trial.

2.14: Distance to the Periphery Measurement

Images containing a 21-step Z stack with either DIC or Brightfield channel, and respective fluorescent channels were used to measure the distance between a protein aggregate to the cell periphery. The diameter of the cell was measured in 4 separate directions (top-bottom, side-side, both diagonals) with the average used to find the radius (r). The coordinates of the edges of the cell and the radius were used to generate a virtual sphere that represents the mathematical periphery of the cell. The coordinates for the protein aggregate were plotted, within the sphere, and the distance between the origin (center) of the sphere can be determined using equation 1, derived from the equation for a sphere.

$$\mathrm{D} = \sqrt{((r - X)^2 + (r - Y)^2 + (r - Z)^2)} \qquad \text{Equation 1}$$

Once the distance between the origin and protein aggregate is determined (D), this value is subtracted from the radius, leaving the distance to the periphery of the cell from the protein aggregate.

2.15: Rate of Movement Quantification

To determine the rate of movement for a protein aggregate, the distance to the periphery is first quantified at each timepoint for the duration of the time

frame being quantified. Next the coordinates for the first time point are used to generate an arbitrary sphere the same size of the cell, however using the coordinates of protein aggregate as the center or origin of the cell. Next, the coordinates of the protein aggregate at it's second time point are plotted within the newly generated sphere, and the distance between the origin (aggregate in the first time point) and the protein aggregate (aggregate at it's second time point) can be determined using equation 1. This distance represents the distance moved over the designated period of time between images in the timelapse.

Each rate was plotted on a graph, and a linear trendline was overlaid. The average slope of the trendlines for a given genetic strain and protein aggregate were averaged.

Mean average deviation (MAD) was determined by taking the difference between each data point of the rate of movement, and substracted from the corresponding value of the trendline at the given time point. The average absolute value of deviations from the trendline represent the MAD value.

2.16: Protein Lysis, Sucrose Gradients, and Western Blotting

Protein lysates were obtained from cell cultures grown overnight under standard conditions in 50mL volume. Cultures were transferred to Oakridge Tubes and centrifuged at 3000rpm for 5 minutes. Supernatant was removed and 25mL of water was added to the pellet. Centrifugation was repeated after the addition of water to wash the cells. Pelleted cells were resuspended in 300µL of 1X Lysis Buffer (Composition) and transferred to a 1.5mL Eppendorf

Microcentrifuge Tube containing 0.5mL of chilled glass beads. Tubes containing cell culture were kept on ice, cold for the remainder of the lysis procedure. 7.5µL of Protease Inhibitor Cocktail (Sigma) was added to each culture. Samples were then vortexed for 30 seconds 20 times, resting on ice for at least 30 seconds between vortexing. Samples were then pelleted at 3000rpm for 1 minute at 4°C. The supernatant, lysate, was collected after centrifugation.

Protein concentration of lysates was determined using optical density readings and Bio-Rad Protein Assay Dye. 1µL of protein lysate was added to 99µL of water in a 1.5mL Eppendorf Microcentrifuge Tube. 1mL of 1X Bio-Rad Protein Assay Dye was added to the diluted sample. All samples were prepared in triplicate. Separate tubes were prepared to generate a standard curve. Protein standard was diluted in water to 100µL total volume (0µL, 5µL, 10µL, 20µL, 30µL, and 40µL of standard), and the Assay Dye was also added. Samples were allowed to site for a few minutes before reading absorbance on spectrophotometer set at 595nm wavelength. The standards were recorded first followed by the samples in triplicate. The standard curve was used to identify protein concentration in the samples, providing an average protein concentration for individual lysates.

For sucrose gradient centrifugation, 2mg of protein were loaded into a 2mL microcentrifuge tube with a continuous gradient previously prepared. The gradient was made of sucrose cushions ranging from 20% up to 60% sucrose. Once loaded, samples were centrifuged for at least 90 minutes at 4°C,

13,000rpm. 7 equal fractions were collected after centrifugation, and the final fraction included the pellet resuspended in lysis buffer.

Prepared samples were run on SDS-PAGE gels. Samples were typically run ranging from 100-300ug of protein total. To prepare that amount of protein, the volume of each fraction of the gradient needed to contain the desired concentration of protein was determined and added to a 1.5mL Eppendorf Microcentrifuge Tube. 4X Sample Buffer Containing Beta-mercapthanol was added to the protein lysate followed by the volume of water needed to dilute the sample buffer to 1X (Typically total volume was kept between 12 and 16µL for ease of calculations). If needed, prepared samples were boiled by placing in a 100°C heating block for 10 minutes. Samples were centrifuged at 3000 rpm for 1 minute after boiling. With prepared samples, they are carefully loaded into a lane on the SDS-PAGE gel (8% Acrylamide Stacking Gel and 10% Acrylamide Resolving Gel). Gels were run until the samples reached the bottom of the resolving gel at 125V (typically around 70 minutes total). Gels were transferred onto PVDF membrane (Immobilon-P Transfer Membranes) at 0.25A for 20-25 minutes. Filter paper was used on either side of the gel and membrane (Whatman by GE Gel-Blotting Paper 150 X 150mm GB005 CAT NO. 10426972).

After transfer, membranes were removed and washed in blocking buffer 3 times for 15 minutes each (I-Block). The appropriate dilution of the primary antibody was then added and incubated for either 1 hour, or overnight at 4°C if needed (See Table 2.5 for antibodies, concentrations, and incubation times). After incubation with primary antibody, membranes were once again washed with

blocking buffer at least 3 times for 15 minutes each wash. Following washes, the secondary antibody was added for 1 hour). The membrane was one again washed in blocking buffer at least three times.

For detection of proteins after incubation with a secondary antibody with alkaline phosphatase conjugate, membranes were washed twice for 5 minutes with 1X Assay Buffer. Membranes were placed on plastic wrap on the benchtop, and covered in CDP-STAR Substrate for 5 minutes. Substrate was carefully blotted off from the corner of the membrane holding it up to drip off excess substrate. After adding substrates the membrane was put between a plastic sheet and taken to the developing room. Film was put over the plastic sheet containing the membrane and inside of a cassette closed tightly to expose the film to the substrates that attached to the protein. Initial exposure starts at 5 minutes, then the film is developed to observe protein levels. If protein levels are low, exposure time is increased with a new film, and the opposite if protein levels are high.

Antibody	Host	Source	Titer	Incubation	Product Description
GFP	Mouse	Sigma	1:10000	1 Hour	Monoclonal Anti-GFP (G1546)
Sup35	Mouse	CoCalico Biologicals	1:10000	Overnight	Monoclonal Anti-Sup35c (BE4)
Mouse	Goat	Sigma	1:5000	1 Hour	Anti-Mouse IgG Alkaline Phosphatase (A3562)
Rabbit	Goat	Sigma	1:5000	1 Hour	Anti-Rabbit IgG Peroxidase Antibody (A9169)

Table 2.5: Antibodies

2.17: 5-FOA Plasmid Swap

myo2Δ strains containing a URA3-selected plasmid expression of Myo2p were transformed with plasmids for expression of *myo2-D1297G*, *myo2-D1297N*, or *myo2-AflII* (each containing HIS as an auxotrophic marker). Transformations were selected on media containing 5-Fluoroorotic acid (5-FOA) and lacking Histidine (similar to procedures as performed by Catlett et al., 1998).

Chapter 3: Characterization of Newly Formed Protein Aggregates in Wildtype Strains

3.1 Introduction

As described in Chapter 1 and in Sharma et al (2017), using Sup35NM-GFP to characterize the formation and behavior of prions has revealed a multi-step process. The initial observation comes from biochemical work that shows a molecular weight species larger than the monomer that appears after just 8 hours of induction, indicating that protein aggregation takes place prior to the visualization of the aggregate (16 hours). The appearance of a higher molecular weight species early during induction reflects the requirement of a certain size of the aggregate in order to become visible microscopically. However, this observation of a size requirement to visualize aggregates was only made with Sup35NM-GFP, and not the endogenous Sup35p, leaving it to speculation that both the overexpressed and endogenous protein aggregate similarly.

Once aggregates are visible, time-lapse microscopy characterized formation of aggregates into two steps subjectively, without quantification. While qualitative or subjective observations are able to identify trends and generalization of behavior, it is difficult to identify differences or changes that may be subtle. Establishing quantifiable measures for behavior enables research that can extrapolate biological mechanisms through the use of differences identified based on genetic backgrounds or exposure to pharmacological agents. For example, quantifying the mobility of early foci in genetic mutants that lack proteins involved in cargo trafficking may provide an understanding of the

mechanism by which early foci are mobile. Measuring characteristics, such as distance and time, is provides more detail about the dynamics of protein aggregate formation and explores particular traits that may be important to explaining behavior that cannot be identified through qualitative approaches. Therefore, the need to develop quantifiable measures to characterize protein aggregate formation is crucial.

Here, the goal of this chapter is to monitor the biochemical aggregation of endogenous Sup35 protein, and establish quantifiable measures to investigate the formation of Sup35NM-GFP aggregates. The formation of Sup35NM-GFP aggregates is monitored using 3D-time-lapse microscopy as previously done (Sharma et al., 2017) and the formation of Sup35NM-GFP aggregates is quantified by three different measurements of Mobility and Coalescence (Step 1), and Sequestration (Step 2). Each quantifies a particular trait of protein aggregate formation that can be used to understand what cellular mechanisms are important in managing *de novo* aggregate formation. A better understanding of the cellular mechanisms managing protein aggregates especially during formation may lead to improved therapeutics to prevent or reduce the symptoms of aggregate related diseases.

3.2 Results

3.2.1 Endogenous Sup35p is found in high molecular weight complexes during prion formation.

As described in Chapter 1, Sharma et al. (2017) showed that Sup35NM-GFP forms SDS-resistant oligomers prior to the visualization of aggregates that

have infectious properties. However, the sedimentation of endogenous Sup35p was not investigated during prion formation. The goal of this section is to determine whether endogenous Sup35p also forms high molecular weight complexes.

Here, I performed sedimentation analysis on induced cultures at specific time points using sucrose gradient centrifugation. Protein lysates were collected from several cultures that have undergone 8 hours, 16 hours, or 24 hours of induction. An un-induced culture was also included as a control to ensure [*psi*-] cultures containing the Sup35NM-GFP plasmid did not contain aggregation prior to induction. I also included strains without the Sup35NM-GFP plasmid that had no prion, [*psi*-], or contained the [*PSI*$^{+}$] prion. Lysates were separately centrifuged into a continuous sucrose gradient ranging from 20% sucrose to 60%, and 7 equal fractions were collected. A sample from each fraction was loaded and run on an SDS-PAGE gel, and probed for endogenous Sup35p. In [*psi*-] strains, Sup35p is not aggregated and should sediment to the lighter fractions (fractions 1-3), compared to [*PSI*$^{+}$] strains where Sup35p is aggregated and sediments to the heavy fractions (fractions 5-7).

I found as early as 8 hours of induction, Sup35p sediments to heavier fractions compared to un-induced and [*psi*$^{-}$] controls (Figure 3.1; Lyke and Manogaran, 2017). By 24 hours, the relative distribution of endogenous Sup35p shifts from lighter to heavier fractions. Since visual fluorescent aggregates do not appear until 12-16 hours after of induction, the sedimentation of Sup35p into heavier fractions by 8 hours corresponds with previous results, which showed

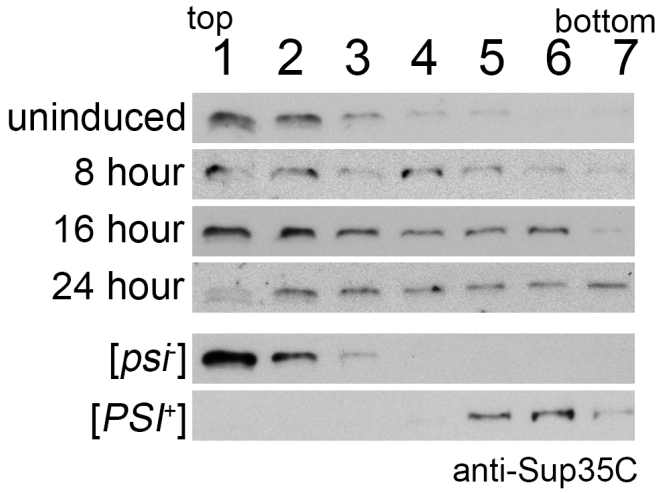

Figure 3.1: Endogenous Sup35p settles into heavier fractions with induction of Sup35NM-GFP. Wildtype cells containing the copper inducible Sup35NM-GFP plasmid (p3032) were either uninduced, or induced with 50μM copper sulfate for 8,16, and 24 hours. [psi-] and [PSI+] cultures without the plasmid were also included. Cultures were lysed using glass beads and protein was immediately separated by a continuous sucrose gradient centrifugation (20-60% sucrose). Seven fractions were collected and run on SDS-PAGE for immunoblotting. Anti-Sup35C monoclonal antibody (1:10,000) was used in immunoblot analysis. Figure was published in Lyke and Manogaran, 2017.

that Sup35NM-GFP forms SDS-resistant oligomers at the same time point (Sharma et al., 2017). These data suggest that aggregation of both endogenous Sup35p and Sup35NM-GFP happen at approximately the same time.

3.2.2 Sup35NM-GFP Aggregate Formation undergoes two distinct steps that can be quantified

To begin to understand the mechanisms of cellular response to visible protein aggregate formation, I analyzed 3D time-lapse videos of newly formed Sup35NM-GFP aggregates. Previous work revealed that the initial formation of

visual Sup35NM-GFP aggregates involves two steps. The first step involves the initial appearance early foci. These early foci are highly mobile for approximately 30-60 minutes (Figure 1B, Sharma et al., 2017). In cells with multiple early foci, fusion can occur with early foci merging together into a single focus that can also be mobile. Together, I define step 1 as consisting of early foci mobility and coalescence, which have been observed to occur simultaneously (Figure 3.2 Left, Lyke and Manogaran, 2017; Sharma et al., 2017). The second step involves the localization of early foci near the cell periphery (Figure 3.2 Right). Early foci are quickly sequestered near the cell membrane, where they grow into either dot, line, or ring like aggregates, and remain for several hours (Mathur et al., 2009; Sharma et al., 2017).

To begin to understand the cellular mechanisms that are involved in aggregate formation, I established several methods to quantify different parts of this two-step process. Mobility is considered the time in which early foci move through the cytoplasm. Using 3D time-lapse microscopy, the mobility of early foci, or movement over time, is determined by measuring the distance individual early foci move per minute. Briefly, the 3D coordinates of the early foci from the one time point and the second are plotted within a sphere representative of the cell. Next, using geometry the distance between the two time points can be extrapolated, representing the distance traveled by the early foci in three dimensions over that time frame.

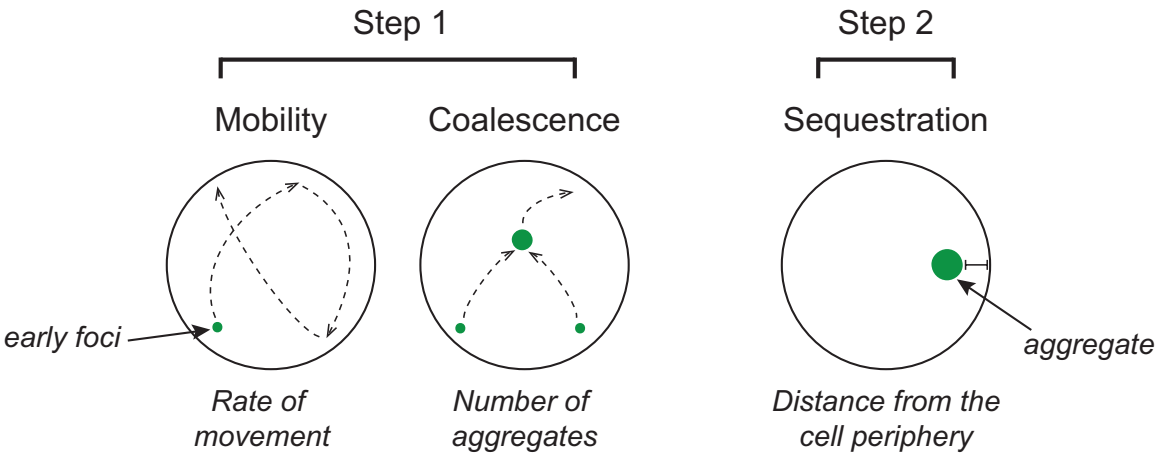

Figure 3.2: Model of Sup35NM-GFP Formation. Left. Step 1 of formation consists of two parts, mobility and coalescence. Mobility happens approximately during the first 30-60 minutes of formation, where the aggregates are observed to move throughout the cell. The mobility of early foci can be quantified by measuring the distance early foci have moved over time. Coalescence (right) also happens within the first 30-60 minutes of formation. It has been observed that multiple early foci can merge together in some cells but not in others (Sharma et al., 2017). The ability to merge or coalesce can be measured by counting the number of aggregates well after step 1 is completed. Right. Step 2 of formation involves the sequestration of matured early foci, or aggregates near the cell periphery. Once positioned to the cell periphery, the aggregate remains relatively static for several hours. The position of the aggregate can be measured spatially in three dimensions in reference to the edge of the cell.

I used two different wildtype genetic backgrounds to determine whether this two-step process could be observed in different backgrounds and whether behavior was similar. The 74D-694 strain is commonly used for prion studies because of the genetic markers available and the ease in which prionogenic proteins aggregate (Chernoff et al., 1995). The BY4741 strain is routinely used by the yeast community, and is the genetic background of the single gene disruption library and GFP-tag collection (Winzler et al., 1999). An analysis of

both wildtype genetic backgrounds showed that the average rate of movement over the first 30 minutes was approximately 0.65μm/min (Figure 3.3). Previous studies observing the rate of movement for heat induced aggregates show a similar rate of 5-15nm/second (0.3-0.8μm/min; Escusa-Toret et al., 2013), possibly suggesting that the initial mobility Sup35NM-GFP aggregates is similar to other types of aggregates. Multiple trials of mobility for both wildtypes show similar patterns of high initial mobility that slows over time (Figure 3.4 Top). While BY4741 strains showed a significantly negative slope by regression analysis, the

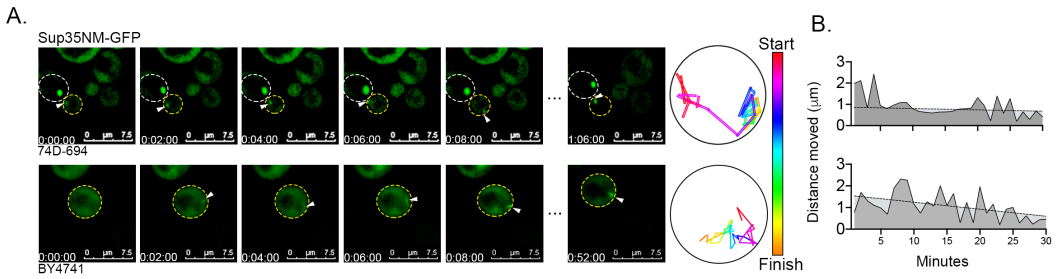

Figure 3.3: Mobility of Sup35NM-GFP Aggregates. A. Sup35NM-GFP was induced for 16 hours in 74D-694 and BY4741 cells. Cultures were then imaged by long-term 3D time-lapse microscopy (see Chapter 2) for the initial appearance of a protein aggregate. Movement of the early foci was tracked using 3D coordinate mapping with representative images shown. The yellow outlined cell for was used for mobility. To the right of the images are a particle trace showing the movement of the individual foci through the recording. B. A graph representing the distance moved per minute for the foci shown in A. On each graph a linear trend is displayed as the dashed line.

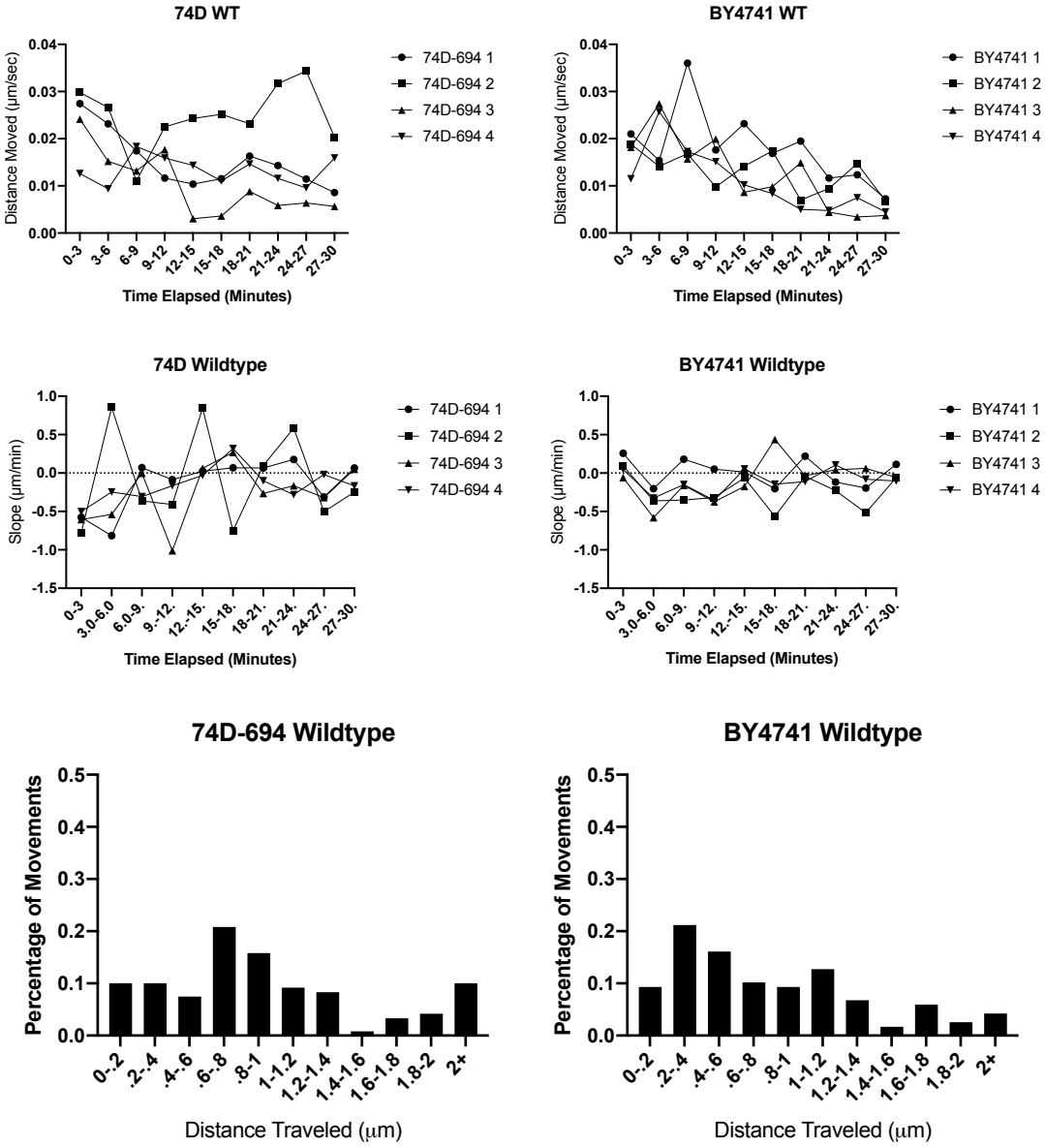

Figure 3.4: Mobility Comparison of Multiple Cells. Sup35NM-GFP was induced for 16 hours in 74D-694 and BY4741 cells, using similar methods to Figure 3.3. Aggregates from four individual cells of each genetic background were recorded. Top: Average distance moved of each aggregate per three minutes of recording. Middle: Average slope of each aggregate per three minutes of recording. Bottom: Percentage of movements by distance moved. Each minute the distance the aggregate moved was recorded and binned into a distance range. After the first 30 minutes of formation, the percentage of movements for each distance range is determined and represented above. Strains were compared using Kolmogorov-Smirnov test.

74D-694 strain did not, suggesting that while the pattern of behavior is similar there may be differences in cellular response (Figure 3.4 Middle). Further comparison of mobility profiles was done by binning the number of events that a particular distance was moved. Similar to the comparison of slopes, the 74D-694 strain was significantly different from the BY4741 strain (Figure 3.5 Bottom). We also looked at mobility during the first 10 minutes and third 10 minutes of formation to better understand where differences between the strains lied in the response to aggregate formation. During the first 10 minutes of formation 74D-694 early foci had an average rate of movement of 1.06μm/min and BY4741 was 1.21μm/min. As expected based on the overall average, the mobility of both strains slowed down by the third 10 minutes to 0.81μm/min and 0.47μm/min for 74D-694 and BY4741 respectively. The variability in the mobility of aggregates can also be assessed through calculating the mean absolute difference (MAD). The MAD value is the absolute difference of each datapoint from the mean value. This statistical tool can be used to investigate the similarity between two separate data sets, such as 74D-694 and BY4741 strains. A high MAD value (0.3 – 0.5) suggests that the mobility of aggregates does not follow a consistent rate similar to the trendline, but rather indicates that the aggregate has times in which movement is high and then low throughout formation that deviate from the consistency of the trendline. Meanwhile, a low MAD value (0.1-0.2) indicates that aggregates remain at a constant rate of movement similar to the trendline. Both wildtype strains exhibited higher MAD values (0.33 for 74D-694 and 0.30 for

	Mean Overall rate Rate (μm/min)	Mean Rate in first 10 minutes	Mean Rate in third 10 minutes	Mean Slope	Mean MAD
74D-694	0.65 +/- 0.58	1.08 +/- 0.63	0.81 +/- 0.60	-0.013 +/- 0.009	0.33 +/- 0.08
BY4741	0.66 +/- 0.55	1.21 +/- 0.52	0.47 +/- 0.38	-0.028 +/- 0.007	0.30 +/- 0.06

Table 3.1: Mobility Quantification of Sup35NM-GFP in wildtype strains. The mean rate of movement was determined by taking the distance moved per minute over approximately thirty minutes, for at least four individual early foci. The slope was determined by plotting a trendline of the movement over time (Fig. 3.3 and 3.4), calculating the slope, and averaging values from at least three early foci. The Mean Absolute Difference (MAD) was determined by taking the deviation of the distance moved per minute from the trendline at that particular time point. Individual deviations are averaged for each data set, and the average deviations from the multiple datasets provide the Mean Absolute Difference (Lyke et al., unpublished).

BY4741; Table 3.1), suggesting that aggregates experience variable rates of movement until their movement eventually slows.

Coalescence reflects the number of aggregates per cell, and the ability of early foci to merge together as a single focus indirectly. If coalescence occurs, there would be one aggregate per cell after 60 minutes. If coalescence does not occur, it would be expected that more aggregates would be observed after 60 minutes. While the majority of 74D-694 cells had one dot, line, or ring aggregate per cell, there was a large range in the number of aggregates in wildtype strain cells (Figure 3.5). 74D-694 ranged from 1 to 15 aggregates while BY4741 ranged from 1 to 6 aggregates. However, coalescence was not significantly different between strains, with a median number of aggregates of 1 for both. I also

investigated the distribution of aggregate phenotypes between the two genetic backgrounds. Previous work showed that 74D-694 cells can contain a single dot, multiple dots, a single line or ring, or multiple lines (Sharma et al., 2017). 74D-694 generally contained an equal distribution in all four possible aggregate pathways, however BY4741 favored cells that contained either single aggregates (Figure 3.6). It has been previously suggested that the number of protein aggregates per cell can be reflective of cellular age (Saarinkangas and Caudron., 2017; Ruan et al., 2018), so I investigated the age of the cell in relation to the number of protein aggregates.

During cell division the dividing cell forms a bud scar where the daughter was attached. A mother cell that has undergone several divisions will have more budscars than a new daughter cell, therefore the number of budscars represents the replicative age of the cell. In 74D-694 cells, more budscars corresponded to higher numbers of protein aggregates per cell, however BY4741 cells generally contained a low number of aggregates regardless of replicative age (Figure 3.7).

Given that older cells had more protein aggregates in 74D-694 cells, I investigated the role age may play on the formation of aggregates. In budding cells, the mother cell is chronologically older than the newly formed daughter, allowing a direct comparison of young and old cells by analyzing mother daughter pairs. 21 time-lapse recordings of Sup35NM-GFP formation in mother-daughter pairs of 74D-694 background was analyzed.

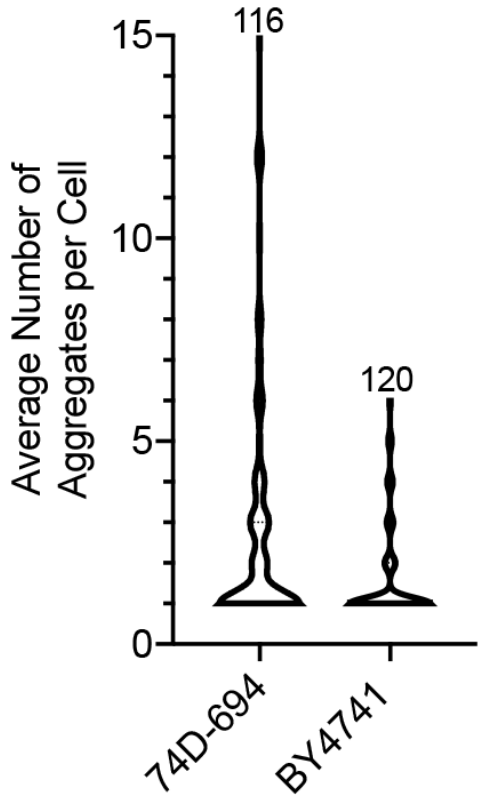

Figure 3.5: Coalescence of Sup35NM-GFP aggregates. Sup35NM-GFP was induced in cultures of either 74D-694 or BY4741 genetic background for 18-22 hours. Cells were imaged and the number of protein aggregates in each cell was quantified to assess coalescence with assistance by Abbey Kuborn. The average number of aggregates per cell is graphed. Moods Median T-Test revealed no significant difference between the two strains. Statistical analysis was performed by Dr. Steve Merrill.

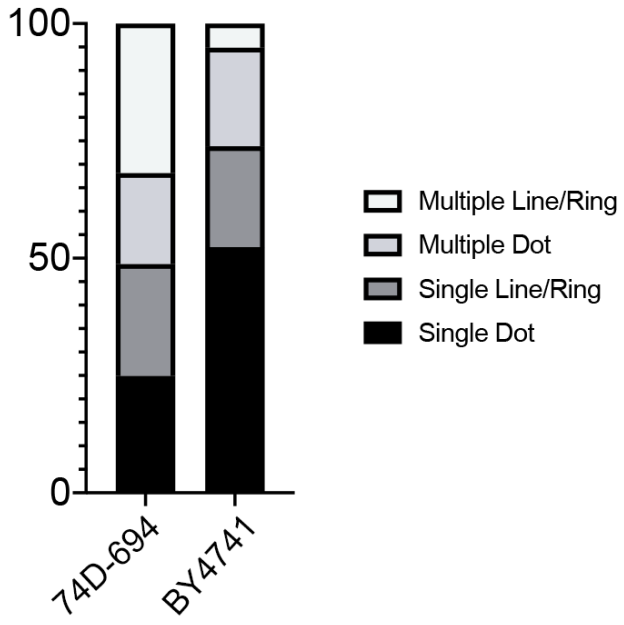

Figure 3.6: Distribution of Sup35NM-GFP Aggregates in cells between two genetic backgrounds. Sup35NM-GFP was induced for 18-22 hours in either 74D-694 or BY4741 and subsequently imaged. Cells were quantified based on the type of aggregate present in the cell with assistance by Abbey Kuborn. Over 200 cells were quantified for both genotypes.

The mother cell always contained a higher number of aggregates compared to the corresponding daughter (Figure 3.8A-C; Lyke and Manogaran, 2017). Interestingly, time-lapse observations of early foci were mobile and coalesced in daughter buds. However, early foci were mobile but generally lacked coalescence in the corresponding mother cell (Figure 3.8A-C). Mother daughter pairs were further analyzed in both 74D-694 and BY4741 backgrounds using snapshot microscopy for higher sample size comparison. Similar to budscar staining experiments, the BY4741 cells contained mostly single aggregates

regardless whether early foci were located in the mother cell or corresponding daughter bud, whereas 74D-694 mother cells had higher aggregate counts compared to corresponding daughters (Figure 3.8D). Taken together, the differences between 74D-694 and BY4741 in the number of aggregates corresponding to age suggests that both genetic background and age may play a role in the ability to coalesce early foci, while maintaining a single aggregate appears to be the preferred pathway by cells.

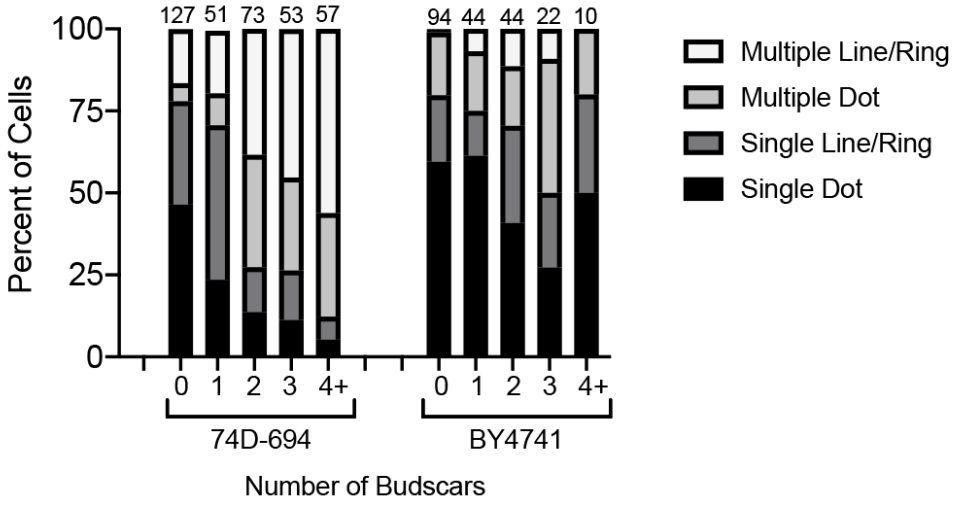

Figure 3.7: Aggregate Distribution by Budscar Number. Sup35NM-GFP was induced for 18-22 hours in either 74D-694 or BY4741 and subsequently stained with Calcafluor White for budscars. Cells were quantified based on the type of aggregate present in the cell and the number of budscars. The number of cells analyzed are shown above each bar. Abbey Kuborn assisted with quantification analysis.

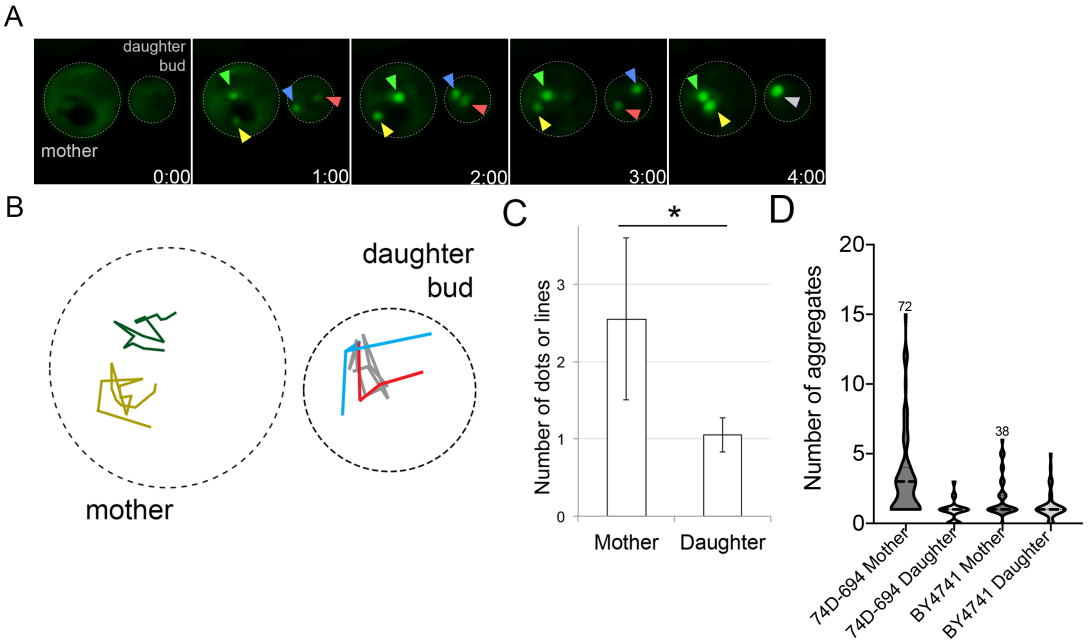

Figure 3.8: Mother cells contain more aggregates compared to corresponding daughter cells. A. Sup35NM-GFP was overexpressed for approximately 18 hours in 74D-694 cells. Diffuse cells were imaged using 3D time-lapse microscopy for an additional 12 hours. Representative images of an early foci appearing in both mother cell and daughter bud (01:00 minute) to their fusion in the daughter bud (04:00 minute) are shown. Yellow and green arrows point to the early foci in the mother cell, while red and blue arrows are in the daughter bud, turning grey when they merge. B. Early foci trajectories (from A) followed for 16 minutes are shown. The movement of each foci was tracked on a 2D plane, with colors corresponding to arrows in A in the mother (left cell) and daughter bud (right cell; Lyke and Manogaran, 2017). C. 20 time-lapse videos were analyzed for the number of aggregates in the mother cell and daughter bud present approximately 1 hour after the initial appearance of the early foci. The graph represents the average number of aggregates per cell, compared by T-test ($p<0.0001$). D. Sup35NM-GFP was overexpressed for approximately 18 hours in 74D-694 or BY4741 cells. Cells were imaged and the number of aggregates per cell was quantified only for cells that were currently dividing (mother cell with daughter bud still attached). The number of mother-daughter pairs analyzed is shown above each mother cell plot. Abbey Kuborn assisted in quantifying aggregates per cell in mother-daughter pairs.

The sequestration step (Step 2) can be quantified as the distance the aggregate is positioned from the cell periphery. To quantify the distance to the periphery, aggregate position was determined within the cell using a 3D coordinate mapping technique (see Chapter 2). This technique extrapolates the distance measured between Sup35NM-GFP aggregates and the edge of the cell. For both wildtype strains, the average distance from the cell periphery was 0.82 μm and 0.88μm for 74D-694 and BY4741 respectively (Figure 3.9), suggesting similar spatial localization of the aggregate. Taken together, these quantification techniques indicate that Sup35NM-GFP formation is mostly similar between two different wildtype backgrounds, albeit with the exception of aging effects.

3.3 Discussion

In this chapter I developed methods to quantify the formation of protein aggregates utilizing data generated from 3D time-lapse recordings. These quantifications allow comparison of the behavior of aggregates in two different genetic backgrounds. Regardless of genotype, the behavior of newly formed Sup35NM-GFP early foci mobility (Figure 3.3) and aggregate sequestration (Figure 3.9) appear to be very similar. The one caveat is the number of protein aggregates formed per cell, especially in aging cells (Figure 3.5-8). While BY4741 cells maintained a low number of dot-like aggregates regardless of age, 74D-694 showed a wide range of aggregate number and type in older cells. It is possible that the 74D-694 strain has weaker protein quality control mechanisms that result in poor management of aggregates especially as cells age

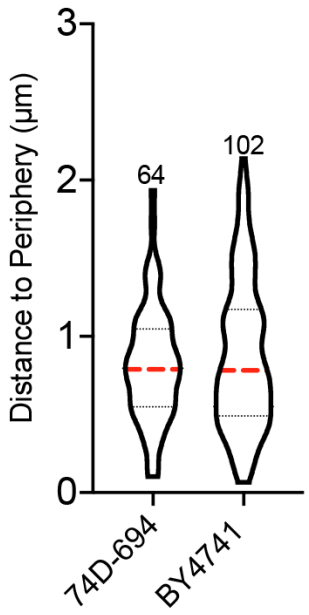

Figure 3.9: Sequestration of Sup35NM-GFP Aggregates. Sup35NM-GFP was overexpressed for 18 hours in 74D-694 and BY4741 cells. Cultures were imaged, and the distance between the aggregate and the periphery in each cell was measured by 3D coordinate mapping. The number of cells assessed are shown above each plot. Unpaired T-Test showed no significant differences between the two strains.

The dynamics of aggregate formation have never been previously characterized in this manner. Zhou et al. (2011) and Zhou et al. (2014) made general claims on the mobility of heat-induced aggregates through observations of time-laspe recordings. Liu et al. (2010) and Escusa-Toret et al. (2013) took similar observations one step further by quantifying the rate of movement, however the aggregates used were heat induced also. Recent work by Sharma et al. (2017) made the first observations of *de novo* Sup35NM-GFP formation using time-lapse microscopy, however the behavior of the aggregate was once again only characterized with generalizations. The work done in this chapter

goes beyond any aggregate behavior characterization previously performed. Innovative quantitative measures developed here allow combined with statistical analysis with the help of Dr. Steve Merrill at Marquette University, allows for a novel approach to characterize aggregate formation and behavior. These new tools can be leveraged to understand the biology of protein aggregate formation.

I observed that in both wildtype strains Sup35NM-GFP aggregates had similar, general formation behavior, starting with high mobility and most cells able to coalesce aggregates together, leading to peripheral sequestration of aggregates. However, using quantifiable methods I found that there were differences between the two strains. Aggregates in BY4741 cells slow down in mobility much quicker than aggregates in the 74D-694 genetic background (Table 3.1). 74D-694 also appear to have difficulty managing aggregates as cells age, with older cells containing multiple aggregates more often than in the BY4741 background (Figure 3.7). It is interesting that the differences between the two strains both occur during the first step in aggregate formation, suggesting that 74D-694 strain cells have trouble managing early foci. The first step of formation involved the movement and fusion of aggregates, which previous work suggests is associated with cellular trafficking mechanisms. Cells with disrupted cytoskeletal networks have an increased number of heat-induced aggregates (Specht et al., 2011), and have reduced observed mobility (Zhou et al., 2011). It is possible that older 74D-694 cells have reduced cytoskeletal networks resulting in poor management of the formation of protein aggregates. Differences, especially during aging, are common between different yeast genetic

backgrounds (Lippuner et al., 2014). Further work to understand the role of the cytoskeleton in protein aggregate formation may not only provide clues to differences observed between wildtype strains, but also begin to explain the mechanism of cellular response to protein aggregate formation.

Together, this chapter demonstrates that the formation of protein aggregates can now be quantified rather than simply observed. The quantification described is reliable, and consistent or Sup35NM-GFP formation in two different genetic backgrounds. The ability to quantify aggregate formation under wildtype conditions allows for a baseline to be set in quantification. This baseline can be used to compare the behavior of protein aggregates formed under different conditions to identify what cellular components are necessary for a normal response to aggregate formation. Understanding what is involved in the mechanism of cellular response could potentially lead to a better understanding of how protein aggregates eventually lead to cellular dysfunction and potential toxicity.

Chapter 4: Actin Plays a Role In Newly Formed Protein Aggregate Dynamics

4.1 Introduction

As described in Chapter 3, early foci are highly mobile upon initial appearance, but slow down over time to statically localize near the cell periphery. The consistency at which aggregates localize to the cell periphery suggests that mobility is not passive or by random diffusion, but rather due to a cellular trafficking mechanism that actively moves aggregates to a retention site. In yeast, protein and organelle trafficking is commonly associated with the actin cytoskeleton (Moseley and Goode, 2006). It is possible that newly formed protein aggregates are trafficked along actin network roadways to a distinct destination in the cell. However, if trafficking does not influence aggregate movement, then it is possible that the slow down is due to aggregate growth over time.

Previous studies have suggested that the movement of heat induced Hsp104p associated aggregates is associated with the actin cytoskeleton. Spatially, Hsp104p aggregates have been shown to localize to the actin network observed by phalloidin staining (Liu et al., 2010; Song et al., 2014). The mobility of stress induced aggregates is impaired when the actin network is disrupted by LatrunculinA (LatA) treatment, an pharmacological actin inhibitor (Zhou et al., 2011). Similar treatment of cells by LatA also results in an increase in the number of heat induced aggregates per cell (Specht et al., 2011), together supporting the role of actin in the formation of protein aggregates. Actin has also been shown to affect the segregation of Hsp104p aggregates between dividing cells. The folding

of actin monomers is impaired in the genetic disruption *sir2Δ*, and in this strain daughter cells have an increase in the number of aggregates they contain, suggesting that the actin network plays a role in managing protein aggregates to restrict inheritance in daughter cells (Liu et al., 2010; Song et al., 2014). These changes to the behavior of aggregates based on the actin network are not unique to stress induced aggregates however, as the human protein Optineuron displays similar effects. Optineuron (OPTN) is a trafficking protein in humans that has been shown to be aggregated in ALS patients. The OPTN protein also aggregates when expressed in yeast. Treatment of cells with LatA caused an increase in the number of OPTN aggregates (Kryndushkin et al., 2012). It is possible that the formation of many other newly formed protein aggregates, such as Sup35NM-GFP, are also depending upon the actin cytoskeleton.

The formation of Sup35NM-GFP aggregates has been shown to be dependent on factors that influence actin assembly. Disruptions associated with endocytosis and the cortical actin patch, such as *sla1Δ*, *sla2Δ*, and *las17Δ* reduce the number of cells that form Sup35NM-GFP aggregates (Ganusova et al., 2006; Manogaran et al., 2011). Similarly, pharmacological disruption and mutations in certain actin polymerizing genes inhibit the formation of oxidative stress induced Sup35NM-GFP aggregates (Speldewinde et al., 2017).

In this chapter, I investigate how the actin cytoskeleton influences the behavior of aggregate formation. Mutations to the *ACT1* gene, which encodes actin in yeast, are used to understand how the actin cytoskeleton alters aggregate behavior. This work supports previous literature and further suggests

a potential role for actin in protein aggregate formation, beginning to add more detail to the cellular response mechanisms.

4.2 Results

4.2.1 Aggregate localization with actin is unclear

Two previous studies indicated that Sup35NM-GFP aggregates colocalize with the actin stain, rhodamine-phalloidin (Ganusova et al., 2006; Speldewinde et al., 2017). However, these observations were made using snapshot microscopy in 2D. To quickly assess the association of actin with Sup35NM-GFP aggregates in cells by 3D microscopy, I investigated colocalization between newly formed aggregates and the actin network. While actin can be visualized by rhodamine-phalloidin stain, I found that the requirement to fix the cells altered the appearance of protein aggregates (Figure 4.1). Altering the appearance of protein aggregates raised questions as to the reliability of colocalization analysis under these conditions.

Therefore, I turned to 3D-live cell imaging techniques to observe the actin cytoskeleton. Actin patches are observed using Cof1-RFP, which is a protein that localizes to depolarizing actin patches (Lin et al., 2010), while actin cables are observed using Abp140-YFP, an actin binding protein (Asakura et al., 1998; Yang and Pon., 2002). Colocalization was quantified using Pearson's Correlation Coefficient (PCC). PCC quantifies the degree of overlap between two different fluorescent channels, with a score of 1 representing perfect colocalization and a score of 0 indicating a lack of overlap. PCC values for aggregates and the actin

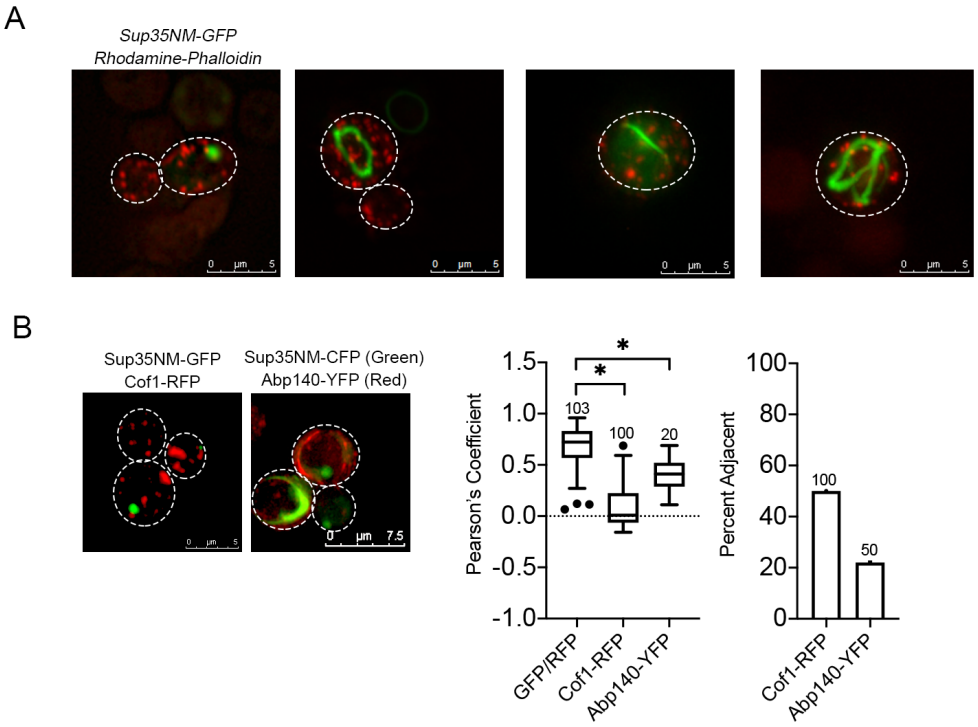

Figure 4.1: Sup35NM aggregate localization with the actin network is unclear. A. Sup35NM-GFP was induced in 74D-694 wildtype cells overnight. Cells were fixed in formaldehyde and stained with Rhodamine Phalloidin. Representative images are shown above. B. 74D-694 cells endogenously expressing Co1-RFP (actin patches) or Abp140-YFP (actin cables) had Sup35NM-GFP or Sup35NM-YFP induced respectively. Representative images are shown. Images were analyzed for co-localization by PCC (Left) and for adjacent localization (Right). A positive control was included in PCC for comparison by T-test analysis ($p < 0.01$).

network were compared to a positive control strain that contained Sup35NM-GFP and Sup35NM-RFP. Adjacent localization was also quantified for aggregates and actin. Structures are considered adjacent when localized within 500nm of each other. No overlap or consistent adjacent localization was observed between either actin structure with Sup35NM aggregates (Figure 4.1). Unfortunately, quantification was difficult to rely on as Cof1-RFP was highly dynamic, and

Abp140-YFP was commonly found throughout the cell, which made colocalization difficult to determine. Therefore, to determine whether actin is involved in the formation of Sup35NM-GFP aggregates, I had turned to assessing aggregate behavior in strains with disrupted actin cytoskeletons.

4.2.2 Mutations in Actin Reduce Sup35NM-GFP Early Foci Mobility

Actin in yeast is encoded by the *ACT1* gene. Deletion of *ACT1* is lethal, but there are many point mutations which are temperature sensitive. Amino acid substitutions of the *ACT1* gene were originally engineered by Wertman et al. (1992) in the BY4741 background. *act1-122* (D80A, D81A) and *act1-120* (E99A, E100A) contain substitutions in or near the Sac6p binding site, the yeast homolog of the fimbrin actin bundling protein (Figure 4.2; Wertman et al., 1992). These mutants show depolarized actin patches, reduced actin cables, and grow normally at permissive temperatures (Wertman et al., 1992; Drubin et al., 1993; Miller et al, 1996; Dorweiler et al., in revision). *act1-101* (D363A, D364A) partially disrupts actin cables, but has no effect on actin patches (Wertman et al., 1992; Drubin et al., 1993; Miller et al, 1996; Dorweiler et al., in revision).

The formation of Sup35NM-GFP aggregates was recorded with 3D time-lapse microscopy in each of the three actin mutant strains and a BY4741 wildtype strain. Each strain contained High [*PIN*$^+$], except *act1-122,* which was µd, which was previously shown to induced [*PSI*$^+$] similar to High [*PIN*$^+$] wildtype strains (Dorweiler et al., in revision). The average rate of movement for both

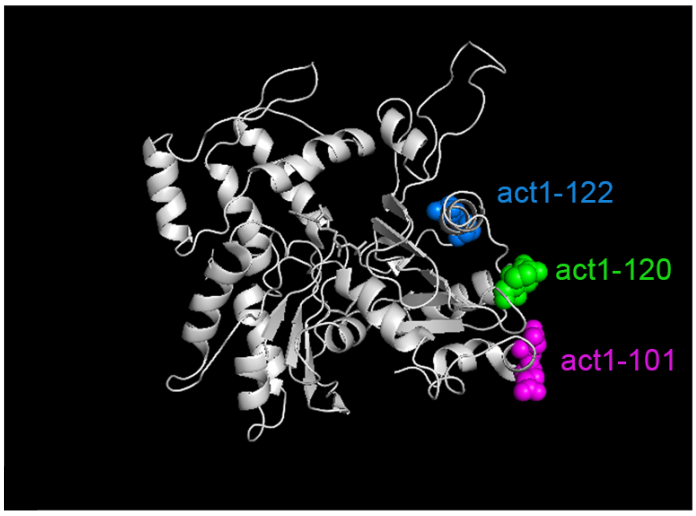

Figure 4.2: The Structure of the Actin Protein. Rendering of an actin monomer is shown with the three point mutant sites designated. The model was created using the Pymol Program with the help of Dr. Jane Dorweiler from the Manogaran Lab.

act1-122 and *act1-120* (0.29μm/min and 0.27μm/min respectively) was significantly reduced compared to the wildtype (0.66μm/min; Figure 4.3). As expected the slopes of the aggregate mobility were also much less negative for *act1-122* and *act1-120* compared to either the wildtype or *act1-101* strains (Figure 4.4). Both of these mutant strains also had the majority of aggregate movements of extremely short distances, which once again was much different than the wildtype and *act1-101* strains (Figure 4.4). Given the difference, I investigated whether mobility was different within the first 10 minutes of appearance when early foci have the highest rate of movement and between 20 and 30 minutes (as done in Table 3.1).

During the first ten minutes of quantification, the average rate of movement for wildtype was 1.2μm/min, while in *act1-122* and *act1-120* the rate

was 0.37μm/min and 0.41μm/min respectively (Table 4.1). In the third ten minute interval (starting 20 minutes after formation), the average rate of movement for wildtype was 0.47μm/min, and in the *act1-122* and *act1-120* mutants 0.29μm/min and 0.19μm/min respectively (Table 4.1). The rates for *act1-122* and *act1-120* suggests that although aggregates appear to slow down in movement over time, aggregates in the *act1-122* and *act1-120* mutants are always slower than the

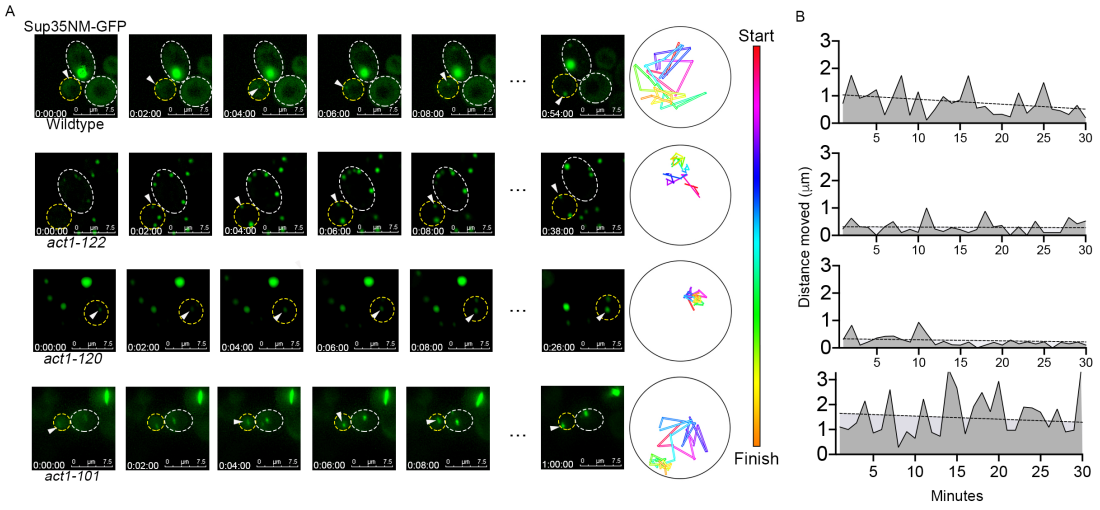

Figure 4.3: Sup35NM-GFP Mobility is reduced in actin mutant strains. A. Sup35NM-GFP was induced in High [*PIN*$^+$] versions of BY4741 wildtype, *act1-120*, *act1-101,* and μd [*PIN*$^+$] BY4741 *act1-122* cells. Strains were imaged in 3D-timelapse with representative images from a single timelapse shown. Aggregates marked with the white caret in the yellow outlined cell were tracked for mobility and a representative particle trace is shown to the right of the images. B The distance moved per minute was graphed for the aggregate shown in A, including the linear trend. Table 4.1 provides statistical analysis of this data.

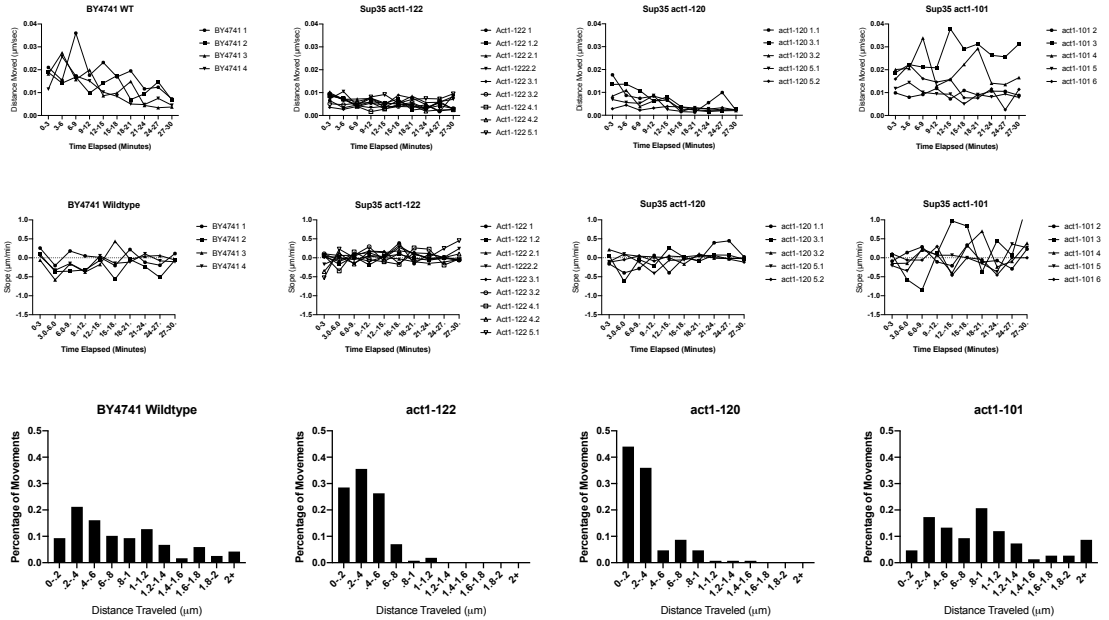

Figure 4.4: Mobility Comparison in Wildtype and actin mutants. Sup35NM-GFP was induced in High [*PIN*$^+$] BY4741 wildtype, *act1-120*, *act1-101,* and μd [*PIN*$^+$] BY4741 *act1-122* cells. Cultures were then imaged by long-term 3D timelapse microscopy (see Chapter 2) for the initial appearance of a protein aggregate. Movement of the early foci was tracked using 3D coordinate mapping. Aggregates from four individual cells of each genetic background were quantified and the rate of movement for each is shown above. Top: Aggregate mobility is shown in three minute increments from initial formation. Middle: The slope of mobility per three minute increment is shown. Bottom: The number of events that moved a particular distance during recordings is shown.

	Mean Overall rate Rate (μm/min)	Mean Rate in first 10 minutes	Mean Rate in third 10 minutes	Mean Slope	Mean MAD
Wildtype	0.66 +/- 0.5	1.2 +/- 0.52	0.47 +/- 0.38	-0.028 +/- 0.007	0.30 +/- 0.06
act1-122	0.29 +/- 0. 2*	0.37 +/- 0.19*	0.29 +/- 0.21	-0.003 +/- 0.004*	0.16 +/- 0.03*
act1-120	0.27 +/- 0.3*	0.41 +/- 0.32*	0.19 +/- 0.10	-0.010 +/- 0.008*	0.15 +/- 0.06*
act1-101	0.92 +/- 0.6*	1.01 +/- 0.57	0.81 +/- 0.69*	-0.015 +/- 0.015	0.39 +/- 0.16*

Table 4.1: Slope and Mean Absolute Difference (MAD) values of Aggregate Mobility. Mann-Whitney Test was used to compare values between actin mutants and wildtype. Analysis revealed *act1-122* and *act1-120* had slower mobility overall and during the first 10 minutes of formation, as well as slopes significantly less negative than wildtype. *act1-101* differed in overall rate and during the third 10 minute interval, and while not different in slope from widltype, *act1-101* also displayed a higher amount of variability within samples of rate of movement compared to wildtype (* $p < 0.01$).

wildtype. The consistent slower mobility in actin mutants is reflected by the slope of the trendline in *act1-122* and *act1-120* being closer to 0 when compared to the negative slope observed in wildtype (Table 4.1). The variability of mobility, as quantified by MAD values, was also much lower in *act1-122* and *act1-120* (Figure 4.4, Table 4.1). The reduced MAD values and negligible slope in *act1-122* and *act1-120* suggest that the mobility of aggregates is consistently very low for the duration of formation. Together, aggregates in *act1-122* and *act1-120* are nearly immobile, appearing and being retained at the same site as initial formation.

In contrast, average early foci mobility was slightly higher in *act1-101* strains (0.921μm/min) compared to wildtype. The increase in average rate can be attributed to aggregates maintaining higher rates of mobility longer in *act1-101* compared to the wildtype, as the rate of movement does not drop as sharply in

the actin mutant between the first ten minutes of appearance to the third ten minutes (1.01μm/min and 0.81μm/min respectively; Table 4.1). While the slope of the *act1-101* mobility trendline was negative, *act1-101* MAD values were higher than wildtype. The negative slope indicates that the overall aggregate mobility is decreasing over time, however the high MAD values suggest that there is more variability in the rate of movement compared to wildtype. These data suggest that mobility is altered differently in the *act1-101* mutant compared to the *act1-122* and *act1-120* mutants.

4.2.3 Actin Mutants Have a Reduced Number of Sup35NM-GFP Aggregates

The number of protein aggregates per cell was also affected by disruptions to actin. *act1-122* and *act1-120* cells contained a median of 2 aggregates per cell, while both wildtype and *act1-101* cells contained 1 aggregate per cell (Figure 4.5). It should be noted that while increased aggregate number may indicate reduced coalescence, it is also possible that actin mutants lead to the formation of more early foci per cell than wildtype strains resulting in more aggregates regardless of coalescence activity. *act1-122* and *act1-120* contain substitutions within the Sac6p binding domain. It is possible that the bundling activity of actin influences aggregate number. Therefore, we looked at a *sac6Δ* generated in the 74D-694 genetic background. Similar to *act1-122 and act1-120* mutants, *sac6Δ* mutants also have depolarized actin patches (Karpova et al., 1998). Compared to a wildtype 74D-694 strain, *sac6Δ* was not significantly different (Figure 4.5). These data suggest that Sac6p mediated actin bundling

does not influence coalescence or aggregate number in the 74D-694 genetic background. The similarity between wildtype and *sac6Δ* strains could be due to the intrinsically high number of aggregates found in the 74D-694 genetic background that could buffer out any observable effects of the genetic mutant.

4.2.4 Disruption to Actin Increases Aggregate Number In Older Cells

Previously, I observed that wildtype BY4741 strain cells typically contained a low number of protein aggregates regardless of age (Chapter 3). Wildtype cells in the 74D-694 background however, had increased numbers of Sup35NM-GFP aggregates in older cells (Chapter 3, Figure 3.7). Given that in actin mutant strains (BY4741 background) I observed an increase in the number of protein aggregates, I tested whether the increase in aggregates corresponded to the age of the cell, similar to that of 74D-694 wildtype cells.

Wildtype and actin mutants were stained with budscars similar to figure 3.7, and the number of aggregates and budscars for each cell was quantified. Both *act1-122* and *act1-120* showed a population of cells that had increased aggregate numbers compared to any population seen in wildtype or *act-101* (Figure 4.6). Interestingly, the population of cells with a high number of aggregates corresponded to cells containing higher numbers of budscars (Figure 4.6). The number of aggregates found in actin mutants by age is reminiscent of wildtype 74D-694 strains (Figure 3.7), suggesting that differences between the 74D-694 BY4741 strains may have to do with the actin cytoskeleton.

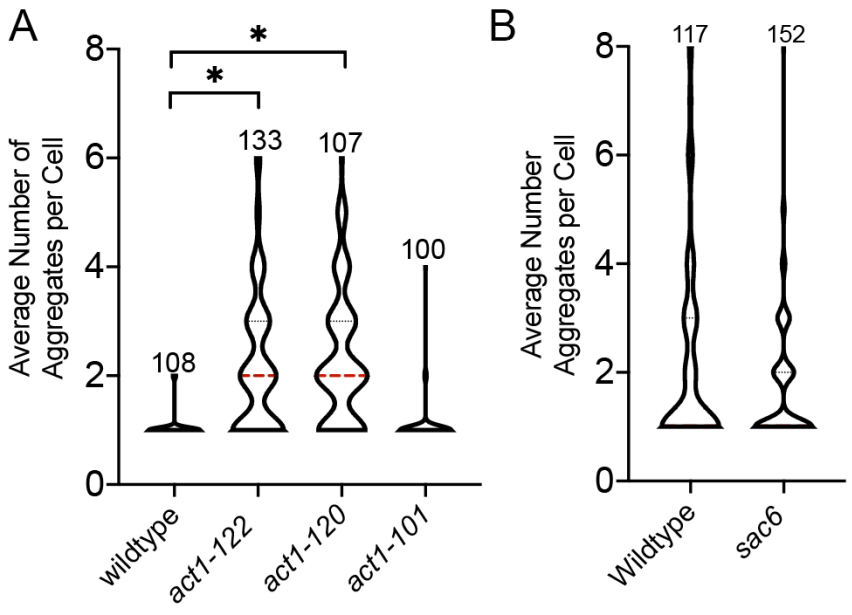

Figure 4.5: Disruption of Actin Alters Coalescence of Newly Formed Sup35NM-GFP Aggregates. A. Sup35NM-GFP was induced in BY4741 wildtype, *act1-120*, *act1-101,* and *act1-122* cells. The average number of protein aggregates was quantified per cell in each strain from still shot microscopy, and is represented in the graph. Aggregate number was compared to the wildtype value using T-test analysis, finding *act1-122* and *act1-120* significantly different. B. Sup35NM-GFP was induced in *sac6*Δ 74D-694 cells. The number of aggregates per cell was quantified, and compared to a wildtype control by T-test analysis. (* $p<0.001$).

4.2.5 Peripheral localization of Sup35NM-GFP aggregates is changed in the presence of actin mutants and actin inhibiting drugs

Next, I investigated whether peripheral localization is affected in the actin mutants discussed above. *act1-122* and *act1-120* mutants showed significantly different peripheral localization profiles compared to wildtype. While the average distance of the aggregate from the cell periphery was 0.88μm in wildtype strains, aggregates were 1.20μm and 1.07μm from the periphery in *act1-122 and act1-*

120 mutants, respectively (Figure 4.7). The peripheral localization of aggregates in both actin mutants is statistically different than wildtype strains. Not all actin mutants impact peripheral localization because aggregates were located approximately 0.89μm in *act1-101* mutants, which is similar to wildtype. Next I asked whether *sac6Δ* mutants, which have depolarized actin patches and are associated with actin bundling, have altered sequestration. Aggregates are found to be on average further from the cell periphery than its isogenic wildtype (Figure 4.7). This data suggests that actin networks influence aggregate sequestration, and possibly it is the Sac6p mediated bundling of actin and/or actin patches that influence aggregate localization.

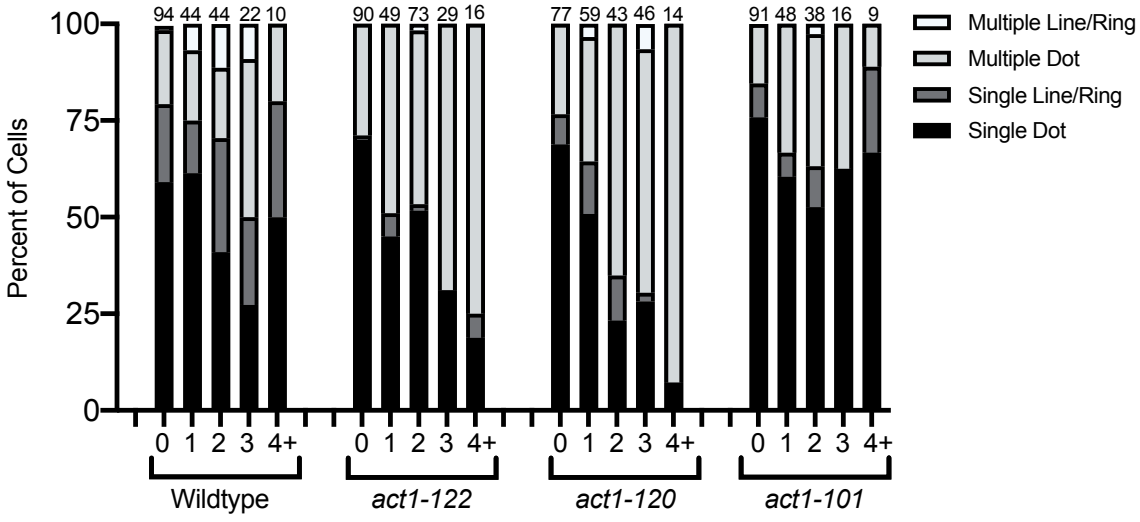

Figure 4.6: Aggregate Distribution by Budscar Age in Actin Mutant Strains. Sup35NM-GFP was induced for 18-22 hours in wildtype BY4741, *act1-122*, *act1-120*, and *act1-101*, and subsequently stained with Calcafluor White for budscars. Cells were quantified based on the type of aggregate present in the cell and the number of budscars. The overall column is the sum of all of the data. Abbey Kuborn assisted with data analysis.

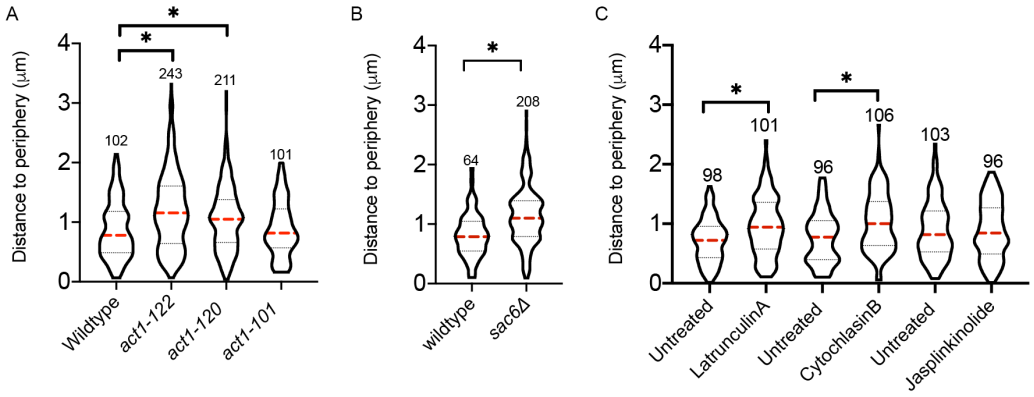

Figure 4.7: Sequestration of Sup35NM-GFP aggregates is altered by disruptions to the actin cytoskeleton. A. Sup35NM-GFP was induced in BY4741 wildtype, *act1-122*, *act1-120*, and *act1-101*. 3D-coordinate mapping was used to quantify distance to the periphery of aggregates in each strain. *act1-122* and *act1-120* were significantly different from wildtype by T-test analysis, while *act1-101* was not. B. Sup35NM-GFP was induced in 74D-694 Wildtype and *sac6Δ*. The localization of protein aggregates was quantified in both strains and analyzed as done in A. C. Sup35NM-GFP was induced in wildtype BY4741 cells and treated with Latrunculin-A, CytochlasinB, Jasplinkinolide, or paired ethanol controls for at least thirty minutes prior to imaging. Protein aggregate localization was quantified after treatment using coordinate mapping. Individual treatments were compared using T-test to their corresponding paired control (ethanol treated). Latrunculin-A and CytochlasinB were significantly different from their corresponding control samples. (* $p<0.01$).

Next, I asked whether peripheral localization of aggregates could be disrupted by transient inhibition of actin by pharmacological agents. Sup35NM-GFP aggregates were allowed to form in wildtype (untreated) cells. Cultures were then treated briefly with actin inhibitors. LatrunculinA (LatA) and CytochlasinB (CytoB) inhibit F-actin polymerization by capping the plus end of actin fibers preventing monomer addition, resulting in a near abolishment of actin cables and actin patches (Ayscough et al., 2000; Yang and Pon., 2002; Kopecka et al., 2015; Macklean-Fletcher and Pollard.,1980). Jasplinkinolide (Jasp.) stabilizes

actin patches and cables by preventing the removal of actin monomers for the minus end of actin fibers (Ayscough et al., 2000). This transient inhibition of the actin cytoskeleton allows Sup35NM-GFP aggregates to form and localize to the periphery of the cell as usual, and then observe localization after disruption. If introduction of an actin inhibitor changes peripheral localization, then it is possible that the actin networks influence the ability to keep Sup35NM-GFP tethered at a specific location. Treatment with LatA or CytoB changed the average localization of aggregates to 0.96μm and 1.03μm respectively, a significantly different distribution compared to their paired untreated controls (0.72μm and 0.77μm respectively, Figure 4.7). Meanwhile, treatment with the actin stabilizing drug Jasp. did not change distribution compared to it's paired control, both having an average localization at 0.89μm. Since disrupting the actin cytoskeleton after aggregates have been sequestered to the periphery results in a change in localization, this suggests that aggregates maintain an association to actin even after mobility is reduced. Actin, both bundled cables and patches, may play a role in holding protein aggregates at a specific, peripheral site in the cell.

4.3 Discussion

Here, I have shown that the formation of Sup35NM-GFP aggregates is impacted by disruption of the actin cytoskeleton. Specifically, *act1-122* and *act1-120* mutants, which disrupt actin patch polarization and actin cable presence, reduced mobility, coalescence, and sequestration of newly formed aggregates. This work provides evidence that the behavior of newly formed aggregates may

not be completely random, but actually involve a universal mechanism of response by the cell.

While there are likely many factors involved in the formation of newly formed aggregates, here I show that the actin cytoskeleton is a major player in the movement of early foci into a single, peripheral inclusion. The rate of movement of early foci in *act1-122* or *act1-120* strain cells was severely impaired, with foci seemingly remaining in the same spot as their initial formation took place (Figure 4.3, 4.4). The lack of mobility presumably also decreased the ability of early foci to merge together, resulting in more aggregates per cell that were localized inconsistently in the cell (Figure 4.5, 4.7). The effect of actin on mobility and the number of aggregates per cell is similar to the results obtained using stress induced aggregates previously. As described above, stress induced aggregates both localize with the actin cytoskeleton, but have mobility impaired by LatA disruption (Liu et al., 2010; Zhou et al., 2011; Song et al., 2014). While actin is made up of both patches and cables, it is unclear whether they serve different functions in aggregate formation. *sac6Δ* is known to alter actin patch polarization (Young et al., 2004), and while the strain exhibits normal coalescence, sequestration is altered (Figure 4.5. 4.7). However, sequestration is also impaired by the disruption of actin cables pharmacologically (Figure 4.7). Therefore, it seems as thought the role of actin cables and patches in the formation of protein aggregate is much more complex then cables being used in step 1 and patches for step 2 of formation.

This is the first study to investigate newly formed Sup35NM-GFP aggregate mobility and coalescence, and the role of the actin cytoskeleton. However, a possible interaction between the actin cytoskeleton and Sup35NM-GFP aggregates has been proposed previously. Ganusova et al. (2006) found that disruption of cortical actin patch proteins resulted in a decrease in the formation of Sup35NM-GFP aggregates, suggesting that there is a link between the formation of aggregates and the actin cytoskeleton. In support of actin having a role in aggregate formation, mutations to a protein called Lsb2, which binds to an actin patch protein, that impair the ability of Lsb2p to bind to actin patches reduces the formation of Sup35NM-GFP aggregates (Chernova et al., 2011). Furthermore, treatment of cells with LatA or in *abp1Δ* strains, an actin nucleation protein, Sup35NM-GFP aggregate formation is also reduced (Speldewinde et al., 2017), adding to the idea that an intact actin cytoskeleton contributes to aggregate formation. It is possible that in these previous studies, Sup35NM-GFP forms aggregates that are not visible microscopically, but could potentially be biochemically as I observed in Chapter 3, Figure 3.1. Together with my work, it could be suggested that the actin cytoskeleton is needed to promote the fusion of early foci together by the associated trafficking mechanism to form a single, large observable aggregate that is much easier for the cell to manage rather than multiple aggregates.

Interestingly, not all actin mutants caused similar behavior of newly formed aggregates. The *act1-101* mutant acted mostly like wildtype, although this mutant displayed higher mobility that slowly declined through recordings. It was

expected that the shortened actin cables in the *act1-101* mutant (Tang et al., 2000) would result in limited mobility, but my data suggests just the opposite. It is possible that early foci are moved along shortened cables but reach the end quickly, resulting in a short period that resulting the aggregate must re-associate with another actin cable. The increased association and dissociation from actin cables may reflect the large variability in mobility that is observed in MAD values, and may explain why aggregates are mobile for a longer period of time as it simply takes longer for aggregates to reach their destination. However, eventually aggregates do reach a peripheral destination, allowing for the negative slope of movement observed.

It is unclear how actin plays a role in the sequestration of newly formed aggregates. In actin mutants, Sup35NM-GFP aggregates have a wide distribution of peripheral localization compared to wildtype cells. However, this distribution in wildtype cells can be disrupted by adding pharmacological inhibitors of actin, becoming more reflective of the sequestration in genetic mutants. This change in localization suggests that the actin cytoskeleton possibly had a role in tethering the aggregate to a specific location, and transient treatment of actin drugs mildly released the aggregate to change localization. On the other hand, drug treatment could release the aggregate, yet due to molecular crowding, the aggregate moves drifts to any space that is available. It is possible aggregates maintain association with the actin cables or patches, after sequestration. This association may function to tether protein aggregates to a single site in the cell or as part of a peripheral protein deposit. Whether

aggregates directly interact with the actin cytoskeleton for sequestration should be further explored to fully understand the role of actin in the cellular response to newly formed aggregates.

The actin cytoskeleton is not only involved in the formation of protein aggregates, but it also appears to play a role in aging. As described previously, *sir2Δ* strains that are used to model premature aging in yeast with misfolded actin have issues with asymmetric inheritance of Hsp104p associated aggregates (Erjavec et al., 2007; Liu et al., 2010; Song et al, 2014). Disruption of actin by LatA has also been observed to decrease the asymmetric inheritance of stress induced aggregates (Zhou et al., 2011). In my study, in the BY4741 wildtype cells, regardless of age cells maintain about 1 aggregate per cell. However, in the *act1-122* or *act1-120* cells while young cells maintain a single aggregate, older cells have multiple (Figure 4.5). The increased number of aggregates in the older actin mutant population is similar to 74D-694 wildtype cells observed previously (Chapter 3). However, previous literature would suggest the opposite effect, that both older and younger cells should have multiple aggregates when actin is disrupted. It is possible that in actin mutants while the ability to traffic aggregates may be lost, the mechanism for asymmetric inheritance is still partially intact to prevent transmission of aggregates into daughter cells. The Sir2p is most likely still functional in our actin mutants, therefore although actin is disrupted Sir2p may still be able to provide enough function to allow for asymmetric inheritance. However, given the weak actin cytoskeleton, older cells continue to have decreased protein quality control

mechanisms and are less efficient at managing the formation of protein aggregates, resulting in the increase of aggregates observed in older, actin mutant cells or 74D-694 wildtype cells, compared to BY4741 strains.

Overall, here I have shown that the actin cytoskeleton plays an important role in the cellular mechanism of response to the formation of protein aggregates. Further work will identify how actin plays this role, such as whether there is a direct interaction between actin and the aggregate, and what other factors could be involved. Given the movement of newly formed protein aggregates, one possibility to explore is the role of actin in cell trafficking. Organelles, vesicles, and other cellular components are trafficked in the cell by motor proteins along the actin cytoskeleton, a mechanism that could similarly be used for the movement of protein aggregates. Further study to understand the role of the actin cytoskeleton in responding to protein aggregate formation may uncover more details of the mechanism by which aggregates can lead to age associated diseases with the potential to identify new therapeutic targets that would prevent or reduce disease symptoms.

Chapter 5: Early Foci Dynamics Require Myo2p.

5.1 Introduction

The goal of this chapter is to determine whether Myo2p has a role in the early formation of protein aggregates. The work done in Chapter 3 established quantifiable measures to characterize *de novo* formation of Sup35NM-GFP aggregates, and this quantification was used to identify a role of the actin cytoskeleton (Chapter 4). However, although actin may directly affect the dynamics of aggregate formation, it is unclear how protein aggregates may be interacting with the cytoskeleton. Recent work has lead to this investigation of the myosin motor protein Myo2p as a potential link between the actin cytoskeleton and protein aggregate.

Myosin motor proteins travel along the actin cytoskeleton moving cargo, such as proteins and organelles, and this movement may provide the mobility of protein aggregates observed. In yeast there are five different known myosin proteins. Myo3p and Myo5p function as part of endocytosis machinery, and Myo1p plays a role in cytokinesis during cell division (Brown., 1997). Meanwhile, Myo2p and Myo4p are both Class V Myosin's that play a role in the transport of cellular components. The role of Myo4p is limited as it does not contain many of the tail regions required to bind cargo, and is mainly responsible for transporting mRNA during cell division through the aid of myosin binding proteins (Brown., 1997; Mermall et al., 1998; Schott et al., 1999). Myo2p however, is responsible for transporting a variety of cellular components such as organelles and vesicles along the actin network (Matsui., 2003; Pruyne et al., 2004; Weisman., 2006;

Fagarasanu et al., 2010). Myo2p is made up of three domains: a motor domain, a coiled coil domain, and a tail domain. The motor domain uses ATP hydrolysis to drive motility function along the actin network while the coiled coil domain allows interaction for Myo2p monomers to bind together as a dimer. The tail domain contains a globular head, which allows interaction with a diverse range of cargo (Cheney et al., 1993). The diverse role of Myo2p makes it a candidate for potentially trafficking protein aggregates in the cell.

Previous work suggests that Myo2p could be the motor protein that is trafficking protein aggregates along the actin network. Point mutations in actin that disrupt the ability of Myo2p to interact with the cytoskeleton causes reduced asymmetric inheritance of heat induced aggregates (Liu et al., 2010), allowing more aggregates to be inherited by daughter cells during division; the change in inheritance suggests that the interaction between Myo2p and actin is necessary for aggregate retention. Mutations to the globular head of Myo2p that disrupt vacuole cargo binding similarly reduce asymmetric inheritance of stress induced aggregates (Bockler et al, 2017). Although Hsp104p heat induced aggregates have been shown to localize with Myo2p (Song et al., 2014), interaction between the aggregate and Myo2p may not be direct. Disruption of either Vac17p or Vac8p, which have both been shown to interact with Myo2p and facilitate vacuole cargo binding, results in a decrease in Hsp104p aggregate asymmetric inheritance, suggesting that an intermediate protein such as Vac17p facilitates interaction. Meanwhile, recent work with pre-existing Sup35NM-GFP aggregates in [*PSI*$^{+}$] cells showed that when Myo2p is depleted from the cell, through an

auxin-inducible degron system, the number of aggregates per cell increases (Kumar et al., 2016). This same lab later showed that deletion of Vps1p, not Vac17p, causes a similar increase in Sup35NM-GFP aggregates as depletion of Myo2p (Kumar et al., 2017). Despite the support in the literature for the influence of Myo2p trafficking along the actin cytoskeleton on protein aggregate mobility, the role of Myo2p in Sup35NM-GFP *de novo* formation has not been addressed. Therefore, I investigated whether disruption to Myo2p affects early foci dynamics.

In this chapter, I used several genetic mutants that disrupt the function of Myo2p to investigate whether the motor protein has a role in the dynamics of protein aggregate formation. Using the same quantification methods discussed previously (Chapter 3 and 4), Myo2p influences step 1, but not step 2 of early foci dynamics. This study begins to shed light onto the mechanism of cellular response to protein aggregate formation.

5.2 Results

5.2.1 *myo2-2* mutant strain reduces newly formed aggregate mobility

Myo2p is essential for viability, localizes cargo to the bud tip, and is involved in organelle movement. A point mutation within the globular tail of Myo2p (*myo2-2,* G1248D; Catlett and Weismann, 1998) leads to defective cargo localization and mislocalization of Myo2p, while maintaining essential function (Catlett and Weismann, 1998; Catlett et al., 2000). Early foci mobility was significantly reduced overall in *myo2-2* mutants (0.33μm/min) compared to the isogenic wildtype strain (0.99μm/min; Figure 5.1). Similar to Chapter 4, given the

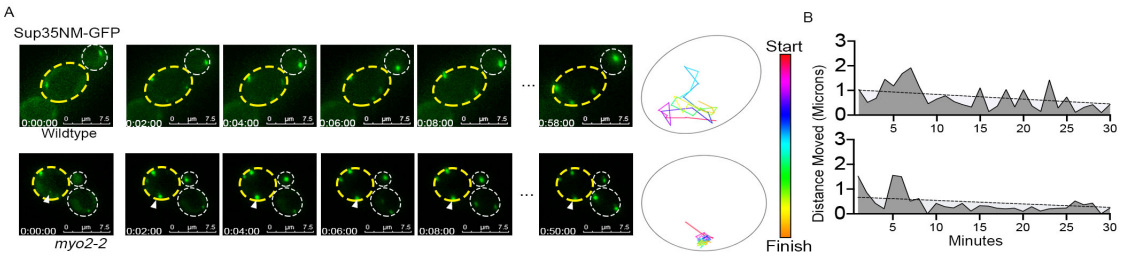

Figure 5.1: myo2-2 mutant displays reduced *de novo* Sup35NM-GFP mobility. A. Sup35NM-GFP was induced in High [*PIN*$^{+}$] wildtype and *myo2-2* strains (Catlett et al. 1998). Strains were imaged in 3D-timelapse with representative images from a single timelapse shown. A particle trace of the white caret marked aggregate in the yellow outlined cell is shown. B. The rate of movement was quantified in individual timelapse recordings using 3D-coordinate mapping, and a representative graph is shown next to each. On each graph a linear trend is displayed as the dashed line.

difference between wildtype and the *myo2-2* strain, both the slope of aggregate mobility and the distance moved was also significantly different between strains (Figure 5.2). I investigated the average rate of movement both during the first 10 minutes of formation and then the third ten minutes. During the first ten minutes of formation, the wildtype strain mobility averaged 1.4μm/min while *myo2-2* was at 0.57μm/min. During the third 10 minute interval, the wildtype strain average mobility was 0.91μm/min and the *myo2-2* mutant was 0.25μm/min (Table 5.1). The low rate of mobility in *myo2-2* mutants was consistent, as the slope for a trendline in multiple trials was nearly zero, and the MAD values were low as well indicating that sample rates did not vary much from the trendline. This is in contrast to isogenic wildtype cells that exhibited a negative slope with large MAD

values indicating that the rate of movement varied throughout formation from a linear trend (Table 5.1). Together, *myo2-2* mutants exhibit a low rate of mobility that does not change or vary throughout formation. These results are reminiscent of observations associated with *act1-120 and act1-122* (Chapter 4, Figure 4.2 and 4.3), indicating that movement behavior is similarly altered in Myo2p and Act1p mutations compared to wildtype strains.

5.2.2 Coalescence of newly formed aggregates is decreased in *myo2-2*

Coalescence of newly formed aggregates also differed in the myo2-2 mutant compared to wildtype. The median number of aggregates per cell in the *myo2-2* mutant was significantly higher (2 aggregates/cell) compared to wildtype (1 aggregates/cell; Figure 5.3). Taken together, these results suggest that either more aggregates form in *myo2-2* cells or aggregates are unable to coalesce like wildtype strains.

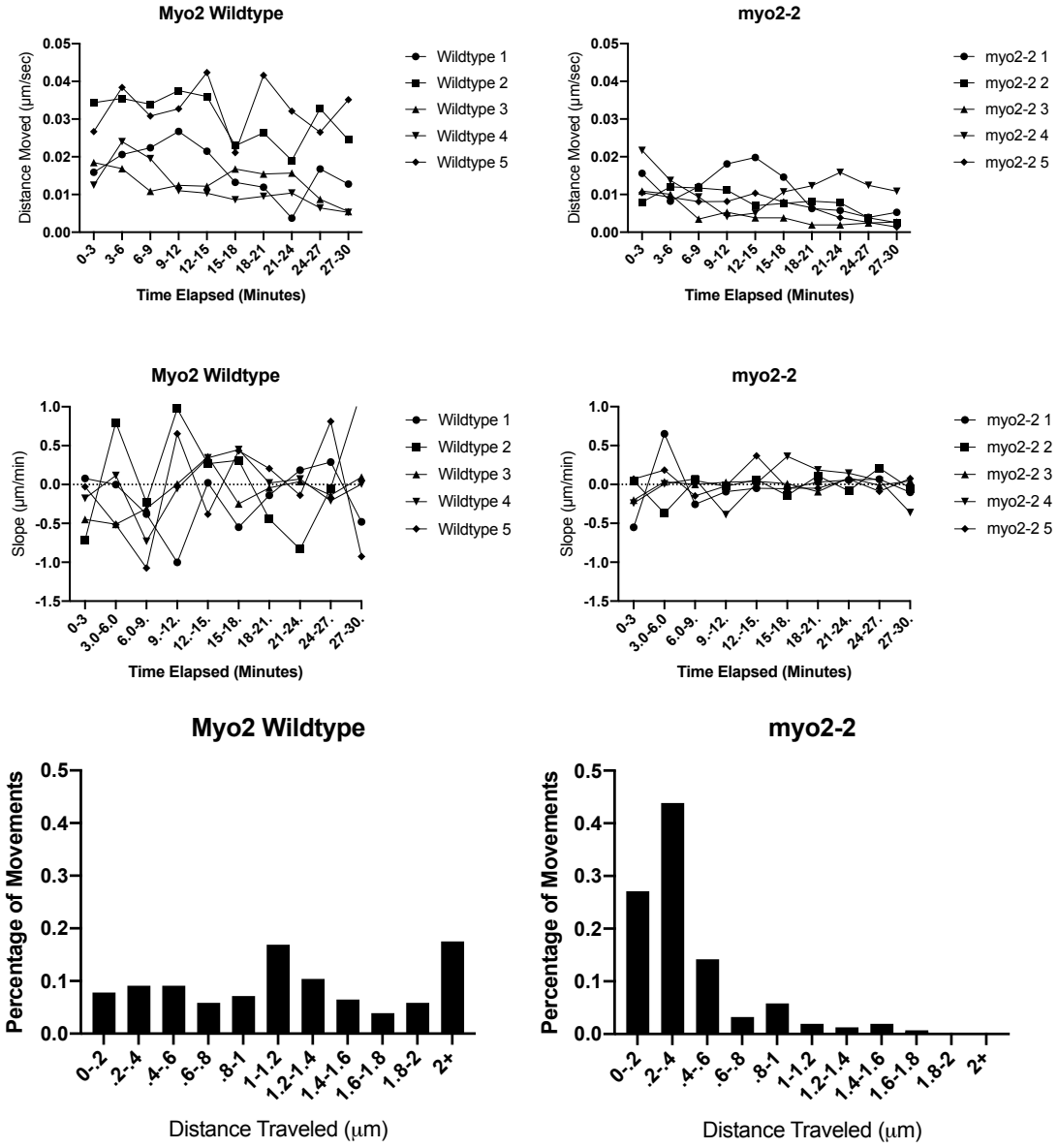

Figure 5.2: Mobility Comparison of Wildtype and *myo2-2*. Sup35NM-GFP was induced for 16 hours in Wildtype and *myo2-2* cells. Cultures were then imaged by long-term 3D timelapse microscopy (see Chapter 2) for the initial appearance of a protein aggregate. Movement of the early foci was tracked using 3D coordinate mapping. Aggregates from five individual cells of each genetic background were quantified. Top: The mobility of each aggregate per three minutes of recording. Middle: Slope of aggregate movement over three minute intervals during formation. Bottom: The number of events during formation separated by the distance moved for each minute recorded.

	Mean Overall rate Rate (µm/min)	Mean Rate in first 10 minutes	Mean Rate in third 10 minutes	Mean Slope	Mean MAD
Wildtype	0.99 +/- 0.8	1.43 +/- 0.74	0.91 +/- 0.73	-0.052 +/- 0.08	0.49 +/- 0.21
myo2-2	0.33 +/- 0.3*	0.57 +/- 0.45*	0.25 +/- 0.19*	-0.01 +/- 0.01*	0.20 +/- 0.05*

Table 5.1: Slope and Mean Absolute Difference (MAD) values of Aggregate Mobility. Statistical significance performed using Mann-Whitney Test (* $p < 0.01$).

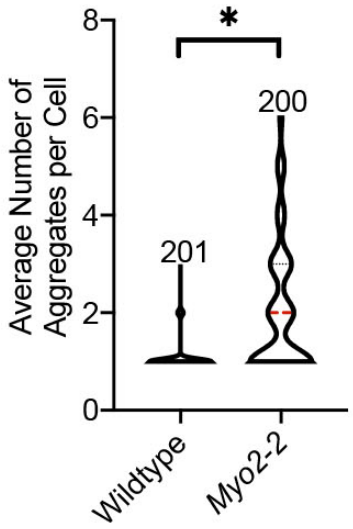

Figure 5.3: *myo2-2* increases the number of protein aggregates per cell. Sup35NM-GFP was induced in High [*PIN*$^+$] wildtype and *myo2-2* strains (Catlett et al. 1998). The average number of protein aggregates was quantified per cell in each strain from still shot microscopy, and is represented in the graph. Aggregate number was significantly different between wildtype and *myo2-2* by T-test analysis. (* $p<.01$)

5.2.3 Coalescence of newly formed aggregates does not depend on [PIN+] in wildtype or *myo2-2* mutants

As described previously, the formation of Sup35NM-GFP aggregates is enhanced by the presence of [*PIN*$^+$] (Chapter 1). Up to this point all of my work in this chapter has been done using strains containing the high [*PIN*$^+$] variant. However, the *myo2-2* strain and isogenic wildtype were gifts from Lois Weisman's lab, and were found to contain an endogenous version of [*PIN*$^+$] that has never been characterized. Both strains were cured by passing on guanidine hydrochloride (Eaglestone et al., 2000), and subsequently cytoduced with high [*PIN*$^+$] for experiments. Given the different behaviors of the wildtype and *myo2-2* strain, I investigated whether there were differences between the endogenous [*PIN*$^+$] or the cytoduced high [*PIN*$^+$] variants on Sup35NM-GFP aggregate coalescence. Coalescence results indicate that the presence of either [*PIN*$^+$] variant did not affect Sup35NM-GFP aggregate coalescence (Figure 5.4).

5.2.4 Coalescence of newly formed aggregates in Myo2p Disruptions

I also investigated three other Myo2p mutants for effects on coalescence to determine whether the previous results were specific to the mutated site on Myo2p or the disrupted function. The three other Myo2p mutants were: *myo2-aflII, myo2-D1297G,* and *myo2-D1297N*. The *myo2-aflII* mutant contains a 33

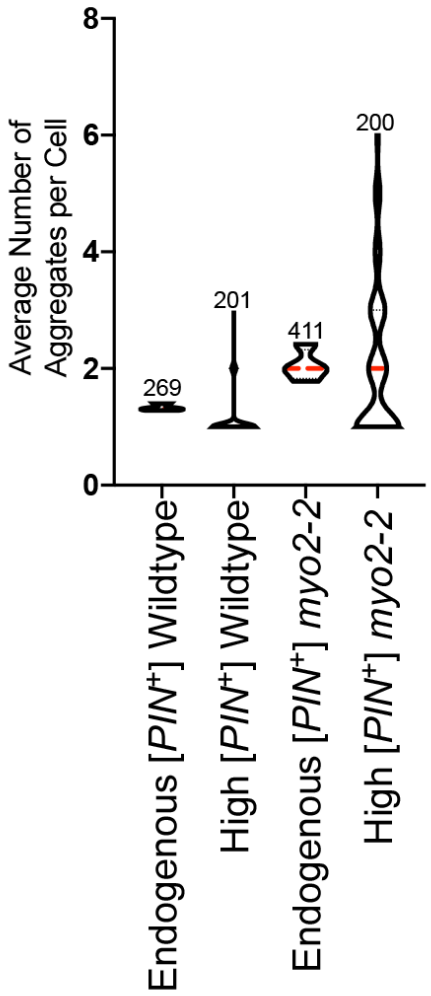

Figure 5.4: [*PIN*$^+$] variant does not alter Sup35NM-GFP aggregate number between wildtype or *myo2-2* strains. Sup35NM-GFP was induced in both High [*PIN*$^+$] and endogenous [*PIN*$^+$] wildtype and *myo2-2* strains. The number of protein aggregates per cell was quantified, with the average displayed in the graph. While it appears that the number of aggregates in High [*PIN*$^+$] *myo2-2* strains have a broader distribution, the median for both *myo2-2* strains was 2 aggregates per cell. T-test analysis showed no significant difference between wildtype strains and *myo2-2* strains respectively.

amino acid deletion in the Myo2p globular tail, and is not able to bind essential cargo causing growth and viability issues (Catlett et al., 2000). The *myo2-D1297G* and *myo2-D1297N* strains are mutations at a site needed for competitive binding of non-essential cargo such as the mitochondria and vacuole (Catlett et al., 2000; Eves et al., 2012). *myo2-D1297G* impairs the inheritance of vacuoles and causes clumped mitochondria (Catlett et al., 2000; Altmann et al., 2008). The *myo2-D1297N* strain only prevents vacuole binding and inheritance (Eves et al., 2012). Interestingly, both the *myo2-aflII* and *myo2-D1297N* had an increased number of aggregates per cell (median of 2 aggregates per cell), whereas the *myo2-D1297G* mutant did not (1 aggregate per cell; Figure 5.5). Similar to previous reports (Catlett et al., 2000), we found that the *myo2-aflII* strain is associated with viability issues and may account for the differences we observed. However, while both *myo2-D1297N* and *myo2-D1297G* both effect interaction with the vacuole, only *myo2-D1297N* also effects potential interaction with protein aggregates.

5.2.5 Myo2p mutants do not alter Sup35NM-GFP aggregate sequestration

The second step of aggregate formation involves early foci localization to the cell periphery and subsequent growth of foci into larger aggregates such as dots, lines, and rings (Chapter 3, Sharma et al., 2017). I asked whether localization of aggregates to the cell periphery was also dependent on Myo2p. *myo2-2* mutants (0.87μm) had similar aggregate sequestration to isogenic wildtype strains (0.92μm, Figure 5.6), as did the *myo2-D1297N* (0.88μm) and

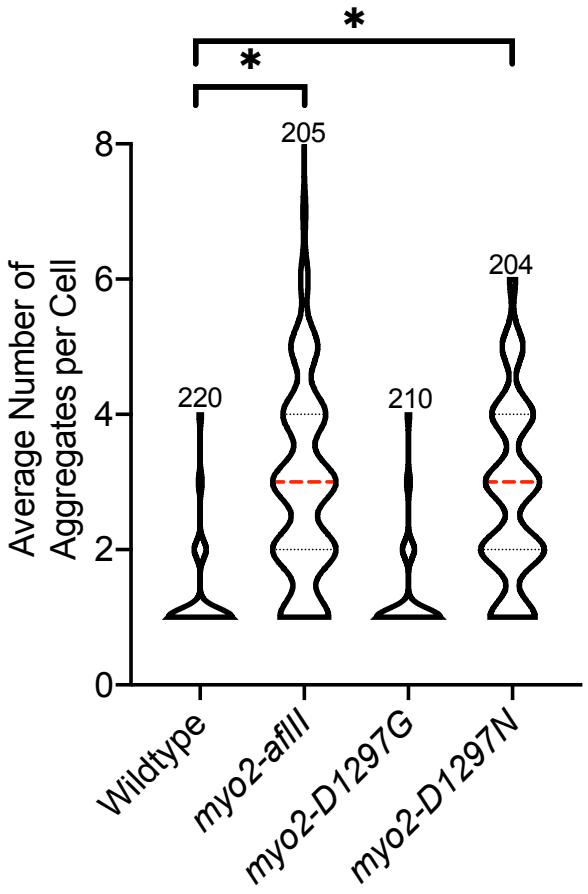

Figure 5.5: Disruptions to Myo2p cause an decrease in Sup35NM-GFP coalescence. Endogenous [*PIN*$^+$] myo2Δ strains expressing *myo2-AflII*, *myo2-D1297G*, or *myo2-D1297N* from a plasmid, and induced to express Sup35NM-GFP were quantified for the average number of protein aggregates per cell. T-test analysis showed significance between all three deletion strains to a wildtype control. (* p<.01)

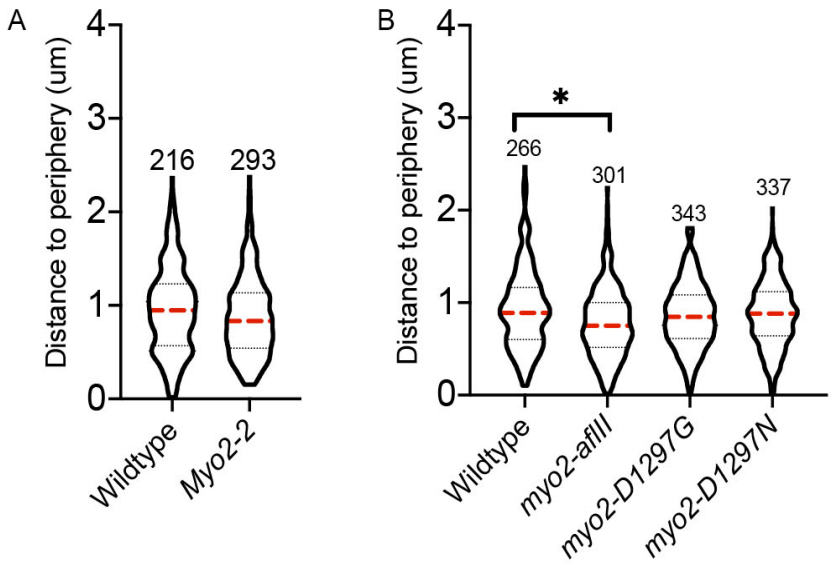

Figure 5.6: Myo2p disruption does not reduce peripheral localization of Sup35NM-GFP aggregates. A. Sup35NM-GFP was induced in High [*PIN*$^+$] wildtype and *myo2-2* strains (Catlett et al. 1998). Protein aggregate localization was quantified with coordinate mapping in both strains. T-test analysis showed no significant difference between wildtype and *myo2-2*. B. Endogenous [*PIN*$^+$] myo2Δ strains expressing *myo2-AflII*, *myo2-D1297G*, or *myo2-D1297N* from a plasmid, and induced to express Sup35NM-GFP were quantified for aggregate distance to the periphery. *myo2-aflII* was significantly different from wildtype by T-test analysis (* p<.01).

myo2-D1297G mutations (0.85μm, Figure 5.6). The *myo2-aflII* strain (0.77μm) however, showed a significant difference in aggregate distribution compared to the isogenic wildtype (Figure 5.6). As with coalescence however, again the effect seen with the *myo2-aflII* strain is more than likely due to issues with viability rather than an effect on aggregate formation. Once again, the presence of either high [*PIN*$^+$] or the endogenous [*PIN*$^+$] did not effect Sup35NM-GFP aggregate sequestration (Figure 5.6).

5.3 Discussion

In this chapter the role of Myo2p was explored in relation to the dynamics of newly formed protein aggregates. In *myo2-2* strains, mobility and coalescence of newly formed Sup35NM-GFP aggregates was reduced, however sequestration remained at wildtype levels. In addition, two other Myo2p mutant strains, *myo2-AflII* and *myo2-D1297N,* reduced coalescence as well. However, *myo2-D1297G* did not change Sup35NM-GFP formation behavior. This work suggests that Myo2p has a role in the management of newly formed protein aggregates, and there are specific cargo binding sites that interact with protein aggregates to potentially traffic aggregates along the actin cytoskeleton.

The *myo2-D1297G* and *myo2-D1297N* mutations are at a competitive binding site on Myo2p for Vac17p and Mmr1p, two “intermediate” proteins that link the vacuole or mitochondria to Myo2p for trafficking respectively. *myo2-D1297N* prevents only Vac17p interaction, while *myo2-D1297G* prevents interaction for both intermediate proteins (Catlett et al., 2000; Altmann et al., 2008; Eves et al., 2012). *myo2-2,* although a mutation at a different site but still within the globular head to bind cargo on Myo2p, has also been reported to impair vacuole interaction with the motor protein (Catlett and Weismann, 1998). Given the effects on mobility and coalescence in these mutants, this would suggest that the interaction with Vac17p may be important for managing aggregate formation. Recent work involving Vac17p interaction with protein aggregates and Myo2p is still unclear. Disruption of Vac17p has been shown to

increase asymmetric inheritance of heat stress induced Hsp104p aggregates supporting interaction between aggregate-Vac17p-Myo2p (Hill et al., 2016). However, work with Sup35NM-GFP aggregates in strains that have the pre-existing [*PSI*$^{+}$] prion has shown the opposite, where disruption of Vacp17p had no effect on protein aggregates, rather deletion of a different protein that interacts with Myo2p, Vsp1p, did cause an increase in the number of Sup35NM-GFP aggregates per cell (Kumar et al., 2017). It is possible that different intermediate proteins facilitate interaction between different protein aggregates and Myo2p. The identification of which intermediate proteins, such as Vac17p or Vps1p, facilitate interaction between different protein aggregates and Myo2p may explain why different mutations to the same site in Myo2p result in different effects on Sup35NM-GFP formation. It will be necessary to continue investigating how protein aggregates interact with Myo2p, specifically the potential relationship that intermediate proteins facilitate with Myo2p and the possibility of a similar mechanism of formation between different protein aggregates.

In contrast to actin disruptions, Myo2p mutants did not affect the sequestration of newly formed Sup35NM-GFP aggregates. While *myo2-aflII* did slightly alter localization, again this was suspected to be a produce of viability issues with the strain rather than changes to sequestration give this mutant maintains the ability to bind to cargo such as the vacuole or mitochondria. The ability to localize aggregates to the periphery normally in Myo2p mutants was surprising as I suspected that localization would be dependent on the ability to move aggregates towards a particular site in the cell. Localization was expected

to be highly variable similar to that in actin mutants (Chapter 4), as aggregates should appear randomly in the cell and due to the lack of mobility by Myo2p, remain at their site of formation. Given that Sup35NM-GFP is still localized at the cell periphery in Myo2p mutants, protein aggregates may form near the periphery of the cell and maintain that localization, with Myo2p only required for mobility and coalescence.

Taken together, this chapter suggests that Myo2p is required for the trafficking of newly formed protein aggregates to a single location in the cell, although it is not necessary for maintaining peripheral localization. It is unclear how protein aggregates interact with Myo2p, and therefore the potential for other factors in this mechanism should be explored. Understanding the role of Myo2p in responding to protein aggregate formation may allow for application to differentiate where older or diseased cells breakdown in management of protein aggregates.

Chapter 6: Sup35p Aggregate Formation Does Not Associate with Vacuole Fragmentation or Protein Inclusions

6.1 Introduction

In Chapter 3 (Figure 3.9) Sup35NM-GFP aggregates were described to localize near the cell periphery regardless of genetic background. The peripheral localization of aggregates is disturbed by mutations to the actin cytoskeleton (Chapter 4, Figure 4.7), but not the Myo2p motor protein (Chapter 5, Figure 5.6). The objective of this chapter is to identify other factors that may dictate the peripheral localization of newly formed protein aggregates.

A screen performed by Manogaran et al., (2011) suggested that there might be a role of vacuole function on protein aggregate formation. The screen identified genetic deletions that altered the formation of Sup35NM-GFP aggregates and/or the later induction of [*PSI*$^{+}$], here referred to as 'prion mutants'. The prion mutants were characterized into two different classes, early or late. Early class deletions reduce Sup35NM-GFP aggregate formation and the induction of [*PSI*$^{+}$], while late class deletions form aggregates but have reduced [*PSI*$^{+}$] induction frequencies. Interestingly, strains containing either early or late class deletions all had fragmented vacuoles. It is possible that changes to vacuole morphology may alter the spatial localization of newly formed aggregates in the cell.

Damaged or aggregating proteins are often collected and held in protein inclusions, holding sites that function to sequester damaged proteins away from the rest of the cellular environment and provide a potential site to either be

refolded or enter degradation pathways. Sup35NM-GFP aggregates have been proposed to localize to a vacuole-associated deposit called the Insoluble Protein Deposit, IPOD (Tyedmers et al., 2010). Rnq1p, a protein of unknown function, has previously been used as a marker for IPOD, and Sup35NM-GFP aggregates are suggested to co-localize with the marker (Tyedmers et al., 2010). Atg8p, an essential component of the autophagy pathway in yeast and the pre-autophagosomal structure, PAS, (Reggiori and Klinosky, 2013) can also be used to identify IPOD (Kaganovich et al., 2008). Observations by snap shot microscopy found Sup35NM-GFP to be colocalized with Atg8p, and authors proposed that IPOD may be the site of aggregate formation (Tyedmers et al., 2010; Arslan et al., 2015). However, these data are in contrast to findings by Mathur et al. (2009), who suggested that aggregates are first sequestered to the cell periphery and then localized to the vacuole much later on. The role of autophagy has also been linked to Sup35NM-GFP aggregation. Disruptions in autophagy related genes that code for proteins in the general autophagy pathway cause aggregates to form in more abundance and faster (Speldewinde et al., 2015). These data suggest that both IPOD and autophagy influence aggregate formation and possibly localization.

In yeast many protein inclusions have been identified, each associated with housing different subsets of the protein population (Saarikangas et al., 2017). Not only have Sup35NM-GFP aggregates been suggested to localize at IPOD and the PAS, but also with Q-Bodies, which are cytoplasmic protein inclusions that are often associated with stress induced protein aggregates

(Arslan et al., 2015). Q-bodies can be identified using Hsp42-GFP. While Sup35NM-GFP aggregates have been shown to co-localize with various protein inclusions, there has yet to be a link established between inclusions and the peripheral localization characterized in the previous chapters.

Here, I explore the link between vacuole morphology, autophagy, and protein inclusions with Sup35NM-GFP formation and localization. My results suggest that vacuole morphology or autophagy do not impact the formation of Sup35NM-GFP aggregates, but also reveal an unexpected finding that the presence of centromeric plasmids in 74D-694 genetic strains result in vacuole fragmentation. I also find that newly formed Sup35NMp aggregates do not localize with Q-Bodies, PAS, or IPOD.

6.2 Results

6.2.1 Characterization of Prion Mutants

Manogaran et al (2011) used the BY4741 background to screen for deletions that reduced prion formation, and confirmed their results by re-engineering the deletions in the 74D-694 background. The original observations of vacuole fragmentation associated with prion mutants were only qualitative. To understand the percentage of cells within a population that are fragmented, I counted the number of cells that had different vacuole phenotypes. Like most organelles in yeast, vacuole morphology can be very dynamic, with vacuoles fragmenting and fusing back together (Weisman., 2003; Efe et al., 2005). When these dynamic processes are altered, persistent fragmentation occurs. The

fragmentation of vacuoles is characterized into three separate classes: wildtype cells consisting of 1-3 individual vacuoles, Class B cells consisting of 4-6 vacuoles, and Class C cells with 7+ vacuoles (Figure 6.1A, Seeley et al., 2002). Two early class mutants (*sac6Δ* and *vps5Δ*) and two late class mutants (*bem1Δ* and *bug1Δ)* were characterized along with the isogenic wildtype. The wildtype strain contained mostly Wildtype Class vacuoles as expected, with 2.5% Class B and 1.6% Class C (Figure 6.1). *bug1Δ* was similar to the wildtype strain with 98% wildtype vacuoles. The *sac6Δ* mutant was also somewhat similar to the wildtype strain, but had an increased number of Class B vacuoles to 7.2%. *vps5Δ* and *bem1Δ* showed much more vacuole fragmentation, with 23.4% and 14.9% Class B vacuoles. Overall there was a large proportion, if not the majority, of cells regardless of genetic stain that contained wildtype class vacuoles. The high number of wildtype vacuoles regardless of genetic strain was unexpected and suggests that vacuole fragmentation itself may not cause a decrease in prion formation.

Meanwhile, if there is a link between prion mutants and IPOD, then it is possible that changes to in IPOD localization could be observed in prion mutant strains. As described above, Atg8p localizes to the perivacuolar inclusion IPOD, but it is also an integral component of autophagy. Cells that have disruptions to autophagy possess multiple GFP-Atg8p foci as they are unable to be taken into the vacuole (Lipatova et al., 2012). I speculated that even low levels of vacuole fragmentation in prion mutants may impair the ability of Atg8p to localize properly. Similar to other studies, I found that wildtype cells contained a median

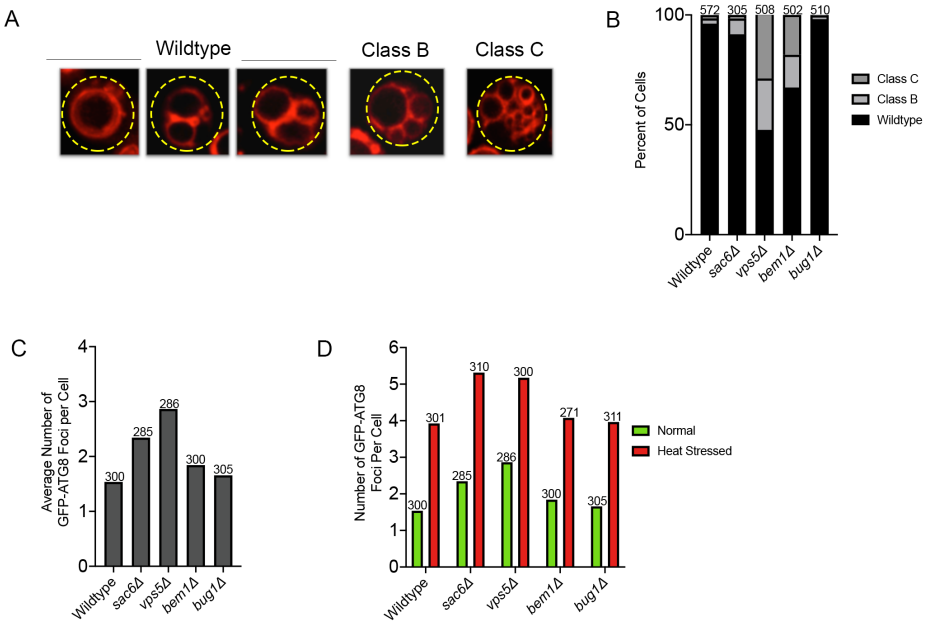

Figure 6.1: Characterization of Vacuoles and GFP-Atg8p in Prion Mutants. A. 74D-694 Cells grown overnight were stained with FM4-64 for the vacuole membrane. Above are images representative for each of the three different vacuole classifications based on morphology. B. 74D-694 strains of cells were grown overnight and stained with FM4-64. Vacuoles were quantified for each genetic strain over three individual trials. C. GFP-Atg8p was expressed in yeast strains overnight. The number of GFP-Atg8p foci was quantified for each strain in three separate trials. D. GFP-ATG8 was induced in cell strains overnight. Each culture was imaged and GFP-ATG8 foci per cell was quantified. After quantification, each culture was subjected to a thirty minute heat shock of 40°C. Immediately following heat stress, cells were imaged again with GFP-ATG8 foci per cell quantified. Above are the average values recorded for each cell strain under normal or heat stressed conditions.

of one GFP-Atg8p focus. Late class deletions, *bem1Δ* and *bug1Δ* also had one GFP-Atg8p focus (Figure 6.1C). However, early class deletions, *sac6Δ* and *vps5Δ,* had a noticeable increase of GFP-Atg8p foci. It should be noted that even though *sac6Δ* and *bug1Δ* strains have wildtype vacuoles, only *sac6Δ* has an increase in GFP-Atg8p foci, suggesting that there is not link between vacuole fragmentation and the number of GFP-Atg8p foci.

However, Atg8p has functions that are independent of autophagy. It was recently shown that Atg8p expression is induced during heat stress as part of a general proteostasis response, rather than autophagy alone (Ishii et al., 2019). Given the additional roles of Atg8p outside of autophagy, I speculated that if prion mutants have altered response to heat stress, than GFP-Atg8p foci may be different than wildtype cells. To assess whether there were changes based on the stress response in prion mutants, I subjected all cell strains to a thirty minute heat shock of 40°C, and then quantified the number of GFP-Atg8p foci per cell. The average number of foci roughly doubled in each of the genetic strains including wildtype after heat stress (Figure 6.1D). Given that each strain responded similarly to heat stress, these data suggest that stress response is not impaired in any of the prion mutants.

6.2.2 Sup35NM-GFP aggregation is independent of vacuole morphology

Although vacuole fragmentation was observed in prion mutants in Figure 6.1, the figure did not investigate whether localization of Sup35NM-GFP changed depending upon the level of vacuole fragmentation. In order to perform this experiment, plasmids containing an inducible Sup35NM-GFP were introduced into 74D-694 and BY4741 strains. Unexpectedly, 74D-694 wildtype strains with Sup35NM-GFP aggregates also had fragmented vacuoles (Figure 6.2). To understand why wildtype cells with the plasmid exhibited fragmented vacuoles, I considered that the presence of the Sup35NM-GFP construct was causing the fragmentation. However, the presence of an empty vector in wildtype 74D-694

resulted in vacuole fragmentation, indicating that the Sup35NM-GFP vector did not cause fragmentation specifically (Figure 6.2). Fragmentation was not a product of the transformation protocol, as cells having gone through transformation without the addition of a plasmid did not cause vacuole fragmentation. Interestingly, BY4741 wildtype cells, with or without Sup35NM-GFP, had higher levels of Class B and C vacuoles compared to the 74D-694 wildtype cells. Given the ability to induce Sup35NM-GFP aggregation in the BY4741 strain (Chapter 3), the fragmentation of the vacuole is most likely not related to changes in aggregate appearance. However, these data do indicate that centromeric plasmids may contribute to vacuole fragmentation.

6.2.3 The role of autophagy in Sup35NM-GFP formation is unclear

Our experiments above indicate there is no link between vacuole fragmentation, the number of Atg8p foci, and prion mutants. However, it is possible that autophagy could still be involved. To explore vacuole function in prion mutants, we used two different methods. The first method was by quinacrine staining. Quinacrine has been commonly used in yeast to visualize the vacuole as it is capable of diffusing across membranes and accumulates in acidic environments (Weisman et al., 1987). As more of the stain accumulates in acidic environments, previous groups have used the intensity of staining to determine the level of acidification in the vacuole (Morano and Klinosky., 1994; Hughs and Gottschling., 2012).

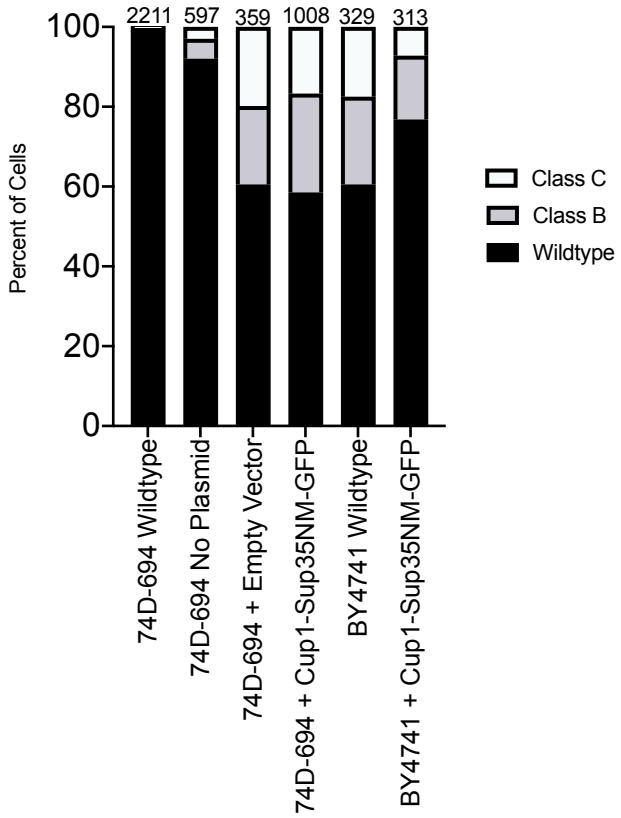

Figure 6.2: Plasmid expression causes vacuole fragmentation. All cells were grown overnight and stained with FM4-64 for vacuole morphology characterization. 74D-694 and BY4741 wildtype cells were used. 74D-694 No Plasmid cells had gone through the transformation procedure without the incorporation of a plasmid.

The pH of the vacuole can vary slightly depending upon the needs of the cell, such as acidification for autophagy function (Nakamura et al., 1997). Therefore, quantifying the intensity of quinacrine staining will be reflective of changes in the function of the vacuole.

Both of the early class mutants (*sac6Δ* and *vps5Δ*) and *bem1Δ* had higher fluorescent intensity compared to the wildtype strain, suggesting a more acidic

vacuole pH (Figure 6.3A). Coincidentally these three mutants also exhibited fragmented vacuoles (Figure 6.1). However, the *bug1Δ* mutant had reduced intensity compared to the wildtype despite reduced [*PSI*$^{+}$] induction. It is possible that *bug1Δ* reduces formation through a different mechanism other than a pathway associated with enhanced vacuole acidification. It should be noted that the intensity of quinicrine can vary greatly between sample preparations, and therefore can display some variability in quantitative comparisons. Therefore, a second measure of vacuole function was used to determine whether aggregate formation is impacted by the vacuoles' level of activity.

Using pharmacological agents, general and selective autophagy processes can be enhanced. Each of these processes leads to degradation in the vacuole, suggesting that if Sup35NM-GFP aggregation is decreased in response to one of these treatments, that autophagy processes and vacuole function influence formation of Sup35NM-GFP. Non-selective autophagy is enhanced through spermidine treatment (Speldewinde et al., 2015). Selective autophagy mechanisms for the mitochondria (mitophagy) and ER (reticulophagy) were also enhanced based on reports of protein aggregates localizing to the surface of either organelle (Zhou et al., 2014). Ethacrynic Acid (EA) enhances mitophagy (Deffieau et al., 2009), and DTT or Tunicamycin (TM) enhance reticulophagy (Cebollero et al., 2012). Enhancing both general autophagy and mitophagy reduced the formation of Sup35NM-GFP aggregates (Figure 6.3B).

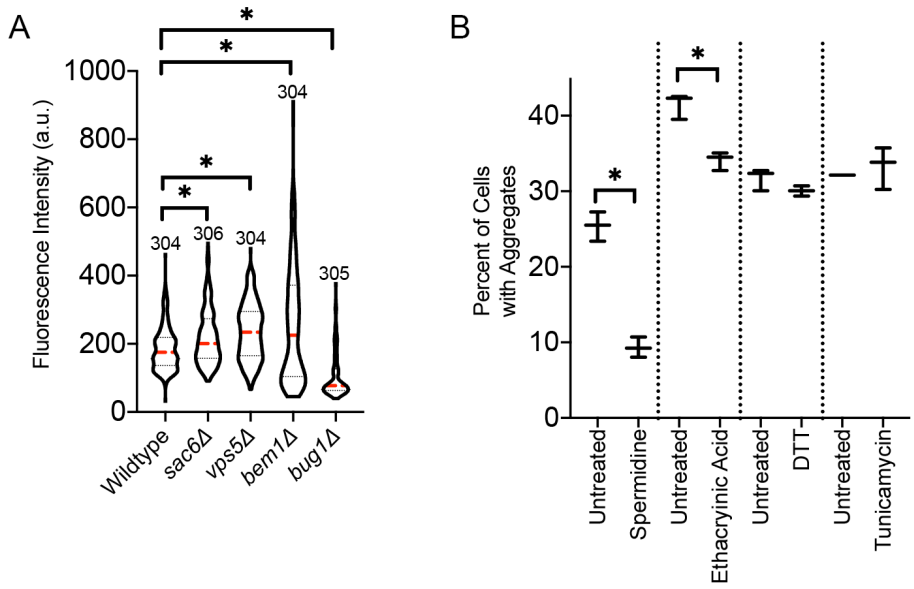

Figure 6.3: Quinacrine staining is increased in prion mutants, while autophagy reduces aggregate appearance. A. All strains were grown overnight and stained with quinacrine to highlight vacuole pH. More acidic vacuole pH values cause an increase in fluorescent intensity. Vacuoles of individual cells had fluorescent intensity values quantified through ImagePro Software. T-test analysis was used to compare mutant strains to the wildtype. B. Wildtype 74D-694 yeast culture was inoculated in 10mL of media for overnight growth and expression of Sup35NM-GFP. Prior to incubation, the culture was split into two 5mL cultures. One culture was left untreated for incubation, while the second was subject to Spermidine treatment, Ethacryinic acid treatment, DTT treatment, or Tunicamycin treatment. After overnight growth of each culture, the percentage of cells expressing Sup5NM-GFP aggregates was quantified in at least 300 cells over three trials for each treatment. Treatments were compared to the corresponding untreated control by T-test analysis (* $p < 0.01$).

Enhancing reticulophagy with either DTT or TM did not alter aggregate appearance. EA enhances mitophagy by binding to glutathione and preventing antioxidant properties, resulting in oxidative stressed mitochondria that are not able to function properly (Schaffer and Buettner., 2001). However, the build up of reactive oxygen species, as EA treatment would be promoting, is also a major

driver of general autophagy (Filomeni et al., 2010). Together, this work supports previous literature (Speldewinde et al., 2015) suggesting that the formation of Sup35NM-GFP is influenced by autophagy mechanisms.

6.2.4 Previously Defined Inclusion Bodies Are Not All Adjacent to the Vacuole

To assess whether aggregates are sequestered to protein inclusions, I first wanted to understand where individual protein inclusions were located in the cell. Of the three inclusions described in the introduction, a separate protein marker identifies each (GFP-Atg8p for the PAS, Rnq1-GFP for IPOD, and Hsp42-GFP for Q-bodies). FM4-64 is a vital dye that is internalized by endocytosis and remains on the vacuolar membrane. As expected, the PAS was localized adjacent to the vacuole in nearly all of the cells quantified (Figure 6.4). However, both IPOD and Q-Bodies were only localized near the vacuole in roughly half of the cells. Sup35NM-GFP was also localized near the vacuole approximately 55% of the cells. Together the localization of Sup35NM-GFP near the vacuole in only roughly half of cell suggests that localization is not associated with the PAS.

6.2.5 Newly Formed Aggregates Do Not Localize with Previously Defined Inclusion Bodies

I then investigated colocalization between Sup35NM-RFP and markers for the PAS, Q-Bodies, and IPOD, and quantified co-localization with snapshot

image capture and Pearson's Correlation Coefficient (PCC). PCC quantifies the degree of overlap between two different fluorescent channels, with a score of 1 representing perfect colocalization and a score of 0 indicating a lack of overlap. PCC values for aggregates and inclusions were compared to a positive control strain that contained Sup35NM-GFP and Sup35NM-RFP. As expected, the positive control gave a PCC median value of 0.67, indicating that PCC can be used to indicate co-localization. No significant colocalization was observed between Sup35NM-RFP and the PAS (0.38; Figure 6.5). However, unexpectedly, no colocalization was also observed between Sup35NM-RFP aggregates and

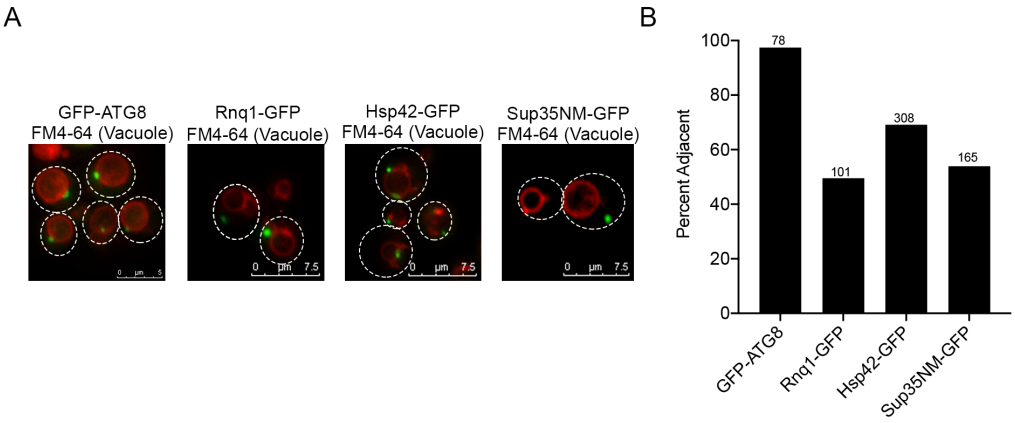

Figure 6.4: Localization of Protein Inclusions near the Vacuole. A. Individual cells expressing protein markers for protein inclusions or aggregates (PAS – GFP-ATG8; IPOD – Rnq1-GFP; Q-Bodies – Hsp42-GFP; APOD – Hsp104-GFP; aggregate – Sup35NM-GFP) were grown overnight and stained with FM4-64 for vacuole visualization. Representative images of each are shown. B. Cells imaged in A were quantified for adjacent localization between the protein marker and the stained vacuole. The percent of cells with adjacent localization is shown in the graph.

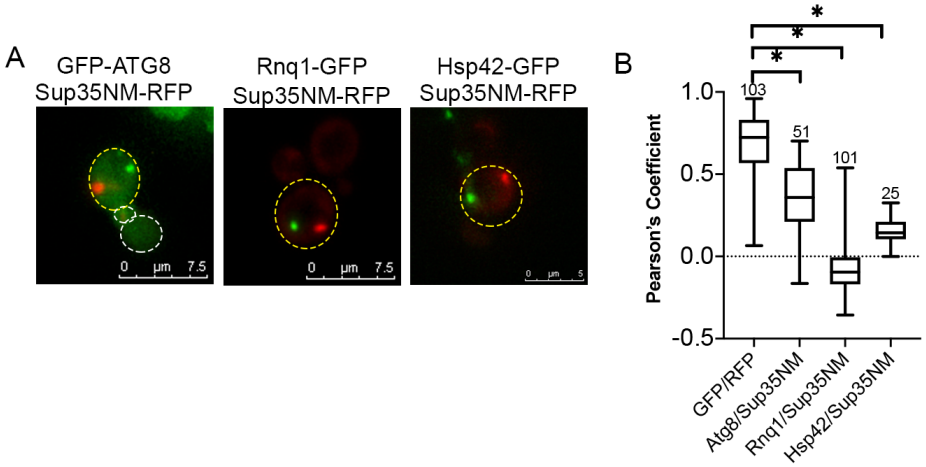

Figure 6.5: Newly formed Sup35NM-RFP aggregates do not localize with previously defined inclusion bodies. A. 74D-694 cells expressing GFP-ATG8 (PAS), Hsp42-GFP (Q-Bodies), or Rnq1-GFP (IPOD) were subjected to Sup35NM-RFP induction. Representative images of each are shown. B. Pearson's Correlation Coefficient (PCC) was used to identify overlap between Sup35NM-RFP and GFP labeled inclusions. 74D-694 cells expressing Sup35NM-GFP and Sup35NM-RFP were used as a positive control. Box plots indicate median and interquartile ranges, with statistical analysis by T-test (*p <0.01).

Atg8p (IPOD; -0.07) or Hsp42p (Q-Bodies 0.16; Figure 6.5), despite the fact that two other studies reported localization (Tyedmers et al., 2010; Arslan et al., 2015).

It is possible that the snapshot image approach did not adequately capture the localization of Sup35NM-GFP. Therefore, I assessed colocalization through the formation of aggregates using time-lapse microscopy to determine whether colocalization was transient. In 26 recordings of Sup35NM-RFP formation, no colocalization was observed (Figure 6.6). The distribution of Sup35NM-GFP aggregate sequestration was also not changed in *hsp42Δ* strains (Figure 6.7).

These data suggest that Sup35NM-GFP localization is not Hsp42p dependent and is not localized to a previously defined inclusion body.

6.3 Discussion

In this chapter I investigated previously identified prion mutants and the mechanism by which these mutations reduce the formation of Sup35NM-GFP aggregates, and whether the aggregates were localized with previously defined inclusion sites. While it was suspected that vacuole fragmentation may influence aggregate formation, my results indicate that changes to vacuole morphology are a product of plasmid expression in yeast. I also found that aggregates were not localized with any of the inclusions previously defined, suggesting that the site initial aggregate localization remains unclear. While this data does not explain why prion mutants alter [*PSI*$^{+}$] formation, it does suggest that aggregate localization is independent of the vacuole and provides characterization that can help target future experiments into the mechanisms of aggregate formation and management.

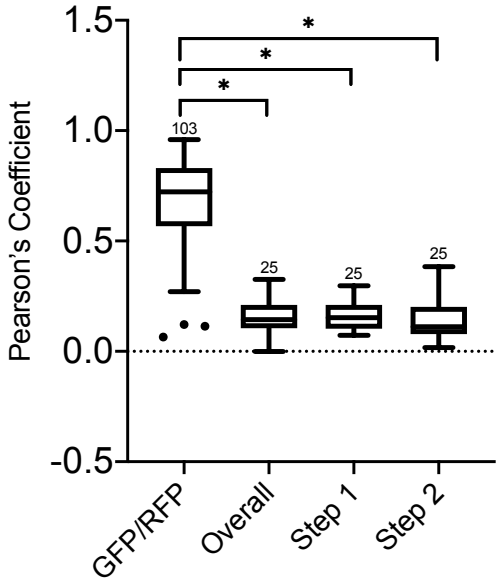

Figure 6.6: Newly formed Sup35NM-RFP aggregates do not colocalize with Hsp42-GFP at any point during formation. Sup35NM-RFP aggregates were induced in cells expressing Hsp42-GFP overnight. The formation of Sup35NM-RFP aggregates was recorded using 3D timelapse microscopy. PCC was used to quantify colocalization between Sup35NM-RFP and Hsp42-GFP throughout the formation process. PCC values were compared to a positive control strain of Sup35NM-GFP and Sup35NM-RFP by T-test analysis (* p<0.01).

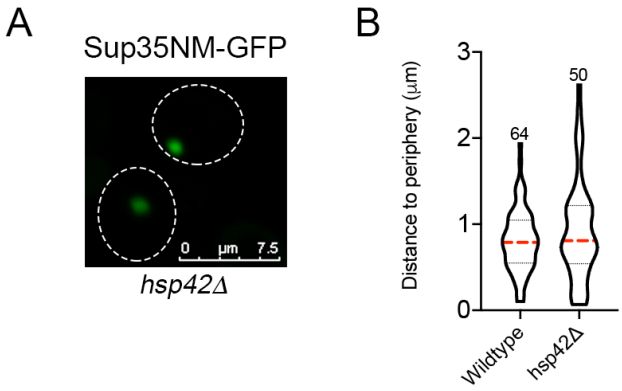

Figure 6.7: Sup35NM-GFP localizes to the cell periphery normally in *hsp42Δ* strains. A. Sup35NM-GFP was induced in 74D-694 *hsp42*Δ cells. B. The distance to the periphery of the Sup35NM-GFP aggregate from cells represented in A was quantified. Statistical analysis by T-test did not show significant difference to wild type.

While Manogaran et al. (2011) proposed that vacuole morphology may influence Sup35NM-GFP formation, my results suggest that vacuole fragmentation does not alter aggregate appearance. As shown, vacuoles were fragmented in wildtype cells that contained plasmids, indicating that Sup35NM-GFP aggregate formation in wildtype cells would also be in the presence of fragmented vacuoles. However, the prion mutants that had fragmented vacuoles also had increased quinacrine intensity, indicating a more acidic vacuole possibly from enhanced autophagy. Autophagy, as my results also suggest, has previously been shown to influence the formation of Sup35NM-GFP (Speldewinde et al., 2015). However, early class mutants also had an increased number of GFP-Atg8p foci. While these mutants also responded to heat stress similar to wildtype, it is possible the increased number of GFP-Atg8p foci is in response to enhanced autophagy from inherent stress caused by the genetic mutation, which in turn reduces the ability to form aggregates.

Most studies have investigated Sup35NM-GFP localization using pre-existing aggregates, or long after formation has occurred. Arslan et al. (2015) did look for colocalization at different time points of formation, however only by using snap shot microscopy at these time points. Here, I used 3D-timelapse microscopy to show that Sup35NM-RFP is not associated with Hsp42-GFP throughout formation (Figure 6.6). It is possible that previous work has found colocalization as a result of 2D microscopy, or collecting snap shots of transient overlap of proteins. Using genetics I further showed that Hsp42p does not

influence the sequestration of Sup35NM-GFP. Together my work provides higher resolution colocalization studies than have been previously used.

The results of this chapter show that newly formed aggregates do not localize to previously defined inclusions, or to the vacuole surface. It is possible that Sup35NM-GFP is localizing to the surface of a different organelle. Work done by Zhou et al. (2014) using heat induced protein aggregates, found that aggregates were localized to the surface of the mitochondria and ER. Chapter 7 explores Sup35NM-GFP localization with the surface of these specific two organelles, and a few others. Defining where newly formed aggregates are localized will provide insight into the mechanisms by which aggregates are managed, and possibly define whether all aggregates are managed similarly.

Chapter 7: Newly Formed Protein Aggregates Localization is Independent of Peripheral Organelles

7.1 Introduction

In this chapter, I investigate the spatial localization of newly formed Sup35NM-GFP aggregates with organelles previously identified to associate with heat-induced protein aggregates (Zhou et al., 2014). Adjacent localization shows that Sup35NM-GFP aggregates are near the surface of both the mitochondria and the ER. However, use of strains with genetic manipulations altering the morphology and localization of organelles suggests that aggregates are not truly associated with either organelle.

7.2 Results

7.2.1 Newly Formed Aggregates are localized near the Mitochondria/ER

Using markers for the vacuole (FM4-64), mitochondria (Mito-dsRED), ER (Sec63-mCherry), Nucleus (DAPI), and Peroxisome (SKL-mCherry), I investigated Sup35NM-GFP localization with each of these organelles. Sup35NM-GFP did not show any significant overlap by PCC with the vacuole, mitochondria, ER, nucleus, or peroxisome (Figure 7.1). However, I found approximately 80% of Sup35NM-GFP aggregates to be localized within 500nm (adjacent) to either the mitochondria or ER structures (Figure 7.1). These data suggest that newly formed Sup35NM-GFP aggregates may be localized to the surface of the mitochondria and ER at the periphery of the cell similar to stress induced aggregates.

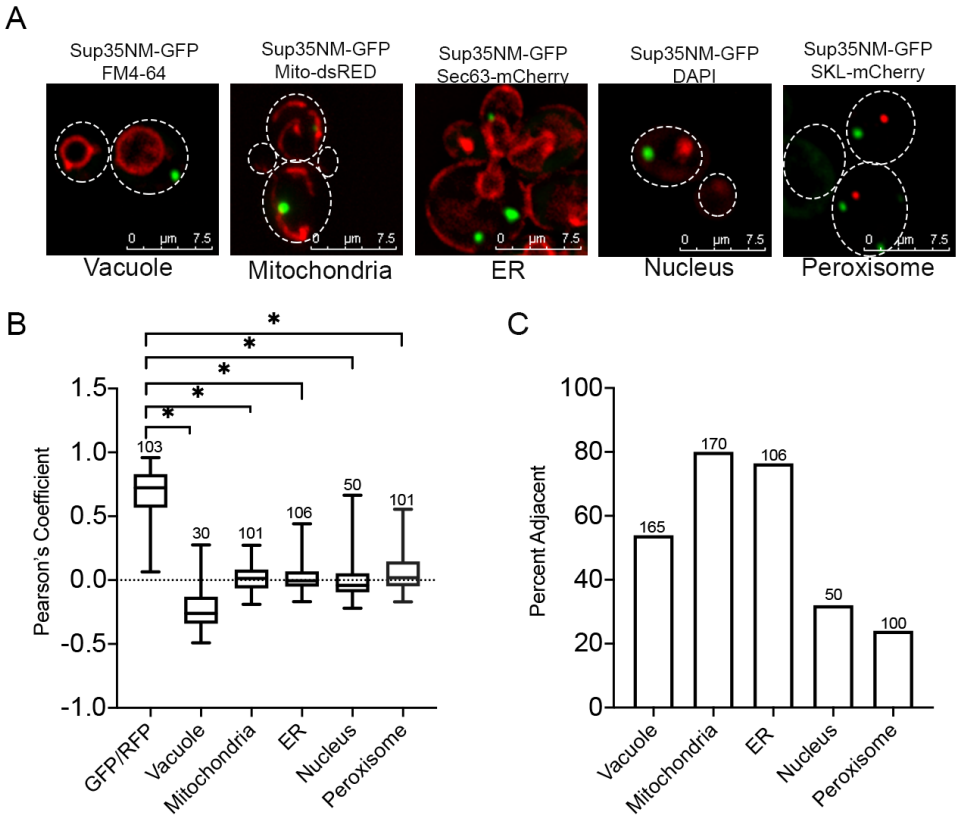

Figure 7.1: Sup35NM-GFP aggregates localize adjacent to the mitochondria and ER. A. 74D-694 cells had Sup35NM-GFP expression induced while either co-expressing Mito-dsRED (mitochondria), Sec63-mCherry (ER), SKL-mCherry (peroxisome), or were stained with FM4-64 (vacuole) or DAPI (nucleus). Representative images of each are shown. B and C. Images were quantified for co-localization by PCC (B) and adjacent localization (C). A positive control was included in PCC for comparison by T-test analysis (* $p < 0.01$).

7.2.2 Sup35NM-GFP aggregate localization is not dependent on the mitochondria or ER

Since I observed Sup35NM-GFP aggregates were localized near the mitochondria and ER surfaces in the majority of cells, I then wanted to determine whether aggregates are truly associated with these organelles or simply localized in the same area. I generated several gene disruptions in the 74D-694

background that alter the localization or morphology of either the mitochondria or ER. The distance of Sup35NM-GFP aggregates from the cell periphery in deletion mutants were assessed and compared to isogenic wildtype strains. Num1p and Mdm36p are mitochondrial tethering proteins (Lackner et al., 2013). Deletion of either gene releases mitochondria from the cellular cortex, however Sup35NM-GFP localization is unchanged in the mutants (Fig. 7.2). Mmm1p and Mdm12p link the mitochondria with the ER (Kornmann et al., 2009). Deletion of either gene leads very condensed mitochondria in the center of the cell, yet also does not alter Sup35 distribution from the cell periphery. Fis1p is a protein that functions in mitochondrial fission (Zhou et al., 2014). Similar to the other deletions impacting mitochondrial morphology, Sup35NM-GFP localization was also unchanged in this mutant. Together, I conclude that changes in mitochondria morphology and position do not impact the sequestration of Sup35NM-GFP.

Ice2p and Cho2p are two proteins that support cortical ER integrity (Lowen et al., 2007; Hermesh et al., 2014), and deletion of either results in less robust cortical ER (Figure 7.2). Sup35NM-GFP is unaltered in either of these

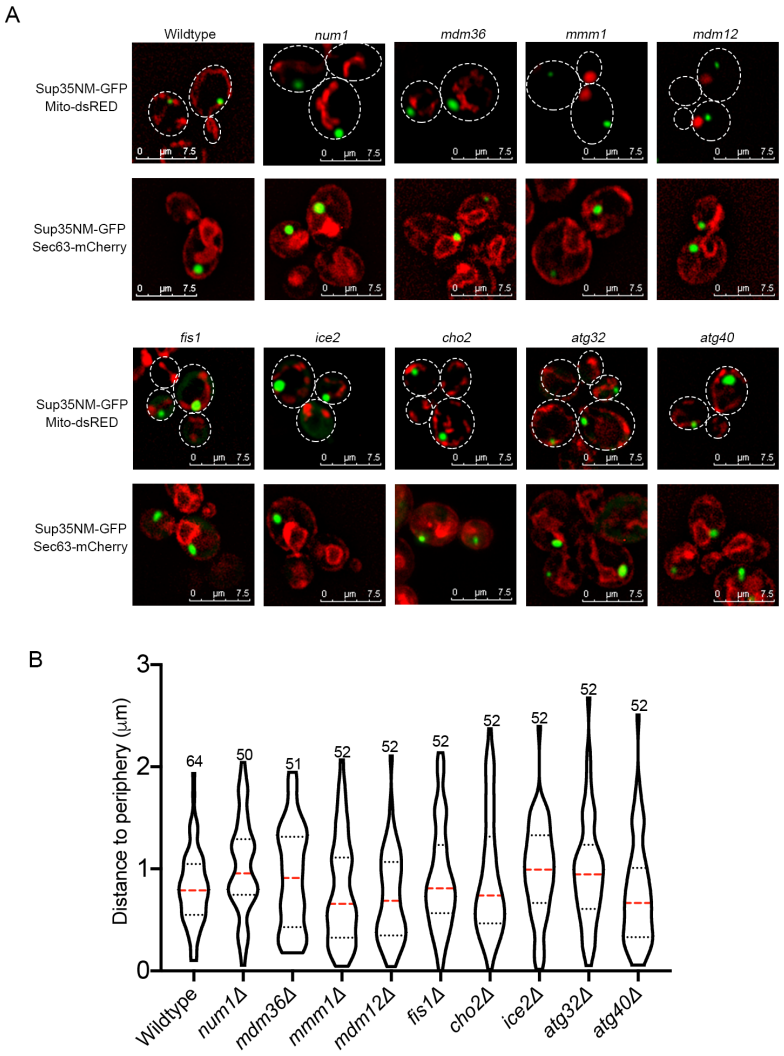

Figure 7.2: Disruptions to the Mitochondria or ER do not alter Sup35NM-GFP aggregate localization. A and B. Sup35NM-GFP was induced in 74D-694 strains individually containing different genetic mutants disrupting mitochondria and/or ER morphology/localization. Representative images of each are shown in A. 3D-coordinate mapping was used to quantify distance to the periphery of aggregates in each strain. No significant difference was found for any deletion strain compared to the wildtype using T-test analysis.

mutants. Similar to changes to the mitochondria, mutations altering cortical ER structure do not change the sequestration of Sup35NM-GFP.

Although changes to the morphology and localization of the mitochondria and ER did not alter sequestration of Sup35NM-GFP, selective autophagy

pathways exist for both organelles. As shown before in Chapter 6, enhancing reticulophagy did not alter the formation of Sup35NM-GFP aggregates, while mitophagy was inconclusive. To confirm that selective autophagy does not impact the formation of aggregates, I disrupted genes that impaired mitophagy (atg32*Δ*; Kanki et al., 2009) and reticulophagy (*atg40Δ*; Mochida et al., 2015). Neither disruption altered Sup35NM-GFP positioning near the cell periphery (Figure 7.2). Taken together, this suggests that Sup35NM-GFP aggregates are localized near the periphery of the cell, but at an unknown site that is independent of most organelles and is influenced by general autophagy.

7.3 Discussion

In this chapter I investigated the spatial localization of newly formed Sup35NM-GFP aggregates with peripherally localized organelles. Despite localization to the mitochondria and ER, disruption of either organelle did not alter the peripheral localization of Sup35NM-GFP, suggesting that sequestration is not dependent on either organelle. Although the localization of existing Sup35NM-GFP aggregates has been proposed to be at distinct inclusions or the surface of organelles, my work suggests that newly formed aggregates have different behavior.

Using 3D microscopy and time-lapse recordings, I have found that the localization of newly formed Sup35NM-GFP aggregates is not as clear as others have described. In Chapter 6 I showed that Sup35NM-RFP aggregates do not localize with the PAS, Q-Bodies, or IPOD as previously expected. In this chapter,

I showed that newly formed aggregates, while they do appear to localize to the surface of the mitochondria and ER, are not associated with either organelle as heat induced aggregates were proposed to be (Zhou et al., 2014). Up to this point, the only change found to alter the sequestration of Sup35NM-GFP aggregates has been the disruption of the actin cytoskeleton (Chapter 4). Mathur et al. (2009) also found that aggregates are peripherally localized initially, but after an extended period of time suggest that aggregates are moved inward in the cell to the vacuole. My data supports that aggregates are not initially localized to the vacuole, and therefore the peripheral localization is not at IPOD. Rather, initial localization of aggregates is to an unknown peripheral site, which I term PPOD, Peripheral Protein Deposit. It is possible that PPOD represents a new retention site for the initial management of protein aggregates near the periphery of the cell, however it is also possible that this peripheral site is simply an unoccupied space in the cell that aggregates can occupy. Further work will be needed to identify what other factors exist as part of PPOD and whether this peripheral sequestration is unique to Sup35NM-GFP or part of a general cellular response to protein aggregate formation, to better explain the biological relevance of the peripheral localization.

Chapter 8: Newly Formed Sup35NM-GFP Aggregates Localize with Hsp104p and Co-chaperones

8.1 Introduction

In the previous chapters I have shown that newly formed Sup35NM-GFP aggregates do not localize with previously defined inclusion bodies (Chapter 6) or to the surface of distinct organelles such as the mitochondria or ER (Chapter 7). However, I have shown that both actin (Chapter 4) and Myo2p (Chapter 5) do play a role in the management of these aggregates. While actin and Myo2p are involved, it is unclear what other molecular factors play a role in the formation of Sup35NM-GFP aggregates. The goal of this chapter is to explore the role of the Hsp104p chaperone complex in protein aggregate formation as a possible molecular factor involved in managing protein aggregate formation.

Using 2D snapshot imaging, Saibil et al. (2012) and Arslan et al. (2015) each showed that *de novo* Sup35NM-GFP aggregates colocalize with Hsp104p, Sis1p, and Ssa1p. Hsp104p is a AAA^{+}-ATPase that binds to co-chaperones Ssa1p and Sis1p. Together, this complex has been shown to extract proteins from within an aggregate through a central pore using ATP hydrolysis. This extraction causes the misfolded protein to unfold as it exits the chaperone (Glover and Lindquist, 1998; Tessarz et al., 2008). Prion propagation is dependent on Hsp104p as the chaperone complex severs aggregates into smaller propagons that can be transmitted to daughter cells (Chernoff et al., 1995; Moriyama et al., 2000; Cox et al., 2003; Shorter and Lindquist, 2004; Kryndushkin et al., 2011).

Based on the role of Hsp104p in prion propagation, one might expect that Hsp104p would disassemble newly formed Sup35NM-GFP aggregates, and therefore reduce aggregate appearance. Conversely, Hsp104p is required for prion formation (Zhou et al., 2001). This requirement is likely due to the fact that Hsp104p is necessary to maintain the [*PIN*$^{+}$] prion, which enhances de novo aggregate formation (Derkatch et al., 2001). However, it has also been suggested that the co-localization of Hsp104p with Sup35NM-GFP aggregates may be needed potentially as a scaffolding function to regulate interaction with other cellular factors allowing for aggregate formation (Saibil et al., 2012). While aggregate in these previous studies were *de novo*, formation had been induced for well over 24 hours, therefore the involvement of Hsp104p with newly formed aggregates has not been established.

Here, I investigate the localization between newly formed Sup35NM-RFP aggregates, and Hsp104p-GFP during the two steps of formation. Using 3D timelapse microscopy, I show the temporal localization of aggregates with Hsp104p throughout step 1 and 2. I also confirm the requirement of Hsp104p in the formation of Sup35NM-GFP aggregates by inducing formation in a genetic strain without Hsp104p. This chapter helps define the temporal association of Hsp104p with newly formed protein aggregates.

8.2 Results

8.2.1 Sup35NM-RFP aggregates co-localize with Hsp104p and associated chaperones

Sup35NM-RFP was overexpressed in strains containing an endogenously tagged Hsp104-GFP. Using 3D-time-lapse microscopy, Hsp104-GFP was normally observed as diffuse cytoplasmic fluorescence, with an occasional single inclusion that was previously characterized to be an age associated deposit (Sarrikangas et al. 2015). Upon the formation of Sup35NM-RFP, early foci appeared to be co-localized with Hsp104p (Figure 8.1A). Throughout the time-lapse, Hsp104-GFP remained associated with Sup35NM-RFP into step 2 when the aggregates were sequestered at the cell periphery. PCC analysis of co-localization during step 1 and step 2 showed values that were similar to the positive control (Sup35NM-GFP and Sup35NM-RFP, Figure 8.1B).

Next, I asked whether Sup35NM-RFP co-localized with Sis1-GFP and Ssa1-GFP, the Hsp104p co chaperones. Focusing solely on sequestered aggregates in step 2, both co-chaperones co-localized with Sup35NM-RFP. Our observations were confirmed by PCC analysis, where PCC values between Sup35NM-RFP and Sis1-GFP or Ssa1-GFP were similar to the positive control (Figure 8.2). Taken together, these results suggest that Sup35NM-RFP aggregates are associated with Hsp104p prior to sequestration, suggesting that the chaperone complex may be involved in the cellular response mechanism to newly formed protein aggregates outside of dissaggregase activity.

8.2.2: Sup35NM-RFP Aggregates Cannot Form without Hsp104p

The formation of Sup35NM-GFP aggregates is dramatically enhanced in the presence of the [*PIN*$^+$] prion (Derkatch et al., 2001; Osherovich et al., 2001), as well as in the presence of several other protein aggregates such as polygluatmine aggregates associated with the Human Huntington's disease. As mentioned above, Sup35NM-GFP does not form aggregates in *hsp104Δ* strains (Zhou et al., 2001), likely due to the loss of [*PIN*$^+$]. However, it has never been tested whether Sup35NM-GFP aggregates can be induced in the presence of other aggregating proteins, such as polyglutamine aggregates associated with Huntingtion's, that do not require Hsp104p (Derkatch et al., 2004). Using an *hsp104Δ* strain, I induced Sup35NM-RFP formation in the presence of a plasmid that contains a galactose inducible expanded glutamine tract associated with exon 1 of the Huntingtin protein, Gal-HttQ103-GFP (Q103-GFP). Q103-GFP aggregates formed within several hours of galactose addition, which often resembled large non-uniform dots or wide lines. Yet, even after 24 hours of both Sup35NM-RFP and Q103-GFP expression, most of the cells continued to display diffuse Sup35NM-RFP fluorescence. While there was an extremely small population of cells that contained Sup35NM-RFP aggregates, these aggregates did not look like typical Sup35NM-GFP as they matched the Q103-GFP aggregate appearance almost perfectly, not appearing as the normal clean dot punctate or thin, crisp ring/lines (Figure 8.3). Therefore the requirement for Hsp104p in Sup35p aggregate formation is supported by the lack of Sup35NM-RFP aggregate formation in these cells.

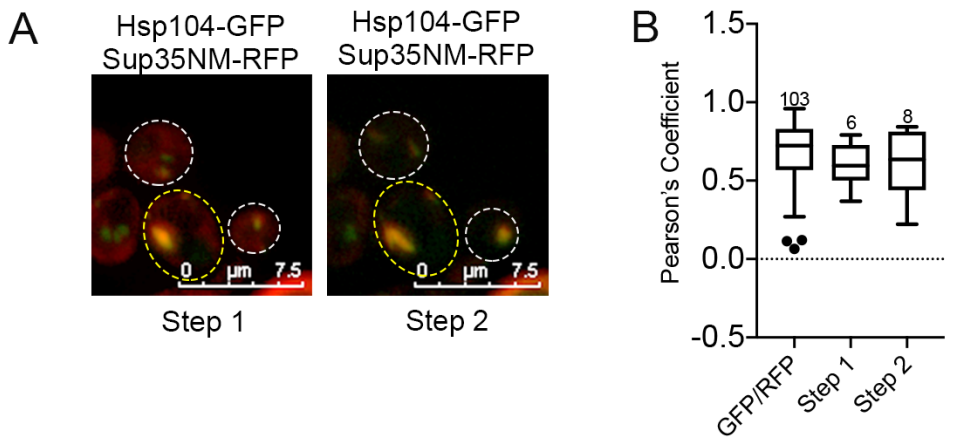

Figure 8.1: Newly formed Sup35NM-RFP aggregates localize with Hsp104p. A. BY4741 cells with endogenously expressed Hsp104-GFP were subjected to Sup35NM-RFP induction that was imaged using 3D timelapse microscopy. Representative images are shown of a de novo formed Sup35NM-RFP aggregate during Step 1 (left image) and Step 2 (right image). B. PCC assessment was performed for the control, and Hsp104-GFP and Sup35NM-RFP at both the mobility/coalescence and sequestration phases.

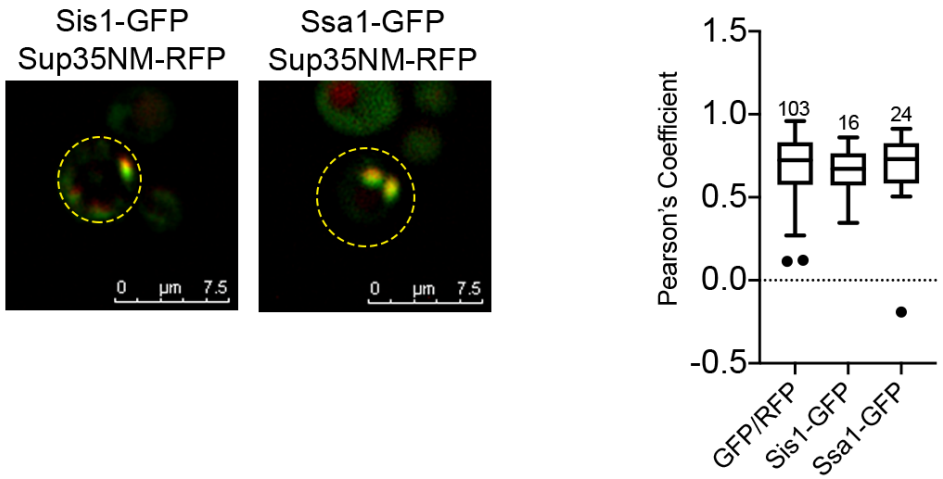

Figure 8.2: Newly Formed Sup35NM-RFP Localizes with Sis1-GFP and Ssa1-GFP. Left. Sup35NM-RFP was induced in 74D-694 cells with either endogenously tagged Sis1-GFP or Ssa1-GFP. Right. PCC assessment of cells represented of the left is shown.

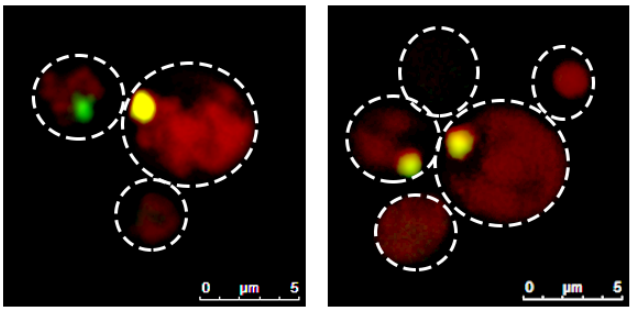

Figure 8.3: Sup35NM-RFP Does Not Form Typical Aggregates in Strains Without Hsp104. Sup35NM-RFP was induced in *hsp104Δ* cells with Q103-GFP expression. Cells were visualized after 24 hours of induction, and nearly all cells contained diffused Sup35NM-RFP expression. Very few cells contained Sup35NM-RFP aggregates as shown in the image.

8.3 Discussion

In this chapter I investigated the role of Hsp104p on the formation of Sup35NM-RFP aggregates. From the detection of early foci, Sup35NM-RFP aggregates colocalize with Hsp104-GFP, and remain co-localized throughout mobility and sequestration steps. Sis1-GFP and Ssa1-GFP are also co-localized with Sup35NM-RFP aggregates. My work also supports the requirement of Hsp104p for the formation of Sup35NM-RFP aggregates. While it is known that Hsp104p functions as a dissaggregase that severs protein aggregates, the role that the chaperone plays in the formation of Sup35NM-GFP aggregates is still unclear.

Both Saibil et al. (2012) and Arslan et al. (2015) have previously shown that Sup35NMp aggregates colocalize with Hsp104p in [*PIN*$^+$] cells at time points after step 2, or aggregate sequestration to the periphery. Now, my data indicates

that this co-localization occurs as soon as the early foci are detected. I postulated that the association between Hsp104p and Sup35NM-GFP aggregates possibly occurs prior to the detection of early foci, when the proteins are forming oligomeric complexes. We attempted protein sedimentation experiments to determine whether Hsp104p would co-sediment with Sup35NM-GFP as soon as 8 hours of induction. While Sup35NM-GFP (Lyke and Manogaran., 2017) and endogenous Sup35p (Fig. 3.1) can sediment as soon as 8 hours of overexpression, we found that Hsp104p sedimented without any Sup35NM-GFP overexpression. The sedimentation without Sup35NM-GFP aggregation is most likely due to Hsp104p's association with Rnq1p because cells are [*PIN*$^{+}$] causing the Rnq1p to sediment with the heavy fractions.

Given the localization during step 1 of formation, it is possible that Hsp104p has another functional role in the management of the aggregate beyond mere severing. Heat stress induced protein aggregates, as detected through Hsp104-GFP, have been shown to exhibit reduced mobility when the actin cytoskeleton is disrupted with LatA (Liu et al., 2010) or decreased asymmetric inheritance in Myo2 mutants (Bockler et al., 2017). Both studies propose a role for Hsp104 in the management of these aggregates. These results are consistent with my findings that Sup35NM-GFP mobility is also reduced in both actin (Fig 4.3; Table 4.1) and Myo2p mutants (Fig. 5.2, Table 5.1). Based on these observations, it is possible that Hsp104p facilitates the interaction between protein aggregates and the Myo2p-actin trafficking network. Hill et al. (2016) suggested that the association between Hsp104p and Vac17p or

Vps1p is needed for interaction between Myo2p and cargo such as the vacuole. Deletion of Vps1p disrupted the ability of Hsp104p associated aggregates to interact with Myo2p (Kumar et al., 2017). Therefore it is plausible that Hsp104p is localized with Sup35NMp aggregates from the initial appearance as the chaperone is providing the interaction with the trafficking mechanism in the cell to properly manage the newly formed aggregate.

Taken together, the Hsp104p chaperone complex may serve multiple functions with the formation of protein aggregates. Understanding what these different functions may be will be important to understand how the cell responds to and manages the formation of protein aggregates. It is also important to note that Hsp104p associates with many protein aggregates, setting up a potential system in which the initial cellular response is similar between multiple aggregates. Further investigation of Hsp104p and the role it plays during protein aggregate formation will be critical to define the cellular mechanisms involved.

Chapter 9: Characterization of Stress Granule Formation

9.1 Introduction

As shown in Chapter 8, Sup35NM-GFP aggregates colocalize with Hsp104-mCherry throughout the process of formation, suggesting that Hsp104p may play a role in aggregate trafficking mechanisms. However, stress granules are often visualized by an Hsp104-GFP marker. Stress granules are membraneless organelles that form in response to cellular stress such as heat and chemical treatment and are comprised of protein and RNA (Protter and Parker, 2016). Contrary to Sup35NM-GFP that irreversibly aggregates, stress granules are reversible. Upon heat or chemical stress, RNA and protein assemble into aggregates yet disassemble upon removal of the stress (Protter and Parker, 2016). The goal of this chapter is to investigate whether the formation of stress granules is managed by similar cellular mechanisms as newly formed Sup35NM-GFP aggregates.

The formation of stress granules is suggested to take place through a multi-step process. Kroshwald et al. (2015) found that the proteins in stress granules go through a liquid-liquid phase prior to coalescing into an aggregate structure. Newly formed heat induced aggregates have been shown to be mobile and coalesce shortly after appearing (Escusa-Toret et al, 2013). The step-wise formation of stress granules is supported by work in mammalian systems that propose three stages of assembly including nucleation, growth, and fusion (Wheeler et al., 2016). In Chapter 3, I demonstrated that the formation of Sup35NM-GFP similarly takes place through a two step process involving

mobility (and coalescence), and sequestration. It is possible that the stress granule undergo similar steps to what I have observed and quantitated with Sup35NM-GFP aggregates.

There is evidence that actin plays a role in the management of stress granules. Hsp104p marked stress granules colocalize with the actin cytoskeleton (Liu et al, 2010). The number of Hsp104p associated stress granules increases in stressed cells treated with the actin inhibitor LatA, suggesting that actin influences the coalescence of aggregates (Specht et al., 2011). While it is unclear whether the interaction between actin and stress granules is similar to that of Sup35NM-GFP, it is possible that the behavior of stress granule formation may be influenced by actin networks.

Here I investigate the formation of Hsp104-mCherry stress granules. Through quantification of formation, stress granules and Sup35NM-GFP aggregates appear to each follow a similar two step process of formation. The formation of stress granules is also effected similarly when disruptions to the actin cytoskeleton are used. This work suggests that Hsp104 associated stress granules all undergo a two step formation process that is influenced by actin networks.

9.2 Results

9.2.1 Stress Granules Follow the 2-Step (Mobility/Coalescence and Sequestration) Process of Formation

To investigate the behavior of stress granules, I induced aggregate formation using sodium azide (NaN_3) in widltype BY4741 cells. NaN_3 treatment has been shown to lead to the aggregation of several stress granule associated proteins including Pab1p and Pbp1p (Buchan et al., 2011), as well as Hsp104p (Cherkasov et al., 2013). Heat stress was not used to induce stress granule formation as our actin mutants are temperature sensitive, therefore chemical stress allows for investigation of stress granule formation under wildtype conditions and in actin mutants. Using 3D-time-lapse microscopy, Hsp104-mCherry foci appear within 15 minutes after sodium azide treatment. These initial Hsp104-mCherry foci, which will be called 'early foci' are very mobile. The average rate of movement is 0.49μm/min. The rate of movement fits into the previously reported range of heat induced aggregates of 0.3-0.8μm/min by Escusa-Toret et al. (2013). The slope of the movement is negative, which is consistent with the slope of movement for Sup35NM-GFP aggregates in the same genetic background (Figure 9.1, Table 9.1). Both Hsp104-mCherry and Sup35NM-GFP have high mobility during the first 10 minutes of formation, and each slow down to similar values by the third 10 minute interval. MAD values between stress granules and Sup35NM-GFP are also similar, suggesting that there the rate of movement is not constant but is constantly changing over time.

Cells induced for stress granules contained a median of 2 Hsp104-mCherry foci per cell after 3-4 hours of stress. These values are higher than the 1 aggregate per cell observed for Sup35NM-GFP (Figure 9.2). However, it

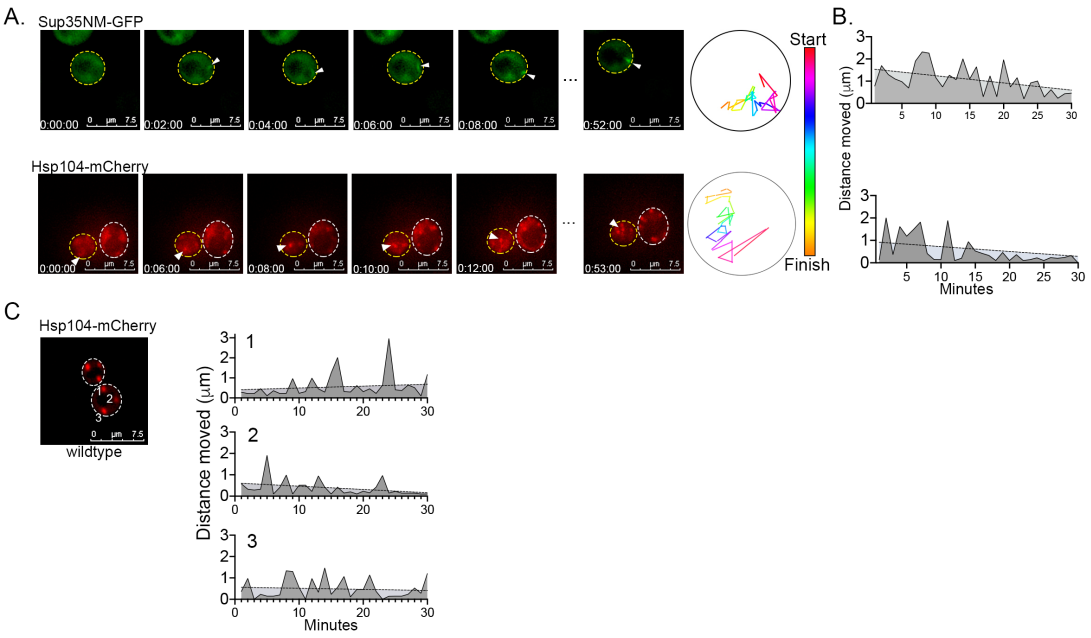

Figure 9.1: Hsp104-mCherry stress granules are mobile initially during formation. A. Sup35NM-GFP or Hsp104-mCherry stress granules were induced in wildtype BY4741 strain cells. 3D-timelapse microscopy was used to record early foci formation, with representative images shown. A representative particle trace for the white caret marked stress foci in the yellow outlined cell is shown. B. The rate of movement is shown in the graph on the right, with a trend line with slope representing change in rate over quantification. C. Stress granule formation was induced in BY4741 wildtype expressing Hsp104-mCherry. 3D-timelapse microscopy was used to record stress foci formation, with representative images shown. The rate of movement is shown in the graph on the right for each of the labeled foci, with a trend line with slope representing change in rate over quantification.

	Overall rate Rate (μm/min)	Rate in first 10 minutes	Rate in third 10 minutes	Slope	MAD
Sup35NM-GFP	0.66 +/- 0.5	1.2 +/- 0.52	0.47 +/- 0.38	-0.028 +/- 0.007	0.30 +/- 0.06
Hsp104-mCherry	0.49 +/- 0.49*	0.84 +/- 0.66*	0.34 +/- 0.36	-0.019 +/- 0.006	0.25 +/- 0.06

Table 9.1: Mobility Comparison of Sup35NM-GFP and Hsp104-mCherry Early Foci in Wildtype Cells. Statistical analysis was performed by Mann-Whitney test (* $p < 0.01$).

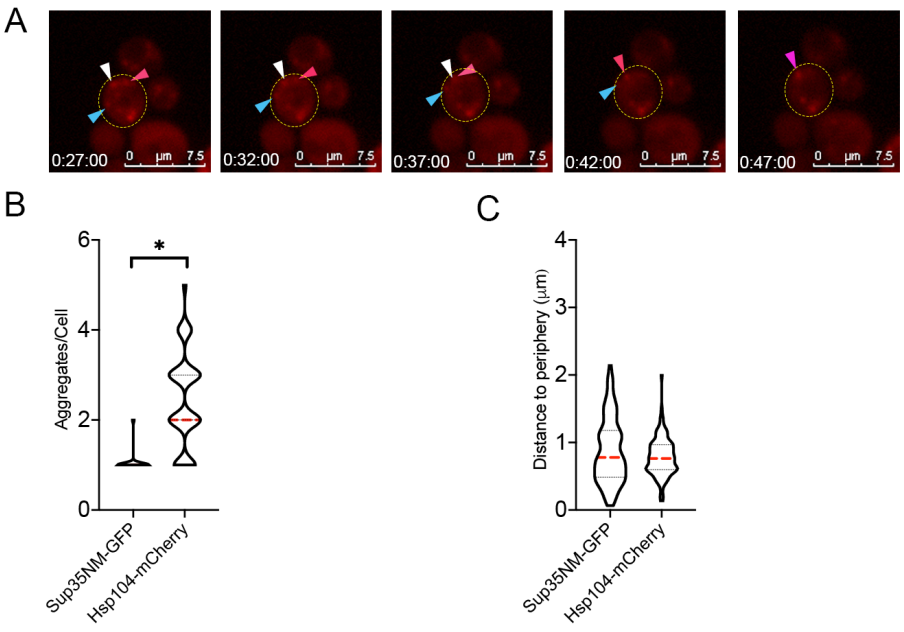

Figure 9.2: Stress Granule Coalescence and Sequestration Compared to Sup35NM-GFP. A. Hsp104-mCherry stress granules were induced in wildtype BY4741 strain cells. 3D-timelapse microscopy was used to record early foci formation, with representative images shown to demonstrate coalescence. Each arrow indicates a separate early foci, with colors merging as foci merge, eventually becoming a purple arrow when all three early foci have coalesced. B. Coalescence was quantified for cells with either Sup35NM-GFP or Hsp104-mCherry induced. T-test was used for comparison (* $p < 0.01$). C. Sequestration was quantified for the same aggregates in B.

should be noted that coalescence still occurs for Hsp104-mCherry foci as observed (Figure 9.2). The increase in aggregate number is more than likely due to the large number of proteins and RNA that is incorporated into stress granules whereas in Sup35NM-GFP induction aggregate formation is mostly due to the transient expression of a single protein. Both aggregates also had similar behavior in the second step of formation, sequestration. Stress granules were localized near the cell periphery (0.79μm) similar to Sup35NM-GFP (0.88μm; Figure 9.2). Taken together, these data suggest that the initial formation of

Hsp104-mCherry associated stress granules exhibit a similar two step formation behavior as Sup35NM-GFP aggregates.

9.2.2: Stress Granule Formation is Effected By Actin Mutation

Similar to Sup35NM-GFP, mobility of Hsp104-mCherry stress granules was decreased in genetic strains with actin mutations. The overall average rate of movement decreased in *act1-122* and *act1-120* strains to 0.24 and 0.28μm/min, respectively (Figure 9.3 and 9.4). During the first ten minutes of formation, the average rate in wildtype was 0.84μm/min, compared to just 0.32μm/min and 0.33μm/min in *act1-122* and *act1-120* respectively. By the third 10 minute interval the average rate in wildtype was 0.34μm/min, while in *act1-122* and *act1-120* the rate hardly changed, decreasing slightly to 0.21μm/min and 0.28μm/min respectively (Table 9.2). The small change in mobility over time for both actin mutants was reflected by a slope that was almost zero (Figure 9.4). These data are very similar to the slope of Sup35NM-GFP aggregates in *act1-122* and *act1*-120 (Table 4.2).

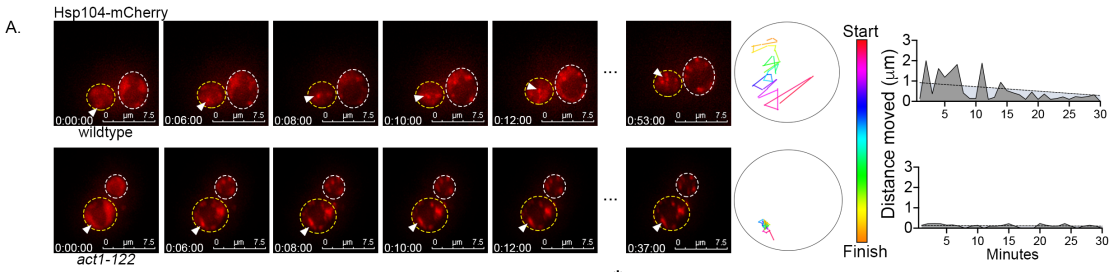

Figure 9.3: Mobility of stress induced Hsp104-mCherry foci in wildtype and *act1-122* strains. A. Stress granule formation was induced in BY4741 wildtype and *act1-122* cells expressing Hsp104-mCherry. 3D-timelapse microscopy was used to record stress foci formation, with representative images shown. A representative particle trace for the white caret marked stress foci in the yellow outlined cell is shown. The rate of movement is shown in the graph on the right, with a trend line with slope representing change in rate over quantification. Slopes were significantly different by MAD analysis.

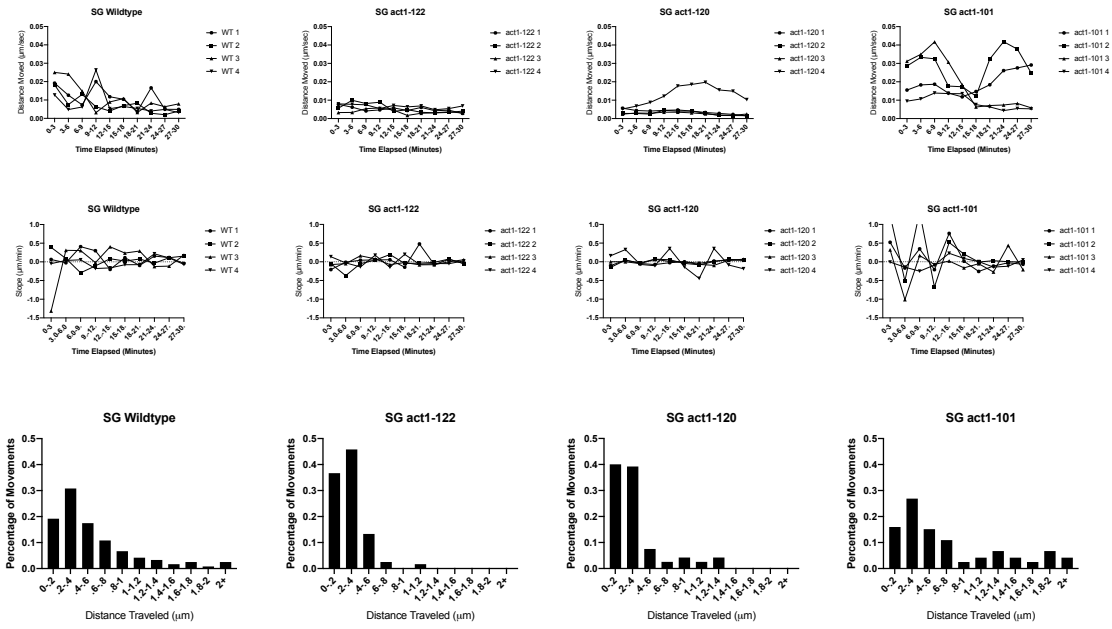

Figure 9.4: Rate of movement quantification in multiple actin mutant strains. Stress granule formation was induced in BY4741 wildtype, *act1-122, act1-120,* and *act1-101* cells expressing Hsp104-mCherry. 3D-timelapse microscopy was used to record stress foci formation, with representative images shown. Top: The Mobility of each individual foci is shown per three minute increment. Middle: The Slope of mobility for each foci is shown every three

minutes. Bottom: The percent of per minute events separated by the distance moved by foci.

	Overall rate Rate (µm/min)	Rate in first 10 minutes	Rate in third 10 minutes	Slope	MAD
Wildtype	0.49 +/- 0.49	0.84 +/- 0.66	0.34 +/- 0.36	-0.019 +/- 0.006	0.25 +/- 0.06
act1-122	0.24 +/- 0.17*	0.32 +/- 0.21*	0.21 +/- 0.16	-0.005 +/- 0.004*	0.09 +/- 0.05
act1-120	0.29 +/- 0.29*	0.33 +/- 0.32*	0.28 +/- 0.28	-0.005 +/- 0.005*	0.14 +/- 0.12
act1-101	0.64 +/- 0.69	1.11 +/- 0.87	0.39 +/- 0.36	-0.028 +/- 0.015	0.40 +/- 0.16

Table 9.2: Quantification of Mobility for Hsp104-mCherry Stress Granules. Statistical Analysis performed using Mann-Whitney Test (* $p < 0.01$).

Meanwhile, *act1-101* increased mobility with a rate of movement during the first 10 minutes of 1.11µm/min, but slowing to 0.39µm/min by the third 10 minute interval. (Figure 9.4, Table 9.2). The change in mobility is reflected by the negative slope for the trendline, and high MAD values indicate that mobility was highly inconsistent over time. Again, the mobility differences of Hsp104-mCherry in the *act1-101* compared to wildtype is similar to observations of Sup35NM-GFP, suggesting that there are similar mechanisms of managing both Sup35NM-GFP and stress granules.

The *act1-122* and *act1-120* strains also showed an increased number of stress granules, and larger distributions in the distance from the cell periphery. While wildtype cells had a median of 2 aggregates per cell, *act1-122* and *act1-120* cells had a median of 3 aggregates per cell after 3-4 hours of stress (Figure 9.5). Some cells had as many as 8 aggregates per cell. These strains also

exhibited a wider distribution of aggregate location from the cell periphery, localizing on average 1.02 and 1.00μm from the cell periphery in *act1-122* and *act1-120* strains (Figure 9.6). Once again, these actin mutants were in contrast to *act1-101*, which did not impact coalescence or sequestration of stress granules. Taken together, the similar quantification of mobility, coalescence, and sequestration of Sup35NM-GFP and Hsp104-mCherry stress granules suggests that the cellular response to newly formed protein aggregates may be a universal response to aggregates associated with Hsp104p.

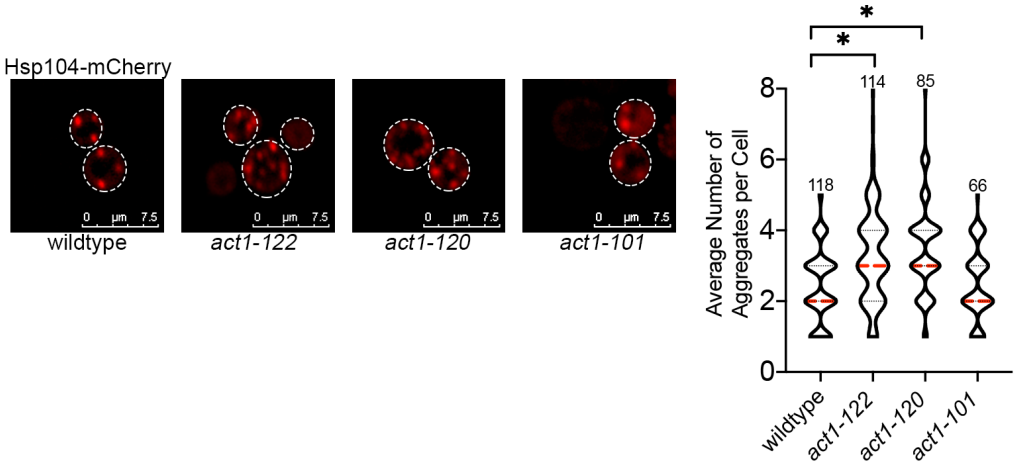

Figure 9.5: Coalescence of Hsp104-mCherry stress granules. Stress granule formation was induced in BY4741 wildtype, *act1-122* , *act1-120*, and *act1-101* cells each expressing Hsp104-mCherry. The number of stress foci per cell was quantified and the average is displayed in the graph. Representative images are also shown for each strain. *act1-122* and *act1-120* strains were significantly different from wildtype by T-test comparison (* $p < 0.01$).

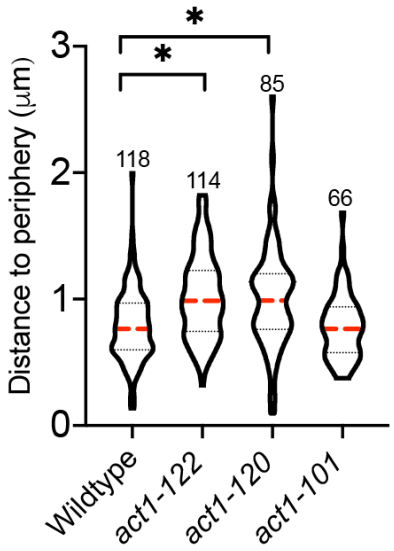

Figure 9.6: Sequestration of Hsp104-mCherry Stress Granules. Stress granule formation was induced in BY4741 wildtype, *act1-122* , *act1-120*, and *act1-101* cells each expressing Hsp104-mCherry. Stress foci localization was quantified using coordinate mapping and is displayed in violin plot. *act1-122* and *act1-120* strains were significantly different from wildtype by T-test comparison. (* p <0.01)

9.3 Discussion

Here I have shown that the formation of Hsp104-mCherry stress granules follows a similar two step process of formation as Sup35NM-GFP aggregates do. For both types of aggregates, formation begins with highly mobile early foci that are capable of coalescing together, and over time become static near the periphery of the cell. The dynamics of formation are also impacted, or reduced, when the actin cytoskeleton is disrupted. Together, this work suggests that both Sup35NM-GFP aggregates and Hsp104-mCherry stress granules are initially managed by similar mechanisms in the cell.

Previous studies have suggested that the formation of stress granules is a multistep process that involves the coalescence of early foci (Kroshwald et al., 2015; Wheeler et al., 2016). My results support a multi-step formation process that involves the mobility and coalescence of early foci. This behavior is also impaired by mutations made to the actin cytoskeleton. While the involvement of the actin cytoskeleton has been implicated previously (Liu et al., 2010; Specht et al., 2011), quantification performed here gives strong evidence that actin does impact the formation of stress granules. Although Zhou et al (2011) proposed that the actin cytoskeleton had an indirect effect on the mobility of stress granules, here my data suggests that actin may have a prominent role in not only the mobility of stress granules, but also in coalescence and sequestration. Given the similarity in behavior between stress granules and Sup35NM-GFP aggregates, it could be possible that actin is responsible for providing the network by which newly formed aggregates are trafficked.

It is unclear whether Hsp104p serves a multifunctional role in the chaperones association with both Sup35NM-GFP aggregates and stress granules. While it is established that Hsp104p is necessary for the reversible nature of stress granules, the chaperone may also function to associate aggregates with cellular response machinery. Recent work suggests that Hsp104p plays a role in the remodeling of the actin network. Tessarz et al. (2009) found that Hsp104p interacts directly with the machinery used to remodel the actin cytoskeleton, and degradation of Hsp104p from the cell results in perturbation of the actin network. It is possible that Hsp104p interacts with the

actin network to link protein aggregates to a distinct site in the cell, that is impaired in actin mutants. What role Hsp104p plays in the formation of protein aggregates should be explored further to better understand the cellular mechanisms used. While humans do not possess a homolog to Hsp104p, it is possible that other factors in protein quality control are involved to manage protein aggregate formation, and this work will provide the foundation to understand what the other factors may be unlocking knowledge into the progression of protein aggregate related diseases.

Chapter 10: Characterization of TDP-43 Aggregate Formation

10.1 Introduction

In the previous chapters, I observed that the behavior of Sup35NM-GFP and stress granules are similar, undergoing a 2-step formation process that appears to be dependent upon actin networks. However, Hsp104p is required for both Sup35NM-GFP aggregate formation and stress granule formation (Sanchez and Lindquist, 1990; Cherkosov et al., 2013). To understand whether Hsp104p plays an important role in this 2-step process, it is important to test protein aggregates that form independently of Hsp104p. The goal of this chapter is to observe the formation of TDP-43 protein aggregates, which form independent of Hsp104p, and use quantification of TDP-43 aggregate formation to better understand the role of Hsp104p in the management of newly formed protein aggregates.

TDP-43 is the human TAR DNA binding protein linked to sporadic amyotrophic lateral sclerosis (Arai et al, 2006; Newmann et al., 2006). While the protein is not endogenous to yeast, a humanized yeast model was first used by Johnson et al (2008) in an effort to better understand localization and aggregation of the protein within an *in vivo* cellular system. These studies found that expression of TDP-43 in yeast results in both cytoplasmic aggregates and cytotoxicity (Johnson et al., 2008).

While both Sup35NM-GFP and TDP-43 both form cytoplasmic aggregates, TDP-43 aggregates are different. TDP-43p does not form aggregates that are amyloid in character, nor are they SDS-resistant (Johnson et

al., 2008). The formation of visual aggregates also does not require Hsp104p, as *hsp104Δ* strains are able to form TDP-43 aggregates that continue to exhibit toxicity (Johnson et al., 2008). However, the formation of aggregates has never been characterized, leaving the role or involvement of Hsp104p in managing aggregate formation unclear. The behavior of newly formed TDP-43 aggregates will provide insight into whether actin networks play a role in managing many different types of newly formed aggregates, and determine the role of Hsp104p on the initial cellular response to protein aggregate formation.

Here, I investigate the dynamics of TDP-43-YFP aggregate formation. Results indicate that the formation of TDP-43 aggregates is a 2-step process, similar to Sup35NM-GFP and stress granules. While somewhat muted, the behavior of TDP-43 aggregates is changed in actin mutants and cells lacking Hsp104p, suggesting a potential role for both the actin network and the molecular chaperone in the initial management of aggregates. This work helps enhance our understanding of the formation process of protein aggregates and the requirements for cellular mechanisms to manage aggregation.

10.2 Results

10.2.1 TDP-43-YFP Aggregate Formation Follows the 2-Step Behavior Previously Observed

A galactose inducible plasmid containing TDP-43-YFP was introduced into the BY4741 genetic background. Strains grown in galactose form TDP-YFP aggregates upon within 3 hours. 3D-time-lapse recordings indicated that newly

formed TDP-43-YFP aggregates were highly mobile (Figure 10.1), with an average overall rate of 0.98μm/min (Table 10.1). At first glance, the rate is higher than the average for both Sup35NM-GFP and Hsp104-mCherry (0.66μm/min and 0.49μm/min respectively). When the rate was analyzed in 10-minute segments, TDP-43 is remained mobile both in the first (1.08μm/min) and third 10-minute interval (0.95μm/min; Table 10.1). In contrast, Sup35NM-GFP and stress granules have considerably less mobility in the third 10-minutes. However, the average slope of the trendlines was still negative, as evidence by the decreased rate between the first ten minutes and third ten minute interval (Table 10.1). MAD values (0.54) also indicate that the rate of movement varied largely from the trendline, suggesting that mobility was not constant. Together, while TDP-43-YFP aggregates display a faster rate of movement compared to Sup35NM-GFP and stress granules, yet the aggregates continue to slows down over time through formation, albeit on a longer timescale. The faster rate and smaller decrease over time is could be due to the constant overexpression of TDP-43-YFP resulting in a large amount of protein that the cell is constantly attempting to incorporate into new aggregates. This constant expression is different from Sup35NM-GFP, which is transiently expressed. It is also possible that the cell is not as efficient in recognizing and/or sequestering an expressed heterologous protein.

While the mobility of TDP-43-YFP aggregates deviated from Sup35NM-GFP and Hsp104-mCherry, both coalescence and sequestration were nearly identical. Cells had a median of 1 TDP-43-YFP aggregate, which was localized

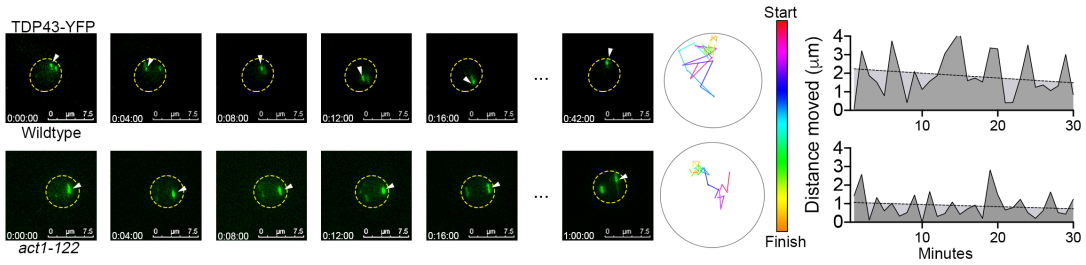

Figure 10.1: Mobility of TDP-43-YFP aggregates in wildtype and *act1-122* strains. TDP43-YFP was induced in High [*PIN*$^+$] BY4741 wildtype and μd [*PIN*$^+$] BY4741 *act1-122* cells. Strains were imaged in 3D-timelapse with representative images from a single timelapse shown. A particle trace representative of the white caret marked aggregate in the blue outlined cell is shown. The rate of movement is shown in the graph on the right, with a trend line with slope representing change in rate over quantification.

	Overall rate Rate (μm/min)	Rate in first 10 minutes	Rate in third 10 minutes	Slope	MAD
Sup35NM-GFP	0.66 +/- 0.5	1.2 +/- 0.52	0.47 +/- 0.38	-0.028 +/- 0.007	0.30 +/- 0.06
Hsp104-mCherry	0.49 +/- 0.49*	0.84 +/- 0.66*	0.34 +/- 0.36	-0.019 +/- 0.006	0.25 +/- 0.06
TDP-43-YFP	0.98 +/- 0.84*	1.08 +/- 0.89	0.95 +/- 0.71*	-0.010 +/- 0.009*	0.54 +/- 0.21

Table 10.1: Mobility Comparison of Different Protein Aggregates. Statistical analysis comparison to Sup35NM-GFP was performed by Mann-Whitney test (* $p < 0.$)

on average 0.75μm from the periphery (Figure 10.2). This similar behavior suggests that the coalescence and sequestration of TDP-43-YFP aggregates in wildtype conditions are very similar to Sup35NM-GFP and stress granules, suggesting that similar mechanisms may be at play for the initial cellular response to general aggregate formation.

10.2.2 Formation of TDP-43-YFP Aggregates in Actin Mutants

Since TDP-43-YFP a 2-step formation process, I investigated whether formation would also be impaired by disruption to the actin cytoskeleton similar to Sup35NM-GFP. Mobility was drastically reduced in *act1-122* and *act1-120* mutants (0.77 and 0.74μm/min respectively; Figure 10.1 and 10.3). Similar to Sup35NM-GFP and stress granules, the mobility observed in *act1-122* hardly changed throughout recording, representing the constant, static positioning of the aggregate. *act1-120* however, exhibited a decrease in mobility that was larger in magnitude than wildtype. The mobility in *act1-101* strains was similar to wildtype at 1.04μm/min overall, although the rate during the first 10 minutes interval was much higher than mobility in wildtype cells (Table 10.2).

Coalescence and sequestration were also quantified for TDP-43-YFP aggregates. As expected based on results with Sup35NM-GFP and Hsp104-mCherry, *act1-122* and *act1-120* cells contained a median of 2 aggregates per cell, with localization of 1.14μm and 0.92μm from the periphery for *act1-122* and *act1-120* respectively (Figure 10.4 and 10.5). In contrast, the *act1-101* strains contained a median of 1 aggregate per cell localized 0.72μm from the cell

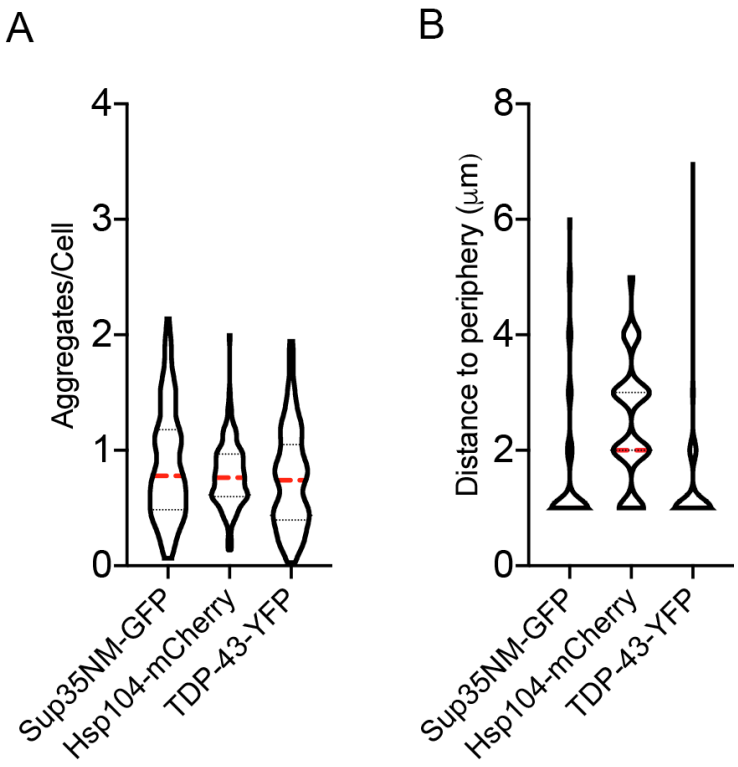

Figure 10.2: Coalescence and Sequestration of Newly Formed Aggregates. A. Sup35NM-GFP, Hsp104-mCherry, and TDP-43-YFP aggregate formation was induced in BY4741 wildtype strain cells. The number of aggregates per cell was quantified and is displayed. B. The same aggregates counted in A were quantified for spatial localization to the cell periphery. Statistical analysis was performed using T-test to Sup35NM-GFP.

	Overall rate Rate (μm/min)	Rate in first 10 minutes	Rate in third 10 minutes	Slope	MAD
Wildtype	0.98 +/- 0.84	1.08 +/- 0.89	0.95 +/- 0.71	-0.010 +/- 0.009	0.54 +/- 0.21
act1-122	0.77 +/- 0.57*	0.84 +/- 0.67	0.79 +/- 0.53	-0.004 +/- 0.010	0.41 +/- 0.08
act1-120	0.74 +/- 0.49*	0.89 +/- 0.63	0.55 +/- 0.27*	-0.018 +/- 0.020	0.37 +/- 0.12
act1-101	1.04 +/- 0.80	1.33 +/- 0.84	0.87 +/- 0.70	-0.020 +/- 0.010	0.55 +/- 0.18

Table 10.2: TDP-43-YFP Mobility Quantification in Wildtype and Actin Mutant Strains. Statistical analysis comparison to Sup35NM-GFP was performed by Mann-Whitney test (* $p < 0.01$).

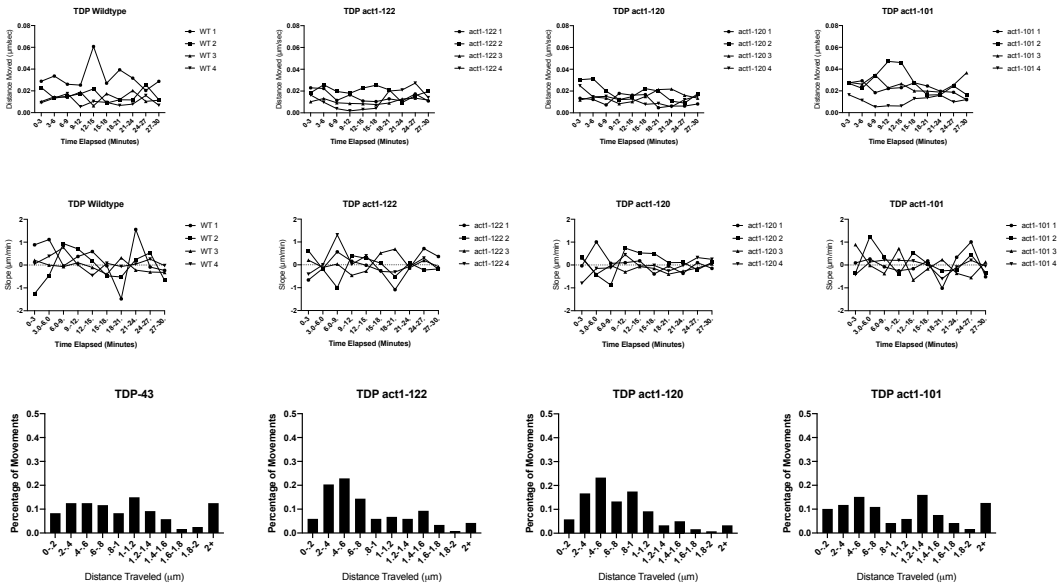

Figure 10.3: Mobility of TDP-43-YFP in actin mutant strains.TDP43-YFP was induced in High [*PIN*$^+$] BY4741 wildtype, *act1-120*, and *act1-101,* and μd [*PIN*$^+$] BY4741 *act1-122* cells. Strains were imaged in 3D-timelapse and the rate of movement for four individual cells was quantified for each. Top: Mobility for individual foci is graphed per three minute increments of recordings. Middle: The slope of the mobility of each individual foci is graphed per three minute increments of recording. Bottom: The distance moved for each foci per minute was recorded and binned by length, and is represented by the percent of events per distance moved.

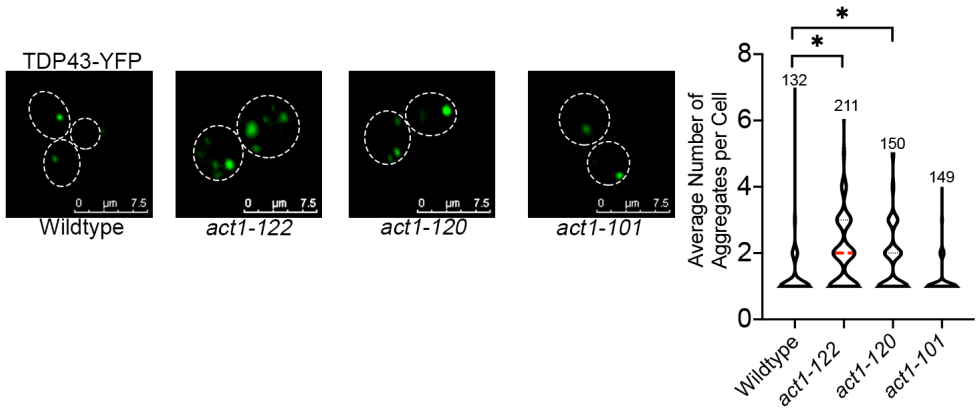

Figure 10.4 Coalescence of TDP-43-YFP aggregates in wildtype and actin mutants. TDP43-YFP was induced in High [*PIN*$^+$] BY4741 wildtype, *act1-120*, and *act1-101,* and µd [*PIN*$^+$] BY4741 *act1-122* cells. The number of protein aggregates per cell was quantified and the average is displayed in the graph. Representative images are also shown for each strain. T-test analysis showed significant difference between the wildtype strain, and *act1-122* and *act1-120* strains (* $p < 0.01$

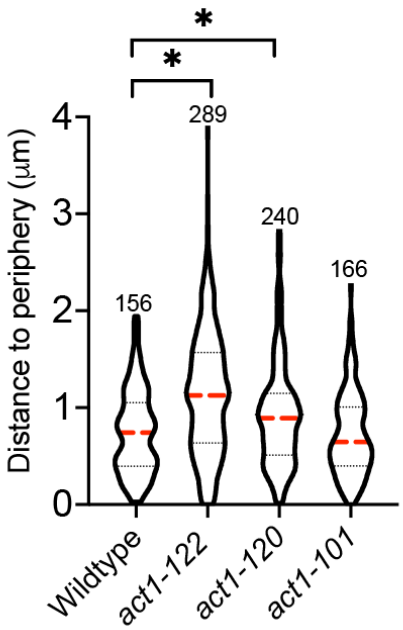

Figure 10.5: Sequestration of TDP-43-YFP Aggregates in wildtype and actin mutant strains. TDP43-YFP was induced in High [*PIN*$^+$] BY4741 wildtype, *act1-120*, and *act1-101,* and μd [*PIN*$^+$] BY4741 *act1-122* cells. Protein aggregate localization was determined in each strain by coordinate mapping, and is displayed in the violin plot. Wildtype was significantly different from *act1-122* and *act1-120* strains by T-test analysis. (* p<0.01)

periphery (Figure 10.4 and 10.5), which was similar to wildtype. Together, the change in aggregate formation suggests that both the formation of TDP-43-YFP aggregates, as well as Sup35NM-GFP and stress granules, with an intact actin cytoskeleton required for proper behavior.

10.2.3 TDP-43-YFP Aggregate Formation is Independent of [*PIN*$^+$] in *act1-122* strains

The formation of Sup35NM-GFP aggregates is dependent on the presence of [*PIN*$^+$], but are not toxic. Cells containing TDP-43p aggregates are

toxic regardless of the [*PIN*$^+$] state (Johnson et al., 2008), however, toxicity appears to be worse in [*PIN*$^+$] strains (Park et al., 2017). Therefore, I wanted to confirm that the behavior observe of TDP-43-YFP aggregates was not a product of our cells containing [*PIN*$^+$] and the possible interaction between them. I found that in [*pin*$^-$] strains, the number of TDP-43-YFP aggregates was consistent with my previous wildtype results (Figure 10.6). Localization of aggregates to the cell periphery was also unchanged between [*PIN*$^+$] and [*pin*-] cells. I also observed that *act1-122* mutants lacking [*pin*-] still have an increased number of aggregates and wider distribution of peripheral localization than wildtype [*pin*-] cells. Since TDP-43-YFP aggregation appeared unchanged in [*pin*-] cells suggests that [*PIN*$^+$] does not play a role in the formation and aggregation of TDP-43.

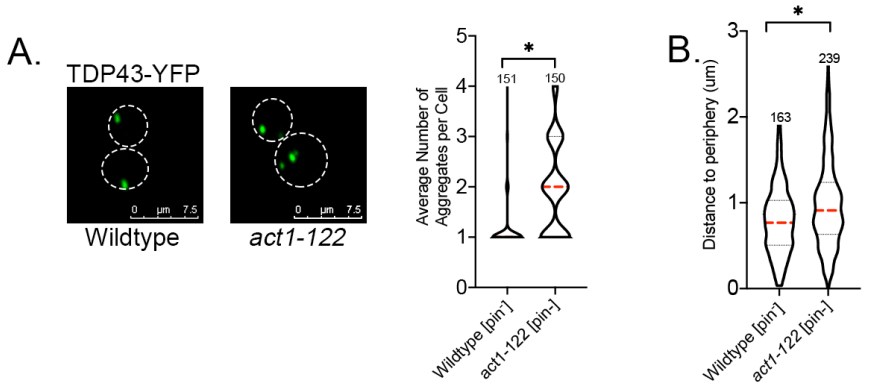

Figure 10.6: The Presence of [PIN+] does not affect TDP43p aggregate dynamics. A. TDP43-YFP was induced in [pin$^-$] BY4741 wildtype and *act1-122* strains. Representative images are shown. The average number of protein aggregates per cell was quantified and is displayed. T-test analysis was used to show significant difference between wildtype and *act1-122* strains. B. Protein aggregate localization was quantified using coordinate mapping. Wildtype and *act1-122* were significantly different by T-test analysis. (* p<0.01)

10.2.4 Hsp104p Impacts Early Foci Formation of TDP-43-YFP

Although previous work has suggested that TDP-43 aggregates are independent of Hsp104p, I wanted to test whether Hsp104p had a role in the behavior of newly formed aggregates. First, I asked whether TDP-43 and Hsp104p are co-localized. Cells containing TDP-43-YFP aggregates did not have distinct Hsp104-mCherry foci supporting a lack of interaction (Figure 10.7). In fact, most cells contained diffuse Hsp104-mCherry fluorescence suggestive that the chaperone was not accumulating at any particular site in these cells.

Next, I tested whether TDP-43 aggregates exhibit the 2-step behavior without Hsp104p, I turned to an *hsp104Δ* strain and quantified the dynamics of aggregate formation. If Hsp104p was required for mobility, then loss of *HSP104* would lead to decreased mobility of TDP-43 aggregates. The average rate of movement in the deletion strain was 0.58 μm/min, which is much lower than the average rate of movement in the wildtype strain (Figure 10.8). During the first 10 minutes of appearance the rate of movement in the *hsp104Δ* strain was 0.89μm/min and slowed to 0.30μm/min by the third 10 minute interval. The rate of movement, slope in trend, and MAD value are all different for the *hsp104Δ* strain compared to wildtype (Table 10.3). Since the mobility of TDP-43-YFP aggregates is much different in the *hsp104Δ* strain, this difference suggests that while Hsp104p may not be necessary for the formation of aggregates, the chaperone does have an important role in the behavior of aggregates.

The coalescence of aggregates was also impaired in the *hsp104Δ* strain. Cells contained a median of 2 aggregates per cell, double the number of

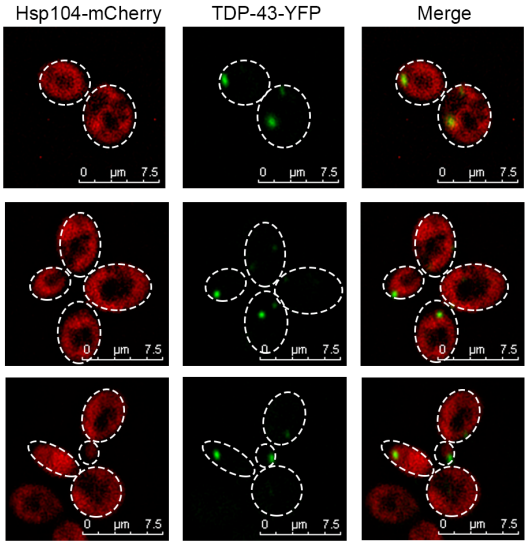

Figure 10.7: TDP-43-YFP does not localize with Hsp104-mCherry. TDP-43-YFP aggregates were induced in wildtype BY4741 cells expressing Hsp104-mCherry. Cells were imaged and assess for colocalization between the two proteins. PCC was not used for quantification as cells containing TDP-43-YFP aggregates contained only diffuse Hsp104-mCherry and artificially show colocalization.

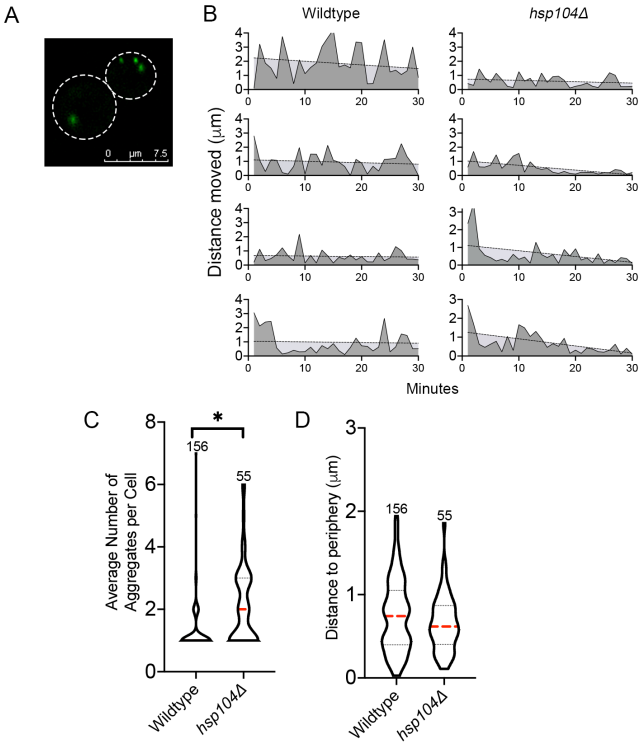

Figure 10.8: Quantification of TDP-43-YFP Formation in *hsp104Δ* strains. A. TDP-43-YFP was induced in *hsp104Δ*. A representative image is shown. B. Strains were imaged in 3D-timelapse and the rate of movement for four individual cells was quantified for each. Graphs for each strain are shown with trend line. C and D. TDP-43-YFP was induced in Wildtype and *hsp104Δ* strains. The number of aggregates per cell was quantified and is shown above. The localization of aggregates was also quantified by measuring the distance to the periphery for each. Statistical analysis was performed using Students T-Test (* $p < 0.01$).

	Overall rate Rate (μm/min)	Rate in first 10 minutes	Rate in third 10 minutes	Slope	MAD
Wildtype	0.98 +/- 0.84	1.08 +/- 0.89	0.95 +/- 0.71	-0.010 +/- 0.009	0.54 +/- 0.21
hsp104Δ	0.58 +/- 0.52*	0.90 +/- 0.71	0.30 +/- 0.23*	-0.029 +/- 0.013	0.37 +/- 0.06

Table 10.3: Quantification of Mobility of TDP-43-YFP aggregates in *hsp104Δ*. Statistical analysis comparison to Sup35NM-GFP was performed by Mann-Whitney test (* $p < 0.01$).

aggregates observed in wildtype strains (Figure 10.8). Previous work that showed TDP-43p still formed aggregates in *hsp104Δ* strains only qualitatively compared the appearance of aggregates (Johnson et al., 2008), potentially overlooking the effect Hsp104p has on aggregate formation. Interestingly, both mobility and coalescence of TDP-43-YFP in *hsp104Δ* strain is similar to TDP-43 mobility and coalescence in *act1-122* and *act1-120* strains, suggesting that the Hsp104p and actin may serve similar roles during the formation of protein aggregates.

The distance to the periphery was also quantified in *hsp104Δ* strains. TDP-43-YFP aggregates were localized 0.66μm from the cell periphery, similar to aggregates in wildtype localized 0.75μm from the periphery (Figure 10.8). The normal localization of aggregates suggests that Hsp104p does not play a role in the second step of formation, however given that the deletion strain effects both mobility and coalescence, Hsp104p may have a role in the first step of aggregate formation.

10.3 Discussion

In this chapter I investigated the formation of TDP-43-YFP aggregates. Although there were subtle differences in quantification between Sup35NM-GFP and Hsp104-mCherry stress granules, TDP-43-YFP displayed a similar trend in behavior. Aggregate formation started with high mobility that was lost over time as aggregates coalesced, eventually localizing near the cell periphery. The first step of formation is impaired by both mutations to actin or disruption of Hsp104p.

However, only actin alters the sequestration of TDP-43-YFP aggregates. Together this work suggests that both actin and Hsp104p are involved in the initial response of protein aggregates, while peripheral localization may be the result of an unknown mechanism that is also actin dependent.

The behavior of TDP-43-YFP aggregate formation has not been characterized previously. While work before has investigated the presence of aggregates and toxicity, the data here represents the first quantification of TDP-43-YFP aggregate formation. As described, aggregates displayed characteristic behavior for the initial appearance of protein aggregates based on my previous work. Sup35NM-GFP, stress granules, and TDP-43-YFP aggregates each initially appear as mobile early foci that are capable of coalescing together. After a short period of time aggregates become static at the cell periphery. The actin cytoskeleton appears to impact step 1 for all three aggregate types, but only step 2 for Sup35NM-GFP and stress granules. Together, this work suggests that the initial formation of protein aggregates is managed by an actin dependent process that may be part of a general response to aggregate formation.

The ability of TDP-43-YFP to aggregate was shown previously to be independent of Hsp104p (Johnson et al., 2008), and my results support this claim (Figure 10.6). However, my work also suggests that Hsp104p does play a role in managing aggregate formation. Unlike previous studies, I quantified the formation of TDP-43-YFP aggregates in cells with and without Hsp104p. Cells lacking Hsp104p had altered dynamics of aggregate formation. The change in formation suggests that while TDP-43-YFP forms aggregates without Hsp104p,

the chaperone plays a role in the cellular response to newly formed TDP-43 aggregates. It is possible that Hsp104p facilitates interaction between protein aggregates and the actin cytoskeleton as disruptions of either alter step one of formation similarly. Hsp104p associated stress granules have been shown to have localization changes in disruption strains of Vac17p or Vps1p (Hill et al. 2016; Kumar et al., 2017). Similarly, mutation to Myo2p to prevent the binding of Vac17p has similar effects on Hsp104p aggregates (Hill et al., 2016; Bockler et al., 2017). Both Vac17p and Vps1p interact with Myo2p to facilitate cargo binding. Taken together, Hsp104p may facilitate interaction between protein aggregates and a protein such as Vac17p or Vps1p, which allows interaction with Myo2p for trafficking along the actin cytoskeleton.

Overall, this chapter has demonstrated that yet another type of protein aggregate follows a similar 2-step process of formation that is impacted by the actin cytoskeleton. Further work is needed to identify what other players are involved in this mechanism and what role they play, such as Hsp104p, to fully understand how the cell is responding to the formation of protein aggregates. Knowing how the cell responds to the formation of protein aggregates may provide clues as to why older cells struggle to manage aggregates and why the formation of protein aggregates is often associated with disease.

Chapter 11: Discussion

11.1: Summary

This dissertation further characterized the behavior and dynamics of newly formed protein aggregates in yeast. Innovative quantifiable techniques to measure the two-step process of aggregate formation were established (Chapter 3). To do this two different wildtype strains were quantified, both having similar aggregate behavior although subtle differences were found in consequence of aging disparities. Using the quantification of wildtype as a baseline, disruption of the actin cytoskeleton was found to impair the dynamics of both step 1 and 2 of formation (Chapter 4). Similarly, mutations to Myo2p disrupted step 1 of aggregate formation (Chapter 5), but not step 2, suggesting that the Myo2p motor protein is necessary for early foci dynamics but not peripheral sequestration. Subsequent work shows that contrary to previous reports, newly formed aggregates are not localized to protein inclusions (Chapter 7) or the surface of distinct organelles (Chapter 8), but rather simply to the periphery of the cell to an undefined location. Here, this final chapter discusses the implications of the results described on the current state of the field, and provides potential future experiments that will help further this knowledge.

11.2: Overall Mechanism

11.2.1 Actin-Myosin Mediated Step 1

Mutations to either actin (Chapter 4) or Myo2p (Chapter 5) decreased the mobility and coalescence of newly formed Sup35NM-GFP aggregates observed

using 3D time-lapse microscopy. Both Hsp104-mCherry stress granules (Chapter 9) and TDP-43-YFP aggregates (Chapter 10) had similar alterations to behavior in mutant yeast strains. My work supports the role of actin and Myo2p on early foci dynamics of stress granules that was previously proposed (Liu et al., 2010; Specht et al., 2011, Zhou et al., 2011; Hill et al., 2016; Bockler et al., 2016). While the effects of mutations to actin or Myo2p are consistent in my study and with others, it remains unclear how exactly early foci behavior is impacted by actin cytoskeleton trafficking mechanisms.

Recent work has explored the relationship between heat induced protein aggregates and Myo2p, finding that a potential interaction between the aggregate and Myo2p exists through an intermediate protein such as Vac17p or Vps1p (Hill et al., 2016; Kumar et al., 2017). Mutations to Myo2p that prevent interaction with Vac17p was found to alter the inheritance of heat induced protein aggregates (Hill et al., 2016; Bockler et al., 2016), suggesting that there may be an association of aggregates either to the vacuole or the intermediate protein directly. Association to the vacuole is unlikely, as I did not observe localization between aggregates and the vacuole (Figure 6.5), therefore it seems likely that newly formed protein aggregates are capable of associating with an intermediate protein to facilitate mobility and coalescence through a mechanism other than organelle attachment.

Both Sup35NM-GFP and stress induced aggregates are highly associated with the chaperone protein Hsp104p. It is possible that Hsp104p facilitates the interaction between protein aggregate and intermediate protein to be trafficked

along the actin-myosin network. This proposed mechanism involving Hsp104p to facilitate interaction with the actin-myosin network is supported by observations that the mobility and coalescence of TDP-43-YFP aggregates is impaired in the absence of Hsp104p (Figure 10.7 and Table 10.2), which does not require Hsp104p for formation suggesting that Hsp104p is important for step 1 of aggregate formation regardless of necessity. Hsp104p may associate with newly formed protein aggregates at or before their visualization, and facilitate interaction with an unknown protein that links the protein aggregate complex to Myo2p for trafficking along the actin cytoskeleton (Figure 11.1A). Further work will be necessary to understand how Hsp104p is able to interact with Myo2p and potentially facilitate the mobility of newly formed protein aggregates.

11.2.2: Actin Mediated Step 2

The second step in the formation of protein aggregates is peripheral localization, or sequestration. Sharma et al (2017) described the static localization of newly formed Sup35NM-GFP aggregates as being at the periphery of the cell, but was not able to quantify this localization. My work suggests that regardless of aggregate type, newly formed aggregates are indeed localized near the periphery of the cell consistently. Previous work suggested that Sup35NM-GFP aggregates localized to the protein deposit IPOD (Tyedmers et al., 2010), however this localization did not seem likely as association of IPOD to the vacuole would mean the inclusion would not always be consistently localized. Consistent with this notion, I found that newly formed aggregates were not

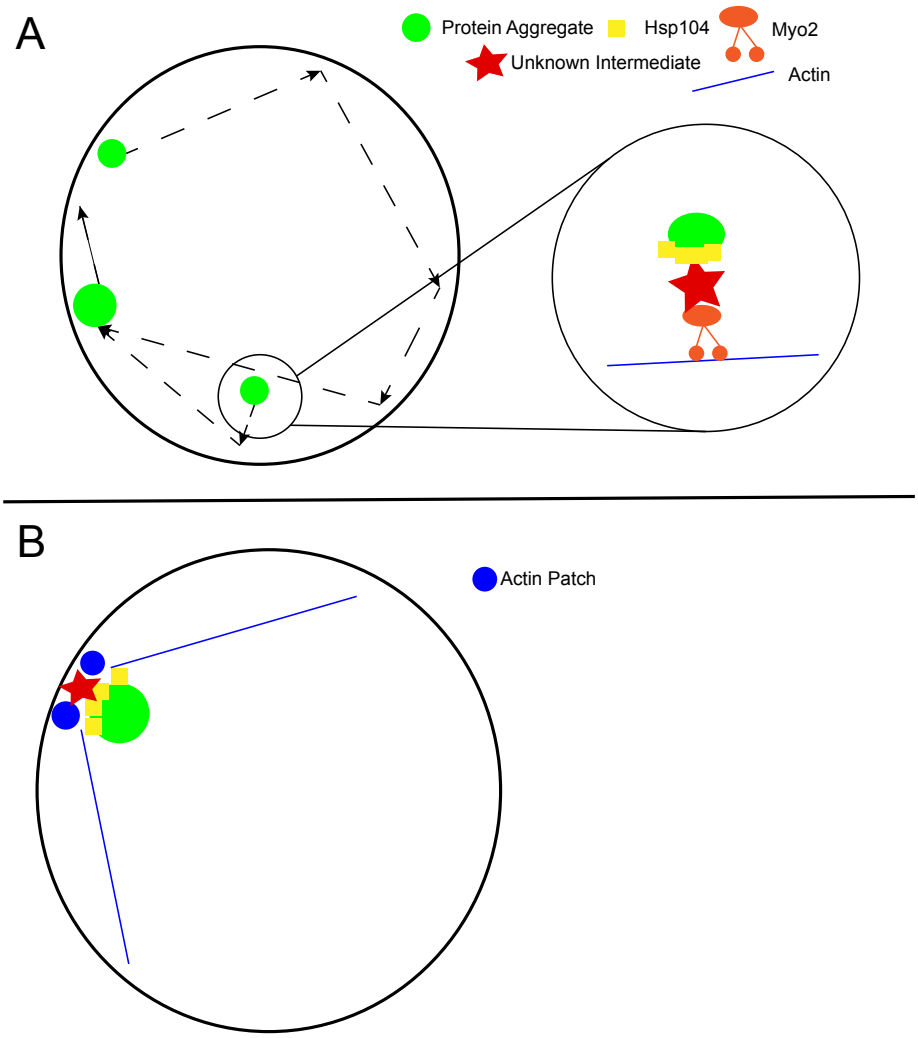

Figure 11.1: Current Model of Step 1 and 2 of Protein Aggregate Formation. A. Early foci are highly mobile in the cell, with the potential to coalesce into a larger aggregate that can remain mobile for some time. The insert shows the proposed association of the early foci with the actin-Myo2p complex, mediated through Hsp104p interaction and an unidentified protein. B. In step 2 of formation, aggregates are localized to the cell periphery, and this localization is dependent on actin, and Hsp104p remains associated with the aggregate. It is unclear however what the association between the aggregate, actin, and Hsp104p are at this point.

localized to any previously defined protein inclusion, including IPOD (Chapter 6), and the consistent localization suggests that Sup35NM-GFP incorporation into IPOD is unlikely initially. Although, it is possible that long after the initial formation of aggregates they are moved to a specialized inclusion, such as IPOD. Mathur et al (2009) described Sup35NM-GFP formation as being peripheral as I have, however over time they found that aggregates are sequestered into the cell by the vacuole, suggesting that the peripheral localization that I observe is only part of the initial response.

Interestingly, despite the static localization, mutations to the actin network that impacted step 1 also alter the peripheral localization of aggregates. Disruption with pharmacological agents in cells with Sup35NM-GFP aggregates resulted in a change of localization, suggesting that the actin cytoskeleton is necessary for maintaining peripheral localization (Chapter 4). Mutations to Myo2p did not alter aggregate localization (Chapter 5), suggesting that the motor protein is only involved in step 1 of formation.

The mechanism by which the actin cytoskeleton impacts the localization of newly formed protein aggregates is undetermined. It is possible that protein aggregates are localized to unoccupied space in the cell, but mutations to actin may cause changes to the localization of organelles and other cellular components. These changes may be enough to alter where and if any unoccupied space in the cell exists, therefore altering localization of the protein aggregate.

It is also possible that the localization of aggregates is determined more directly to the actin cytoskeleton. Disruptions to cortical actin patch proteins decreases the formation of Sup35NM-GFP aggregates, however are also associated with an increase in toxicity with induction (Ganusova et al., 2006), suggesting that there is a link between cortical actin and protein aggregates. It is possible cortical actin is used to hold protein aggregates to a single site at the periphery of the cell until protein quality control is able to manage the aggregates through a different pathway. Heat induced aggregates have been proposed to be tethered by actin to deposition sites given the requirement of actin for asymmetric inheritance and localization (Song et al., 2014). Given our understanding of the mechanism of step 1 of formation, protein aggregates may be trafficked along actin networks to dense actin patches at the periphery of the cell, where aggregates remain associated with the actin patch for static localization through an unknown interaction (Figure 11.1B). Given that improper localization of aggregates can lead to enhanced toxicity, furthering our understanding of the mechanisms behind sequestration of protein aggregates is necessary. Identification of where protein aggregates localize at the periphery of the cell may help define how protein aggregates are managed.

11.2.3: Age-Related Decline in Managing Protein Aggregates

Many protein aggregate related diseases are prevalent in an aging population, and this is reflected in studies of protein aggregate biology. Older cells or those with genetic disruptions that mimic accelerated aging in yeast,

contain more protein aggregates and loss of asymmetric inheritance of protein aggregates during cell division (Erjavec et al., 2007; Speldewinde et al., 2017). Similarly, I found that in the 74D-694 background cells that had gone through many cell divisions had more protein aggregates than those who had rarely divided, suggesting a role of age in managing protein aggregates (Chapter 3). Although wildtype BY4741 did not display this effect, this genetic background with mutations to the actin cytoskeleton did (Chapter 4). Given that the number of protein aggregates in the cell appears to be mostly impacted by age, one might infer that step 1 of aggregate formation is impaired by an age related effect. This age effect could be related to the actin cytoskeleton, which when impaired results in more aggregates per cell in older cells, and since the actin cytoskeleton is necessary for proper coalescence. It is possible that finding a mechanism by which to enhance the robustness of the actin cytoskeleton would counteract the reduction of coalescence observed in older yeast strains, and could decrease toxicity associated with protein aggregation. Determining whether the number of protein aggregates influences the toxicity associated to aggregation will help future understanding of the implications of age related effects.

11.3: Comparison of Different Aggregate Types

As described in Chapter 1, there are three main methods to induce protein aggregation in yeast: overexpression, stress, and heterologous expression. In this study I quantified the formation of a protein aggregate from each of the three different methods of aggregation expression (Hsp104-mCherry stress granules,

Sup35NM-GFP, and TDP-43-YFP). Since the expression for these aggregates is different, the behavior of each is expected to be different. Hsp104-mCherry stress granules form rapidly within minutes of the addition of chemical stress, while Sup35NM-GFP aggregates take the longest of the three to form at 12-16 hours for visible early foci. TDP-43-YFP forms aggregates at an intermediate rate compared to the other two, forming in just a couple of hours from initial expression. Given these differences in the rate of formation, it was expected that the behavior of the aggregates might be different. Stress granule formation is so fast and incorporates a large portion of cytosolic components, that it may be difficult for the cell to respond to and manage each of the early foci that appear, whereas the slow formation rate of Sup35NM-GFP should be much easier for the cell to act on. TDP-43-YFP is constantly overexpressed to ensure there is always protein available in the cell to aggregate, but this overexpression combined with the protein being non-endogenous to yeast may make it difficult to respond to or even recognize. Despite these differences, all three aggregates generally had similar formation behavior: mobile early foci that slowed over time, coalescence of early foci, and peripheral localization.

Given a similar initial behavior in the cell, it seems likely that the same cellular mechanism is responsible for recognizing and responding to aggregate formation. I suspect that the chaperone Hsp104p is an important part of this initial cellular response. Without Hsp104p, TDP-43-YFP aggregates have reduced mobility and coalescence, suggesting a role for the chaperone in step 1 of formation. However, neither Sup35NM-GFP or stress granule formation can be

quantified in cells lacking Hsp104p due to requirements for formation. As previously described, Hsp104p may facilitate interaction between protein aggregate and the trafficking machinery in yeast.

Aggregate recognition may also be associated with sHSP's. In fission yeast, Hsp16p is necessary for aggregate fusion and asymmetric inheritance of stress induced aggregates (Coelho et al., 2014). Similarly, in budding yeast Hsp42p and Hsp26p have proposed roles in aggregate recognition and localization (Specht et al., 2011; Malinovska et al., 2012). However, my data suggests that Hsp42p is not involved with Sup35NM-GFP aggregate formation. Rather, the Hsp104p co-chaperone Ssa1p is known to recruit Hsp104p to protein aggregates (Winkler et al., 2012). It is possible that Ssa1p initially recognizes the formation of protein aggregates, and subsequently recruits Hsp104p to facilitate interaction with the trafficking mechanism for proper management of the aggregate. Identifying how protein aggregates are initially recognized in the cell may be difficult to assess as recognition may take place prior to visualization of aggregates. Given the association of Hsp104p with Sup35NMp aggregates at the initial appearance of aggregates, this suggests that the cellular response to protein aggregate formation is prior to visualization. While biochemical methods can be used to interpret aggregate association prior to visualization, current techniques do not allow for a reliable approach to address this question or understand the mechanism by which aggregates would be recognized by the cell.

11.4: Implications

As described previously, the quantitative techniques used to describe the behavior of aggregate formation are novel. Previous studies have investigated the formation of protein aggregates, but not to the extent that I have done here. These techniques set the stage for future experiments and expanded use of 3D time-lapse microscopy to explore the behavior of different processes in yeast. This quantification will be extremely useful in understanding the mechanisms of aggregate formation beyond what I have described here. However, it is feasible that these same methods can be applied to other mechanisms of yeast cellular biology. Processes such as autophagy or the inheritance of organelles can now be quantified in real time for their behavior, and enhance our understanding of these cellular mechanisms.

The two-step behavior of protein aggregate formation described here will also be influential in creating more targeted experiments in the future to understand protein aggregate associated disease. Similar to protein aggregates in yeast, aggresomes in mammalian cells have been found to be trafficked by dynein motor proteins along microtubule networks (Olzmann et al., 2008). While the systems and components are different, the mechanisms of managing protein aggregates appear to be very similar. Understanding protein aggregate formation in a simple system like yeast may direct studies in higher organisms to homologous cellular components, expediting our understanding. This in turn has the potential to lead to new therapeutics that target prevention or early treatment

of human diseases, rather than the current approaches that are focused on dissolving existing aggregates.

Together, this dissertation identifies a novel approach to characterize the formation of protein aggregates in yeast. This approach and subsequent study has uncovered many details about the mechanisms managing protein aggregates that were previously unknown, changing the dogma of the current field. Further work using these techniques will strengthen our understanding of protein aggregate formation, and potentially lead to the development of strategies to treat or prevent protein aggregate associated diseases much more efficiently.

BIBLIOGRAPHY

Alberti, S. (2017). Phase separation in biology. *Current Biology*. 27(20) 1097-1102

Altmann, K., Frank, M., Neumann, D., Jakobs, S., and Westermann, B. (2008). The class v myosin motor protein, myo2, plays a major role in mitochondrial motility in saccharomyces cerevisiae. *Journal of Cell Biology*. 181(1) 199-130

Arai, T., Hasegawa, M., Akiyama, H., Ikeda, K., Nonaka, T., Mori, H., Mann, D., Tsuchiya, K., Yoshida, M., Hashizume, Y., and Oda, T. (2006). TDP-43 is a component of ubiquitin-positive tau-negative inclusions in frontotemporal lobar degeneration and amyotrophic lateral sclerosis. *Biochemical and Biophysical Research Communications*. 351(3) 602-611

Arslan, F., Hong, JY., Kanneganti, V., Park, SK., and Liebman, SW. (2015). Heterologous aggregates promote de novo prion appearance via more than one mechanism. *PLoS Genetics*. 11(1).

Asakura, T., Sasaki, T., Nagano, F., Satoh, A., Obaishi, H., Nishioka, H., Imamura, H., Hotta, K., Tanaka, K., Nakanishi, H., and Takai, Y. (1998). Isolation and characterization of a novel actin filament-binding protein from Saccharomyces cerevisiae. *Oncogene*. 16(1) 121-130

Ayscough, KR. (2000). Endocytosis and the development of cell polarity in yeast require a dynamic F-actin cytoskeleton. *Current Biology*. 10(24) 1587-1590

Bleem, A., and Daggett, V. (2017). Structrual and functional diversity among amyloid proteins: agents of disease, building blocks of biology, and implications for molecular engineering. *Biotechnology and Bioengineering*. 114(1) 7-20

Bockler, S., Chelius, X., Hock, N., Klecker, T., Wolter, M., Weiss, M., Braun, RJ., and Westermann, B. (2017). Fusion, fission, and transport control asymmetric inheritance of mitochondria and protein aggregates. *Journal of Cell Biology*. 216(8) 2481-2498

Bradley, ME., Edskes, HK., Hong, JY., Wickner, RB., and Liebman, SW. (2002). Interactions among prions and prion “strains” in yeast. *PNAS* 99: 16392-16399

Bradley, ME., and Liebman, SW. (2004). The Sup35 domains required for maintenance of weak, strong, or undifferentiated yeast [PSI+] prions. *Molecular Microbiology*. 51(6). 1649-1659

Braun, RJ., Sommer, C., Carmona-Gutierrez, D., Khoury, CM., Ring, J., Buttner, S., and Madeo, F. (2011). Neurotoxic 43-kDA TAR DNA-binding protein (TDP-43) triggers mitochondrion-dependent programmed cell death in yeast. *Journal of Biological Chemistry*. 286(22) 19958-19972

Brett, CL., Kallay, L., Hua, Z., Green, R., Chyou, A., Zhang, Y., Graham, TR., Donowitz, M., and Rao, R. (2011). Genome-wide analysis reveals the vacuolar pH-stat of saccharomyces cerevisiae. *PLOS ONE*

Brown, SS. (1997). Myosins in yeast. *Current Opinions in Cell Biology*. 9(1) 44-48

Buchan, JR., and Parker, R. (2009). Eukaryotic stress granules: the ins and outs of translation. *Molecular Cell*. 36(6) 932-941

Buchan, JR., Yoon, JH., and Parker, R. (2011). Stress-specific composition, assembly, and kinetics of stress granules in saccharomyces cerevisiae. *Journal of Cell Science*. 124(2) 228-239.

Buchan, JR., Kolaitis, RM., Taylor, JP., and Parker, R. (2013). Eukaryotic stress granules are cleared by autophagy and Cdc48/VCP function. *Cell*. 153(7) 1461-1474

Catlett, NL., and Weisman, LS. (1998). The terminal tail region of a yeast myosin-v mediates its attachment to vacuole membranes and sites of polarized growth. *PNAS*. 95(25) 14799 - 14804

Catlett, NL., Duex, JE., Tang, F., and Weisman, LS. (2000). Two distinct regions in a yeast myosin-v tail domain are required for the movement of different cargoes. *Journal of Cell Biology*. 150(3) 513-526

Cebollero, E., van der Vaart, A., and Reggiori, F. (2012). Understanding phosphatidylinositol-3-phosphate dynamics during autophagosome biogenesis. *Autophagy*. 8(12) 1868-1870

Cheney, RE., O'Shea, MK., Heuser, JE., Coelho, MV., Wolenski, JS., Espreafico, EM., Forscher, P., Larson, RE., and Mooseker, MS. (1993). Brain myosin-v is a two-headed unconventional myosin with motor activity. *Cell*. 75(1) 13-23

Cherkasov, V., Hofmann, S., Druffel-Augustin, S., Mogk, A., Tyedmers, J., Stoeklin, G., and Bukau, B. (2013). Coordination of translational control and protein homeostasis during severe heat stress. *Current Biology*. 23(24) 2452-2462

Chernoff, YO., Lindquist, SL., Ono, B., Inge-Vechtomov, SG., and Liebman, SW. (1995). Role of the chaperone protein Hsp104 propagation of the yeast prion-like factor [PSI+]. *Science*. 268(5212) 880-884

Chernova, TA., Romanyuk, AV., Karpova, TS., Shanks, JR., Ali, M., Moffatt, N., Howie, RL., O'Dell, A., McNally, JG., Liebman, SW., Chernoff, YO., and Wilkinson, KD. (2011). Prion induction by the short-lived, stress-induced protein lsb2 is regulated by ubiquitination and association with the actin cytoskeleton. *Molecular Cell*. 43(2) 242-252

Chiti, F., and Dobson, CM. (2006). Protein misfolding, functional amyloid, and human disease. *Annual Review of Biochemistry*. 75: 333-366

Chiti, F., and Dobson, CM. (2017). Protein misfolding, amyloid formation, and human disease. A summary of progress over the last decade. *Annual Review of Biochemistry*. 86: 27-68

Cox, B., Ness, F., and Tuite, MF. (2003). Analysis of the generation and segregation of propagons: entities that propagate the [PSI+] prion in yeast. *Genetics*. 165(1) 23-33

Deffieu, M., Bhatia-Kissova, I., Salin, B., Galinier, A., Manon, S., and Camougrand, N. (2009). Glutathione participates in the regulation of mitophagy in yeast. *Journal of Biological Chemistry*. 284(22) 14828-14837

Derkatch, IL., Chernoff, YO., Kushnirov, VV., Inge-Vechtomov, SG., and Liebman, SW. (1996). Genesis and variability of [*PSI*] prion factors in *Saccharomyces cerevisiae. Genetics*. 144(7) 1375-1386

Derkatch, IL., Bradley, ME., Zhou, P., Chernoff, YO., and Liebman, SW. (1997). Genetic and environmental factors affecting the de novo appearance of the [PSI+] prion in saccharomyces cerevisiae. *Genetics*. 147(2) 507-519

Derkatch, IL., Bradley, ME., and Liebman, SW. (1998). Overexpression of the Sup45 gene encoding a Sup35p-binding protein inhibits the induction of the de novo appearance of the [PSI+] prion. *PNAS*. 95(5) 2400-2405

Derkatch, IL., Bradley, ME., Masse, SV., Zadorsky, SP., Polozkov, GV., Inge-Vechtomov, SG., and Liebman, SW. (2000). Dependence and independence of [PSI+] and [PIN+]: a two-prion system in yeast?. *EMBO Journal*. 19(9) 1942-1952

Derkatch, IL., Bradley, ME., Hong, JY., and Liebman, SW. (2001). Prions affect the appearance of other prions: the story of [PIN+]. *Cell*. 106(2) 171-182.

Dorweiler, JE., Lyke, DL., Reilly, JA., Wisniewski, BT., Davis, E., Kuborn, AM., Oddo, MJ., Merril, SJ., and Manogaran, AL. (In Revision). The actin cytoskeletal network plays a role in prion transmission and contributes to prion stability. *Molecular Microbiology*.

Drummond, DA., and Wilke, CO. (2009). The evolutionary consequences of erroneous protein synthesis. *Nature Reviews Genetics*. 10(10) 715-724

Drubin, DG., Jones, HD., and Wertman, KF. (1993). Actin structure and function: roles in mitochondrial organization and morphogenesis in budding yeast and identification of the phalloidin-binding site. *Molecular Biology of the Cell*. 4(12) 1277-1294

Eagleston, SS., Ruddock, LW., Cox, BS., and Tuite, MF. (2000). Guanidine hydrochloride blocks a critical step in the propagation of the prion-like determinant [PSI(+)] of saccharomyces cerevisiae. *PNAS* 97(1) 240-244

Escusa-Toret, S., Vonk, WI., and Frydman, J. (2013). Spatial sequestration of misfolded proteins by a dynamic chaperone pathway enhances cellular fitness during stress. *Nature Cell Biology*. 15(10) 1231-1243

Efe, JA., Botelho, RJ., and Emr, SD. (2005). The fab1 phosphatidylinositol kinase pathway in the regulation of vacuole morphology. *Current Opinions in Cell Biology*. 17(4) 402-408

Ellis, RJ. (2001). Macromolecular crowding: obvious but underappreciated. *Trends in Biochemical Science*. 26(10) 597-604

Erjavec, N., Larsson, L., Granthan, J., and Nystrom, T. (2007). Accelerated aging and failure to segregate damaged proteins in sir2 mutants can be suppressed by overproducing the protein aggregation-remodeling factor hsp104p. *Genes and Development*. 21(19) 2410-2421

Eves, PT., Jin, Y., Brunner, M., and Weisman, LS. (2012). Overlap of cargo binding sites on myosin v coordinates the inheritance of diverse cargoes. *Journal of Cell Biology*. 198(1) 69-85

Fagarasanu, A., Mast, FD., Knoblach, B., and Rachubinksi, RA. (2010). Molecular mechanisms of organelle inheritance: lessons from peroxisomes in yeast. *Nature Reviews of Molecular Cell Biology*. 11(9) 644-654

Farrawell, NE., Lambert-Smith, IA., Warraich, ST., Blair, IP., Saunders, DN., Hatters, DM., and Yerbury, JJ. (2015). Distinct partitioning of als associated tdp-43, fus, and sod1 mutants into cellular inclusions. *Scientific Reports*. 5:13416

Filomeni, G., Desideri, E., Cardaci, S., Rotilio, G., and Ciriolo, MR. (2010). Under the ROS…thiol network is the principal suspect for autophagy commitment. *Autophagy*. 6(7) 999-1005

Franzmann, TM., and Alberti, S. (2018). Prion-like low-complexity sequences: Key regulators of protein solubility and phase behavior. *Journal of Biological Chemistry*. 294(18) 7128-7236

Franzmann, TM., Jahnel, M., Pozniakovsky, A., Mahamid, J., Holehouse, AS., Nuske, E., Richter, D., Baumesiter, W., Grill, SW., Pappu, RV., Hyman, AA., and Alberti, S. (2018). Phase separation of a yeast prion protein promotes cellular fitness. *Science*. 359(6371)

Galina, I., Colding, C., Henriksen, P., Beli, P., Nakamura, K., Offman, J., Mathiasen, DP., Silva, S., Hoffmann, E., Groth, A., Choudhary, C., and Lisby, M. (2015). Cmr1/WDR76 defines a nuclear genotoxic stress body linking genome integrity and protein quality control. *Nature Communications*. 6:6533

Ganusova, EE., Ozolins, LN., Bhagat, S., Newnam, GP., Wegrzyn, RD., Sherman, MY., and Chernoff, YO. (2006). Modulation of prion formation, aggregation, and toxicity by the actin cytoskeleton in yeast. *Molecular Cell Biology*. 26(2) 617-629

Gautschi, M., Mun, A., Ross, S., and Rospert, S. (2002). A functional chaperone triad on the yeast ribosome. *PNAS* 99(7) 4209-4214

Gidalevitz, T., Prahlad, V., and Morimoto, RI. (2011). The stress of protein misfolding: from single cells to multicellular organisms. *Cold Spring Harbor Perspectives Biology*. 3(6).

Gietz, RD., and Woods, RA. (2002). Transformation of yeast by lithium acetate / single-stranded carrier DNA / polyethylene glycol method. *Methods Enzymology*. 350 87-96

Glover, JR., and Lindquist, S. (1998). Hsp104, Hsp70, and Hsp40: a novel chaperone system that rescues previously aggregated proteins. *Cell*. 94(1) 73-82

Greenwald, J., and Riek, R. (2010). Biology of amyloid: structure, function, and regulation. *Structure*. 18(10) 1244-1260

Gregersen, N., Bross, P., Vang, S., and Christensen, JH. (2006). Protein misfolding and human disease. *Annual Review of Genomics and Human Genetics*. 7: 103-124

Haslberger, T., Zdanowicz, A., Brand, I., Kirstein, J., Turgay, K., Mogk, A., and Bukau, B. (2008). Protein disaggregation by the AA+ chaperon ClpB involves partial threading of looped polypeptide segments. *Nature Structural Molecular Biology*. 15(6) 641-650

Hermesh, O., Genz, C., Yofe, I., Sinzel, M., Rapaport, D., Schuldiner, M, and Jansen, RP. (2014). Yeast phospholipid biosynthesis is linked to mRNA localization. *Journal of Cell Science*. 127(15) 3373-3381

Hill, SM., Hao, X., Gronvall, J., Spikings-Nordby, S., Widlund, PO., Amen, T., Jorhov, A., Josefson, R., Kaganovich, D., Liu, B., and Nystron, T. (2016). Asymmetric inheritance of aggregate proteins and age reset in yeast are regulated by vac17-dependent vacuolar functions. *Cell Reports*. 16(3) 826-838

Hipkiss, AR. (2006). Accumulation of altered proteins and aging: causes and effects. Experimental Gerontology. 41(5) 464-473

Hughes, AL., and Gottschling, DE. (2012). An early age increase in vacuolar pH limits mitochondrial function and lifespan in yeast. *Nature*. 492(7428) 261-265

Hund, E. (2012) Familial amyloidotic polyneuropathy: current and emerging treatment options for transthyretin-mediated amyloidosis. *Applied Clinical Genetics* 18(5) 37-41

Imran, M., and Mahmood, S. (2011). An overview of human prion diseases. *Viology Journal*. 8:559

Ishii, A., Kurokawa, K., Hotta, M., Yoshizaki, S., Kurita, M., Koyama, A., Nakano, A., and Kimura, Y. (2019). Role of atg8 in the regulation of vacuolar membrane invagination. *Scientific Reports*. 9:14828

Johnson, BS., McCaffery, JM., Lindquist, S., and Gitler, AD. (2008). A yeast TDP-43 proteinopathy model: exploring the molecular determinants of TDP-43 aggregation and cellular toxicity. *PNAS*. 105(17) 6439-6444

Johnson, BS., Snead, D., Lee, JJ., McCaffery, JM., Shorter, J., and Gitler, AD. (2009). TDP-43 is intrinsically aggregation-prone, and amyotrophic lateral sclerosis-linked mutations accelerate aggregation and increase toxicity. *Journal of Biological Chemistry*. 284(30) 20329-20339

Kaganovich, D., Kopito, R., and Frydman, J. (2008). Misfolded proteins partition between two distinct quality control compartments. *Nature*. 454(7208) 1088-1095

Kanki, T., Wang, T., Cao, Y., Baba, M., and Klinosky, DJ. (2009). Atg32 is a mitochondrial protein that confers selectivity during mitophagy. *Developmental Cell*. 17(1) 98-109.

Karpova, TS., Moltz, SL., Riles, LE., Guldener, U., Hegemann, JH., Veronneau, S., Bussey, H., and Cooper, JA. (1998). Depolarization of the actin cytoskeleton is a specific phenotype in saccharomyces cerevisiae. *Journal of Cell Science*. 111(17) 2689-2696

Kato, M., Han, TW., Xie, S., Shi, K., Du, X., Wu, LC., Mirzaei, H., Goldsmith, EJ., Longgood, J., Pei, J., Grishin, NV., Frantz, DE., Schnieder, JW., Chen, S., Li, L., Sawaya, MR., Eisenberg, D., Tycko, R., and McKnight, SL. (2012). Cell-free formation of rna granules: low complexity sequence domains form dynamic fibers within hydrogels. *Cell*. 149(4) 753-767

Kopecka, M., Yamaguchi, M., and Kawamoto, S. (2015). Effects of the F-actin inhibitor latrunculin A on the budding yeast saccharomyces cerevisiae. *Microbiology*. 161(7) 1348-1355

Kornmann, B., Currie, E., Collins, SR., Schuldiner, M., Nunnari, J., Weissman, JS., and Walter, P. (2009). An ER-mitochondria tethering complex revealed by a synthetic biology screen. Science. 325(5939) 477-481

Kroshwald, S., Munder, MC., Maharana, S., Franzmann, TM., Richter, D., Ruer, M., Hyman, AA., and Alberti, S. (2018). Different material states of pub1 condensates define distinct modes of stress adaptation and recovery. *Cellular Reports*. 23(11) 3327-3339

Kumar, J., Nawroth, PP., and Tyedmers, J. (2016). Prion aggregates are recruited to the insoluble protein deposit (IPOD) via myosin 2-based vesicular transport. *PLOS Genetics*. 12(9)

Kumar, J., Neuser, N., and Tyedmers, J. (2017). Hitchhiking vesicular transport routes to the vacuole: amyloid recruitment to the insoluble protein deposit (IPOD). *Prion* 11(2) 71-81

Kroschwald, S., Maharana, S., Mateju, D., Malinovska, L., Nuske, E., Poser, I., Richter, D., and Alberti, S. (2015). Promiscuous interactions and protein disaggregases determine the material state of stress-inducible RNP granules. *eLife* 4

Kryndushkin, DS., Alexandrov, IM., Ter-Avanesyan, MD., and Kushnirov, VV. (2003). Yeast [PSI+] prion aggregates are formed by small Sup35 polymers fragmented by Hsp104. *Journal of Biological Chemistry*. 278(49) 49636-49643

Kryndushkin, DS., Engel, A., Edskes, H., and Wickner RB. (2011). Molecular chaperone hsp104 can promote yeast prion generation. *Genetics*. 188(2) 339-348

Kryndushkin, DS., Ihrke, G., Piermartiri, TC., and Shewmaker, F. (2012). A yeast model of optineurin proteinopathy reveals a unique aggregation pattern associated with cellular toxicity. *Molecular Microbiology*. 86(6) 1531-1547

Kryndushkin, D., Pripuzova, N., Burnett, BG., and Shwmaker, F. (2013). Non-targeted identification of prions and amyloid-forming proteins from yeast and mammalian cells. *Journal of Biological Chemistry*. 288(38) 27100-27111

Labbadia, J., and Morimoto, RI. (2015). The biology of proteostasis in aging and disease. *Annual Reviews Biochemistry*. 84 435-464

Lackner, LL., Ping, H., Graef, M., Murley, A., and Nunnari, J. (2013). Endoplasmic reticulum-associated mitochondria-cortex tether functions in the distribution and inheritance of mitochondria. *PNAS*. 110(6) 458-467

Lancaster, AK., Bardill, JP., True, HL., and Masel, J. (2010). The spontaneous appearance rate of the yeast prion [PSI+] and its implications for the evolution of the evolvability properties of the [PSI+] system. *Genetics*. 184(2) 393-400

Laurent, JM., Young, JH., Kachroo, AH., and Marcotte, EM. (2016). Efforts to make and apply humanized yeast. *Briefings in Functional Genomics*. 15(2) 155-163

Leeuwen, W., and Rabouille, C. (2019). Cellular stress leads to the formation of membraneless stress assemblies in eukaryotic cells. *Traffic*. 20(9) 623-638

Leopold, PE., Montal, M., and Onuchic, JN. (1992). Protein folding funnels: a kinetic approach to the sequence-structure relationship. *PNAS* 89(18) 8721-8725

Levine, CG., Mitra, D., Sharma, A., Smith, CL., and Hegde, RS. (2005). The efficiency of protein compartmentalization into the secretory pathway. *Molecular Biology of the Cell*. 16(1) 279-291.

Liebman, SW., and Chernoff, YO. (2012). Prions in yeast. *Genetics*. 191(4) 1041-1072

Lin, MC., Galletta, BJ., Sept, D., and Cooper, JA. (2010). Overlapping and distinct functions for cofilin, coronin, and Aip1 in actin dynamics in vivo. *Journal of Cell Science*. 123(8) 1329-1342

Lipatova, Z., Belogortseva, N., Zhang, XQ., Kim, J., Taussig, D., and Segev, N. (2012). Regulation of selective autophagy onset by a Ypt/Rab GTPase module. *PNAS*. 109(18) 6981-6986

Lippuner, A., Julou, T., and Barral, Y. (2014). Budding yeast as a model organism to study the effects of age. *FEMS Microbiology Reviews*. 38(2) 300-325

Liu, B., Larsson, L., Caballero, A., Hao, X., Oling, D., Grantham, J., and Nystrom, T. (2010). The polarisome is required for segregation and retrograde transport of protein aggregates. *Cell* 140(2) 257-267

Liu-Yesucevitz, L., Bilgutay, A., Zhang, YJ., Vanderweyde, T., Citro, A., Mehta, T., Zaarur, N., McKee, A., Bowser, R., Sherman, M., Petrucelli, L., and Wolozin, B. (2010). Tar DNA binding protein-43 (TDP-43) associates with stress granules: analysis of cultured cells and pathological brain tissue. *PLoS One*. 5(10).

Liu, G., Coyne, AN., Pei, F., Vaughan, S., Chaung, M., Zarnescu, DC., and Buchan, JR. (2017). Endocytosis regulates TDP-43 toxicity and turnover. *Nature Communications*. 8: 2092

Loewen, CJ., Young, BP., Tavassoli, S., and Levine, TP. (2007). Inheritance of cortical ER in yeast is required for normal septin organization. *Journal of Cell Biology*. 179(3) 467-483

Lyke, DR., and Manogaran, AL. (2017). Spatial sequestration and oligomer remodeling during de novo [PSI+] formation. *Prion*. 11(5) 332-337

Maclean-Fletcher, A., and Pollard, TD. (1980). Mechanism of action of cytochlasin B on actin. *Cell*. 20(2) 329-341

Malinovska, L., Kroshwald, S., Munder, MC., Richter, D., and Alberti, S. (2012). Molecular chaperones and stress-inducible protein-sorting factors coordinate the spatiotemporal distribution of protein aggregates. *Molecular Biology of the Cell*. 23(16) 3041-3056

Manogaran, AL., Hong, JY., Hufana, J., Tyedmers, J., Lindquist, S., and Liebman, SW. (2011). Prion formation and polyglutamine aggregation are controlled by two classes of genes. *PLOS Genetics*. 7(5)

Mathur, V., Taneja, V., Sun, Y., and Liebman, SW. (2009). Analyzing the birth and propagation of two distinct prions, [PSI+] and [Het-s]$_y$ in yeast. *Molecular Biology of the Cell*. 21(9) 1449-1461

Matsui, Y. (2003). Polarized distribution of intracellular components by class v myosins in saccharomyces cerevisiae. *International Review of Cytology*. 229 1-42

Meriin, AB., Zhang, X., He, X., Newnam, GP., Chernoff, YO., and Sherman, MY. (2002). Huntington toxicity in yeast model depends on polyglutamine aggregation mediated by a prion-like protein rnq1. *Journal of Cell Biology*. 157(6) 997-1004

Mermall, V., Post, PL., and Mooseker, MS. (1998). Unconventional myosins in cell movement, membrane traffic, and signal transduction. *Science* 279(5350) 527-533

Miller, CJ., Wong, WW., Bobkova, E., Rubenstein, PA., and Reisler, E. (1996). Mutational analysis of the role of the N terminus of actin in actomyosin interactions. Comparison with other mutant actins and implications for the cross-bridge cycle. *Biochemistry*. 35(51) 16557-16565

Miller, SB., Ho, CT., Winkler, J., Khokrina, M., Neuner, A., Mohamed, MY., Guilbride, DL., Richter, K., Lisby, M., Schiebel, E., Mogk, A., and Bukau, B. (2015). Compartment-specific aggregases direct distinct nuclear and cytoplasmic aggregate deposition. *EMBO Journal*. 34(6) 778-797

Mochida, K., Oikawa, Y., Kimura, Y., Kirisako, H., Hirano, H., Ohsumi, Y., and Nakatogawa, H. (2015). Receptor-mediated selective autophagy degrades the endoplasmic reticulum and the nucleus. *Nature*. 522(7556) 359-362

Molliex, A., Temirov, J., Lee, J., Coughlin, M., Kanagarai, AP., Kim, HJ., Mittag, T., and Taylor, JP. (2015). Phase separation by low complexity domains promotes stress granule assembly and drives pathological fibrillization. *Cell*. 163(1) 123-133

Morano, KA., and Klionsky, DJ. (1994). Differential effects of compartment deacidification on the targeting of membrane and soluble proteins to the vacuole in yeast. *Journal of Cell Science*. 107(10) 2813-2824

Moreno-Gonzalez, I., and Soto, C. (2011). Misfolded protein aggregates: mechanisms, structures, and potential for disease transmission. *Seminar of Cell Developmental Biology*. 22(5) 482-487

Moriyama, H., Edskes, HK., and Wickner, RB. (2000). [URE3] prion propagation in saccharomyces cerevisiae: requirement for chaperone hsp104 and curing by overexpressed chaperone ydj1p. *Molecular Cell Biology*. 20(23) 8916-1922

Moseley, JB., and Goode, BL. (2006). The yeast actin cytoskeleton: from cellular function to biochemical mechanism. *Microbiology and Molecular Biology Reviews*. 70(3) 605-645

Nakamura, N., Matsuura, A., Wada, Y., and Ohsumi, Y. (1997). Acidification of vacuoles is required for autophagic degradation in the yeast, saccharomyces cerevisiae. *Journal of Biochemistry*. 121(2) 338-344.

Nandi, D., Tahiliani, P., Kumar, A., and Chandu, D. (2006). The ubiquitin-proteasome system. *Journal of Bioscience*. 31(1) 137-155

Ness, F., Ferreira, P., Cox, BS., and Tuite, MF. (2002). Guanidine hydrochloride inhibits the generation of prion "seeds" but not prion protein aggregation in yeast. *Molecular Cell Biology*. 22(15) 5593-5605

Neumann, M., Sampathu, MD., Kwong, LK., Truax, AC., Micsenyi, MC., Chou, TT., Bruce, J., Schuck, T., Grossman, M., Clark, CM., McCluskey, LF., Miller, BL., Masliah, E., Mackenzie, IR., Feldman, H., Feiden, W., Kretzschmar, HA., Troianowski, JQ., and Lee, VM. (2006). Ubiquitinated TDP-43 in frontotemporal lobar degernation and amyotrophic lateral sclerosis. *Science*. 314(5796) 130-133.

Nishikawa, SI., Fewell, SW., Kato, Y., Brodsky, JL., and Endo, T. (2001). Molecular chaperones in the yeast endoplasmic reticulum maintain the solubility of proteins for retrotranslocation and degradation. *Journal of Cell Biology*. 153(5) 1061-1070

Ogle, JM., and Ramakrishnan, V. (2005). Structural insights into translational fidelity. *Annual Reviews Biochemistry*. 74 129-177

Olzmann, JA., Li, L., and Chin, LS. (2008). Aggresome formation and neurodegenerative diseases: therapeutic implications. *Current Medical Chemistry*. 15(1) 47-60

Osherovich, LZ., and Weissman, JS. (2001). Multiple Gln/Asn-rich prion domains confer susceptibility to induction of the yeast [PSI+] prion. *Cell*. 106(2) 183-194

Park, SK., Hong, JY., Arslan, F., Kanneganti, V., Patel, B., Tietsort, A., Tank, EM., Li, X., Barmada, SJ., and Liebman, SW. (2017). Overexpression of the essential sis1 chaperone reduces TDP-43 effects on toxicity and proteolysis. *PLoS Genetics*. 13(5)

Paushkin, SV., Kushnirov, VV., Smirnov, VN., and Ter-Avanesyan, MD. (1996). Propagation of the yeast prion-like [psi+] determinant is mediated by oligomerization of the Sup35-encoded polypeptide chain release factor. *EMBO Journal*. 15(12) 3127-3134

Protter, DS., and Parker, R. (2016). Principles and properties of stress granules. *Trends in Cell Biology*. 26(9) 668-679

Prusiner, SB., and McCarty, M. (2006). Discovering DNA encodes heredity and prions are infectious proteins. *Annual Reviews of Genetics*. 40 25-45

Pruyne, D., Legesse-Miller, A., Gao, L., Dong, Y., and Bretscher, A. (2004). Mechanisms of polarized growth and organelle segregation in yeast. Annual *Reviews of Cell Developmental Biology*. 20 559-591

Rambaran, RN., and Serpell, LC. (2008). Amyloid fibrils: abnormal protein assembly. *Prion*. 2(3) 112-117

Reggiori, F., and Klionsky, DJ. (2013). Autophagic processes in yeast: mechanism, machinery, and regulation. Genetics. 194(2) 341-361

Riback, JA., Katanski, CD., Kear-Scott, JL., Pilipenko, EV., Rojek, AE., Sosnick, TR., and Drummond, DA. (2017). Stress-triggered phase separation is an adaptive, evolutionarily tuned response. *Cell*. 168(6) 1028-1040

Ruan, L., Zhang, X. and Li, R. (2018). Recent insights into the cellular and molecular determinants of aging. *Journal of Cell Science*. 131

Ruberg, FL., and Berk, JL. (2012). Transthyretin (TTR) cardiac amyloidosis. *Circulation*. 126(10): 1286-1300

Saarikangas, J., and Barral, Y. (2015). Protein aggregates are associated with replicative aging without compromising protein quality control. *Elife*. 4

Saarikangas, J., and Caudron, F. (2017). Spatial regulation of coalesced protein assemblies: lessons from yeast to diseases. *Prion*. 11(3) 162-173

Saibil, H. (2013). Chaperone machines for protein folding, unfolding, and disaggregation. Nature Reviews: Molecular Cell Biology. 14(10) 630-642

Saibil, HR., Seybert, A., Habermann, A., Winkler, J., Eltsoy, M., Perkovic, M., Castano-Diez, D., Scheffer, MP., Haselmann, U., Chlanda, P., Lindquist, S., Tyedmers, J., and Frangkis, AS. (2012). Heritable yeast prions have a highly organized three-dimensional architecture with interfiber structures. *PNAS*. 109(37) 14906-14911

Salas-Marco, J., and Bedwell, DM. (2004). GTP hydrolysis by eRF3 facilitates stop codon decoding during eukaryotic translation termination. *Molecular Cell Biology*. 24(17) 7769-7778

Sanchez, Y., and Lindquist, SL. (1990). Hsp104 required for induced thermotolerance. *Science*. 248(4959) 1112-1115

Schafer, FQ., and Buettner, GR. (2001). Redox environment of the cell as viewed through the redox state of the glutathione disulfide/glutathione couple. *Free Radical Biological Medicine*. 30(11) 1191-1212

Scholtzova, H., Chianchiano, P., Pan, J., Sun, Y., Goni, F., Mehta, PD., and Wisniewski, T. (2014). Amyloid B and tau alzheimer's disease related pathology is reduced by toll-like receptor 9 stimulation. *Acta Neuropathology Communications*. 2: 101

Schott, D., Ho, J., Pruyne, D., and Bretscher, A. (1999). The Cooh-terminal domain of myo2p, a yeast myosin v, has a direct role in secretory vesicle targeting. *Journal of Cell Biology*. 147(4) 791-808

Seeley, ES., Kato, M., Margolis, N., Wickner, W., and Eitzen, G. (2002). Genomic analysis of homotypic vacuole fusion. *Molecular Biology of the Cell*. 13(3) 782-794

Shaknovich, E. (2006). Protein folding thermodynamics and dynamics: where physics, chemistry, and biology meet. *Chemistry Reviews*. 106(5) 1559-1588

Sharma, J., and Liebman, SW. (2012). [PSI+] prion variant establishment in yeast. *Molecular Microbiology*. 86(4). 866-881

Sharma, J., Wisniewski, BT., Paulson, E., Obaoye, JO., Merrill, SJ., and Manogaran, AL. (2017). De novo [PSI] prion formation involves multiple pathways to form infectious oligomers. *Scientific Reports*. 7(76)

Sherman, F., Fink, GR, and Hicks, JB. (1986). Methods in yeast genetics. *Cold Spring Harbor Lab*.

Shorter, J., and Lindquist, S. (2004). Hsp104 catalyzes formation and elimination of self-replicating Sup35 prion conformers. *Science*. 304(5678) 1793-1797

Sondheimer, N., and Lindquist, S. (2000). Rnq1: an epigenetic modifier of protein function in yeast. *Molecular Cell*. 5(1) 163-172

Song, J. (2013). Why do proteins aggregate? "Intrinsically insoluble proteins" and "dark mediators" revealed by studies on "insoluble proteins" solubilized in pure water. *F1000 Research* 2:94

Song, J., Yang, Q., Yang, J., Larsson, L., Hao, X., Zhu, X., Malmgren-Hill, S., Cvijovic, M., Fernandez-Rodriguez, J., Granham, J., Gustafsson, CM., Liu, B., and Nystrom, T. (2014). Essential genetic interactors of sir2 required for spatial sequestration and asymmetrical inheritance of protein aggregates. *PLOS Genetics*.

Specht, S., Miller, SB., Mogk, A., and Bukau, B. (2011). Hsp42 is required for sequestration of protein aggregates into deposition sites in Saccharomyces cerevisiae. *Journal of Cell Biology*. 195(4) 617

Speldewinde, SH., Doronina, VA., and Grant, CM. (2015). Autophagy protects against de novo formation of the [PSI+] prion in yeast. *Molecular Biology of the Cell*. 26(25). 4541-4551

Speldewinde, SH., Doronina, VA., Tuite, MF., and Grant, CM. (2017). Disrupting the cortical actin cytoskeleton points to two distinct mechanisms of yeast [PSI+] prion formation. *PLOS Genetics* 13(4)

Spokoini, R., Moldavski, O., Nahmias, Y., England, JL., Schuldiner, M., and Kaganovich, D. (2012). Confinement to organelle-associated inclusion structures mediates asymmetric inheritance of aggregated protein in budding yeast. *Cell Reports*. 2(4) 738-747.

Stansfield, I., Grant, CM., Akhmaloka., and Tuite, MF. (1993). Errors in stop codon recognition in a temperature sensitive mutation of yeast. *Biochemical Society Transactions*. 21(4) 329S

Tang, HY., Xu, J., and Cai, M. (2000). Pan1p, End3p, and S1a1p, three yeast proteins required for normal cortical actin cytoskeleton organization, associate with each other and play essential roles in cell wall morphogenesis. *Molecular Cell Biology*. 20(1) 12-25

Ter-Avanesyan, MD., Dagkesamanskaya, AR., Kushnirov, VV., and Smirnov, VN. (1994). The SUP35 omnipotent suppressor gene is involved in the maintenance of the non-mendelian determinant [psi+] in the yeast saccharomyces cerevisiae. *Genetics*. 137(3) 671-676

Tessarz, P., Schwarz, M., Mogk, A., and Bukau, B. (2009). The yeast AAA+ chaperone hsp104 is apart of a network that links the actin cytoskeleton with the inheritance of damaged proteins. *Molecular Cell Biology*. 29(13) 3738-3745

Thumm, M. (2000). Structure and function of the yeast vacuole and its role in autophagy. *Microscopy Research and Technique*. 51(6) 563-572

Tyedmers, J., Treusch, S., Dong, J., McCaffery, JM., Bevis, B., and Lindquist, S. (2010). Prion induction involves an ancient system for the sequestration of aggregated proteins and heritable changes in prion fragmentation. *PNAS*. 107(19) 8633-8638

Uemura, N., Yagi, H., Uemura, MT., Hatanaka, Y., Yamakado, H., and Takahashi, R. (2018). Inoculation of a-synuclein preformed fibrils into the mouse gastrointestinal tract induces lewy body-like aggregates in the brainstem via the vagus nerve. *Molecular Neurodegeneration*. 13(1) 21

Vishveshwara, N., and Liebman, SW. (2009). Heterologous cross-seeding mimics cross-species prion conversion in yeast model. *BMC Biology*. 7:26

Wallace, EW., Kear-Scott, JL., Pilipenko, EV., Schwartz, MH., Laskowski, PR., Rojeck, AE., Katanski, CD., Riback, JA., Dion, MF., Franks, AM., Airoldi, EM., Pan, T., Budnik, BA., and Drummound, DA. (2015). Reversible, specific, active aggregates of endogenous proteins assemble upon heat stress. *Cell*. 162(6) 1286-1298

Weids, AJ., Ibstedt, S., Tamas, MJ., and Grant, CM. (2016). Distinct stress conditions result in aggregation of proteins with similar properties. *Scientific Reports*. 18(6) 24554

Weisman, LS., Bacallao, R., and Wickner, W. (1987). Multiple methods of visualizing the yeast vacuole permit evaluation of its morphology and inheritance during the cell cycle. *Journal of Cell Biology*. 105(4) 1539-1547

Weisman, LS. (2003). Yeast vacuole inheritance and dynamics. *Annual Reviews of Genetics*. 37 435-460

Weisman, LS. (2006). Organelles on the move: insights from yeast vacuole inheritance. *Nature Reviews Molecular Cell Biology*. 7(4) 243-252

Wertman, KF., Drubin, DG., and Botstein, D. (1992). Systemic mutational analysis of the yeast ACT1 gene. *Genetics*. 132(2) 337-350

Wheeler, JR., Matheny, T., Jain, S., Abrisch, R., and Parker, R. (2016). Distinct stages in stress granule assembly and disassembly. *Elife*. 5

Wickner, RB. (1994). [URE3] as an altered URE2 protein: evidence for a prion analog in *Saccharomyces cerevisiae*. *Science*. 264(5158) 566-569

Winkler, J., Tyedmers, J., Bukau, B., and Mogk, A. (2012). Hsp70 targets hsp100 to substrates for protein disaggregation and prion fragmentation. *Journal of Cell Biology*. 198(3) 387-404

Winzeler, EA., et al. (1999). Functional characterization of the S. cerevisiae genome by gene deletion and parallel analysis. *Science*. 285(5429) 901-906

Yang, F., Durfee, LA., and Huibregtse, JM. (2013). A cotranslational ubiquitination pathway for quality control of misfolded proteins. *Molecular Cell*. 50(3) 368-378

Yang, HC., and Pon, LA. (2002). Actin cable dynamics in budding yeast. *PNAS*. 99 751-756

Young, JC., Agashe, VR., Siegers, K., and Hartl, FU. (2004). Pathways of chaperone-mediated protein folding in the cytosol. *Nature Reviews: Molecular Cell Biology* 5(10) 781-791

Young, ME., Cooper, JA., and Bridgman, PC. (2004). Yeast actin patches are networks of branched actin filaments. *Journal of Cell Biology*. 166(5) 629-635

Zhou, P., Derkatch, IL., Liebman., SW. (2001). The relationship between visible intracellular aggregates that appear after overexpression of Sup35 and the yeast prion-like elements [PSI(+)] and [PIN(+)]. *Molecular Microbiology*. 39(1) 37-46

Zhou, C., Slaughter, BD., Unruh, JR., Eldakak, A., Rubinstein, B., and Li, R. (2011). Motility and segregation of Hsp104-associated protein aggregates in budding yeast. *Cell*. 147(5) 1186-1196

Zhou, C., Slaughter, BD., Unruh, JR., Guo, F., Yu, Z., Mickey, K., Narkar, A., Ross, RT., McClain, M., and LI, R. (2014). Organelle-based aggregation and retention of damaged proteins in asymmetrically dividing cells. *Cell*. 159(3). 530-542.